

The cover artwork was digitalized with *Inkscape*[1], from a picture by my sister **Marta**. It's been inspired by a scene in the Warner Bros. movie *The Matrix*¹, and partially by the painting *Nuestra imagen actual*, by David Alfaro Siqueiros. This and all other graphical and text content in the present book have been generated using Free Software, except *Matematica*[2], which is commercial, and *Raster3D*[3], which is gratis but not free. No *Microsoft* product was ever used either in the research activity leading to this Thesis or in the creation of the Thesis book itself.

The author of this work intends to release it under the **Creative Commons Attribution-NonCommercial-NoDerivs 2.5** License. To view a copy of this license, visit <http://creativecommons.org/licenses/by-nc-nd/2.5/> or send a letter to Creative Commons, 543 Howard Street, 5th Floor, San Francisco, California, 94105, USA. However, a substantial part of it (most of Chapters 2, 3 and 4) has been published in scientific journals[4, 5], and therefore its copyright holder is the Publisher (the American Chemical Society). Graphical content in the whole Thesis, plus all other content not in Chapters 2, 3 and 4 is copyrighted under the aforementioned Creative Commons license.

¹for an explanation, search for *bluepill* and *redpill* in the Wikipedia.

Ethylene Polymerization by Group IV
Transition Metal Metallocenes

Doctoral Dissertation

Iñaki Silanes

Director: Jesus M. Ugalde



**TESIAREN ZUZENDARIAREN BAIMENA
TESIA AURKEZTEKO**

Jesus M. Ugalde Uribe-Etxebarria jaunak **Ethylene Polymerization by Group IV Transition Metal Metallocenes** izenburua duen doktorego-tesiaren zuzendari naizenak, tesia aurkezteko baimena ematen dut, defendatua izateko baldintzak betetzen dituelako. **Iñaki Silanes Cristóbal** doktoregai jaunak egin du aipaturiko tesia, **Polimeroen Zientzia eta Teknologia** sailean.

_____, _____ (e)ko _____ ren _____ a

TESIAREN ZUZENDARIA

Izpta.: Jesus M. Ugalde Uribe-Etxebarria



SAILAREN ADOSTASUNA

Polimeroen Zientzia eta Teknologia Saileko Kontseiluak, _____(e)ko bileran, **Ethylene Polymerization by Group IV Transition Metal Metallocenes** izenburua duen doktorego-tesia aurkeztearen alde dagoela adierazi du. **Jesus M. Ugalde Uribe-Etxebarria** jaunaren zuzendaritzapean egin den tesi hori **Iñaki Silanes Cristóbal** jaunak aurkeztu du sail honetan.

_____, _____ (e)ko _____ ren _____ a

O.E. SAILEKO ZUZENDARIA

SAILEKO IDAZKARIA

Izpta.: _____ Izpta.: _____

Acknowledgements

When I read the acknowledgements of other Doctoral Dissertations, I always get the feeling that the author must have been a living Hard Drive²: they remember so many names!

I wish I could mention everyone who deserves being here. Probably I should just say “I thank everybody”, and not risk leaving out more people than I actually mention... This is the part of the Thesis where one earns a handful of enemies, much like with the relatives you fail to invite to your wedding³.

I could not help but begin these acknowledgements thanking Prof. Jesus M. Ugalde. He made me an enormous honor when he offered me a position as part-time collaborator, back in summer of 1998, when I had just finished the third course of my B.Sc. degree. The working environment was so nice that I hardly had any doubt to stay in the group after getting my degree in Chemistry, in order to proceed with my Ph.D. Jesus has always supported my job and encouraged me to go on. Eskerrik asko, Jesus.

It would be pretty accurate to say that I begun my part-time collaboration time work at Jesus’ group under the supervision of Dr. Arantxa Irigoras. She has always been a bit in the tight side, but I don’t regret a single minute of the long hours she spent shouting at me and hitting me with the whip. She taught me a fairly important set of fundamentals that have lasted longer in my mind than the whip-wounds on my skin.

Although I do not intend to arrange this section in any preferential order, my next thanks should go to one of the most important figures in my formation as a scientist. That would, of course, be St. Txema Mercero. Oops, I meant “Dr.”. He has been probably acknowledged in every thesis coming out of Jesus’ group (and some other groups as well) because he has spent a great deal of effort keeping our machines up and kicking with unearthly skill. I

²for the non computer-savvy, HD has nothing to do with driving, and little with being hard. It’s just the internal disk of a computer

³or maybe it’s the ones you *do* invite who hate you. As Chuck Berry said, you never can tell.

VI

would further add that he's kept all of *us* active as well. He has always been willing to listen to our questions, witty enough to find the proper answer, kind enough not to pinpoint the fact that we already asked him that question three times the last week, and so good tempered that he's always made me strain my brain to find new silly questions to push his temper's limits.

Since Txema has been the *guru* that taught me most of what I know about computer science, this might be a good place to mention Doctors Joseph Fowler and Elmer Valderrama, who also contributed. Joseph has always been a walking example of the kind of North American you don't see on the CNN or the Hollywood movies. He brought us the sweet poison of GNU/Linux from the country of the Redmond Evil, and it would not be far-fetched to say he did also open our minds in scientific and personal ways. Elmer is also American, just from Colombia, not the USA. The jury is still out whether he masters to a higher degree the entrails of GNU/Linux or DFT, but the first time someone told me about Perl it was him, and my life has not been the same since⁴.

From the beginnings of my Ph.D. I should also recall Doctors Willy Roa and América García. Willy, humorous and witty⁵, always had the proper word to make you laugh, and also to make you think. And sometimes at the same time. América, her entry in the British Encyclopedia should read longer than the one of the continent she was named after.

The review to the “elderly” part of my colleagues would be seriously lacking if I were to forget about Dr. Xabier López. Xabi is perhaps the most theoretical one of the lot, bird of a flock to all kind of heathens such as Physicists and Organic Chemists. I never had a theoretical question he couldn't help me get straight, and only scarcely I found something I *did* understand and he could not make me de-understand through jokes.

The “younger” crew in Jesus' group deserves a thankful mention at this point. Eider, *moreover* the most remarkable woman east of the Mississippi, as remarkable are Elena, Eli and (in a more manly way, mind you) Joni, Txoni and Julen. They all compiled my kernel when my code was buggy, in a manner of speaking. Among the youngsters (in spirit, if not otherwise) I'd like to thank Drs Mario Piris and Jian Wang, for the science, the *salsa* and the laughs. *Shie-shie*, Jian. Gracias, Mario.

I should not forget that not only my group helped or supported me, inside the Faculty, during these years. Prof. Fernando P. Cossío's Organic Chemistry group not only made my lunches fun, but widened my views on chemistry⁶. Big thanks to Aizpea, Ana, Begoña, Edurne, Eneko, Fernando and Mirari

⁴I don't mean it's been *better*, just different. Scripting in Perl or *shell* has saved me long hours of handwork, at the cost of spending a few days writing down the script.

⁵Typical combination in our group. E.g., Txema's so witty, and Xabi's so humorous.

⁶and also other subjects not suitable for publishing in a Thesis.

(alphabetical order here).

Many names should be added, corresponding to teachers, collaborators and friends, such as Joxemari Elorza, Cecilia Sarasola, Russ Boyd, Nelaine Mora, Leif Eriksson, Carlos Silva, Olalla Faza and Eduardo Ludeña. The latter has become a particularly relevant collaborator, sharing not only good science and good ideas, but also culture and even philosophy. Thanks also to Marce Goñi, the Department Secretary, for her kindness and attention.

My heartily thanks should also go to Doctors Paul Sherwood and Huub van Dam, who made my stay at Daresbury Laboratory (UK) kind and fruitful.

In the personal field, I am grateful to my friends, who showed me there is more to life than sitting in front of a computer 24/7. They are too many to cite them all, but some should not go without mention: Izar, Larraitz and Oihana, thanks for all the *Estropadak* and *Sagardo Egunak*. I would also like to thank Lonore, who made me discover hitherto unknown dimensions in friendship and life, and made a remarkable display of the patience required by the friends of any Ph.D. student.

As an extra, many thanks should go to: Linus Torvalds, for creating and maintaining Linux, the kernel of the OS I have so joyfully used during the Ph.D.; Richard Stallman, founder of the FSF and *guru* of the GNU movement; Larry Wall, creator of Perl, most useful tool for a computer, short of the screen, the keyboard, and maybe the mouse; Donald E. Knuth for creating T_EX and Leslie Lamport for transforming it into L^AT_EX⁷, which is the typographic program exclusively used for producing this book; Patrick Volkerding, creator and maintainer of Slackware, the *distro* I began my steps in GNU/Linux with; Debra and Ian Murdock, founders and former maintainers of Debian, the *distro* I have finally settled for, after trying many; and all the FLOSS community for providing me, and millions others, with high quality and free software.

Finalmente, últimos pero primeros en mi corazón, mi familia. A vosotros os agradezco que me hayáis apoyado incondicionalmente en mi doctorado, animado a seguir con ello pese a los malos momentos, y aguantado cuando os he dado la vara con temas tan apasionantes para un lego como la administración de un *cluster* de PCs, los estados ionizados de un átomo en un plasma caliente, o la ausencia de correlación en un cálculo Hartree-Fock.

⁷To quote “*The Not So Short Introduction to LaTeX2e, v3.20*” (2001):

L^AT_EX also has some disadvantages [...]:

- 1) It is very hard to write unstructured and disorganized documents
- 2) Your hamster might, despite some encouraging first steps, never be able to fully grasp the concept of Logical Markup

“Siguiendo el camino más duro, que aún así no es tan duro como el camino más fácil. Aprendí de los trolls y los enanos y las personas. Hasta de los guijarros.”

*Lores y damas, Terry Pratchett*⁸

*“Doctor, my eyes have seen the years
And the slow parade of fears without crying
Now I want to understand
I have done all that I could
To see the evil and the good without hiding
You must help me if you can
Doctor, my eyes
Tell me what is wrong”*

Doctor my eyes, Jackson Browne

⁸“Following the hardest road, which is not as hard as the easiest one. I learnt from the trolls and dwarves and people. Even from pebble.” *Lords and Ladies*, Terry Pratchett

Foreword

“The scientific theorist is not to be envied, for Nature, or more precisely experiment, is an inexorable and not very friendly judge of his work. It never says “yes” to a theory. In the most favorable cases it says “maybe”, and in the great majority of cases simply “no”... probably every theory will some day experience its “no” - Most theories, soon after conception.”

Albert Einstein, Nov 11, 1922

“When you leave out the impossible, the remaining, although improbable, must be the truth”

Sherlock Holmes

“Experience is what you get when you don’t get what you want”

Tori Filler

I can’t say I haven’t learnt many things during these years doing my Ph.D. One of them is that science, and probably research in general, is an excellent way of getting experience, in a *fillerian* way. Mostly experience on what does not work, but hopefully also in *why* it doesn’t work.

I would have given my reign for a... well, not a horse, but the understanding of what was going wrong with the many dead ends I have stumbled upon during the last years. And this is what I think research is really for: finding out why things don’t work.

Scientific knowledge is, indeed, of a negative nature. The renowned philosopher Sir Karl Popper, when pondering about what is and what is not science, pointed out that any hypothesis, aimed at being scientific, had to be able to become subject of denial. In other words, the proposal that all the swans are white is scientific, in the sense that if one would find a single black swan, then that “swan-whiteness law” would be found false. On the other hand, most of

XII

the contents of religious dogmas and pseudo-scientific theories is non-scientific by nature, since there is no conceivable way of ever finding any counter evidence. It is not only that no counter evidence has been found so far, but that it is not *possible* to imagine any.

The way science looks for the “truth”, then, is similar to the way an artisan produces a wooden figure by carving the “excess” wood out of the log.

From my point of view, a scientist is someone who can cope with ignorance. Her⁹ own ignorance, to be precise. Both ufologists and scientists seek the truth out there, scientists just don’t make it up when they can’t find it by rigorous ways¹⁰. Management of what is not known, and trying to understand why it is not, is half of the task in taking bold steps into the unknown. Or at least trying not to embarrass ourselves more than strictly necessary in the process.

If an ufologist comes across some mysterious lights in the dark sky, while getting back home after a long party night, she might start thinking what the lights *could* be. A scientist will think of what she *could not* say it is, and also what she could say it is *not*.

This negative nature of the scientific knowledge is, without doubt, its strongest point, for its robustness is built upon that principle. But it is also a source for considerable shock among the scientists-to-be as myself while I write these lines. It is also a force that drives the academic and layman communities apart, since a *medium* telling you that your late grandpa is fine in Heaven is far more comforting than a scientific physician saying that we still can’t really say whether there is an afterlife or not, much less communicate with the dead.

All this ravings have the sole purpose of asking forgiveness from the reader, would she finish the reading of this book with a sense of incompleteness. After all it’s supposed to be scientific. The actual answers belong in Nostradamus’ Prophecies, or some 806 phone number.

⁹I find it ridicule to keep using “his/her” every time a pronoun is used in neutral context. Since using the masculine form alone is accepted practice, I see no reason not to use the feminine alone for the same purpose. I just wish I had found a more feminist context to begin using it.

¹⁰At least, not as a general rule.

Contents

1	General Introduction	1
1.1	From natural rubber to polyolefins	2
1.2	Theoretical introduction	5
1.2.1	DFT methods	8
1.2.2	But there are other methods!	11
1.2.3	What about the building bricks?	14
2	Model Validation	17
2.1	Know thy enemy. Then strawman her	18
2.1.1	Dances with MAOs	18
2.1.2	Users of a lesser CPU	20
2.1.3	Beautiful models	21
2.1.4	If the shoe fits	23
3	Mechanism Elucidation	29
3.1	Introduction	30
3.2	Selected characteristics of metallocene catalyzed α -olefins	33
3.2.1	The reaction rate order of the monomer predicted by theory does not match experiment	33
3.2.2	The effect of Lewis bases (including MAO ⁻ counterion) is controversial	34
3.2.3	The growing chain flipping behavior is still unexplained	34
3.3	Methods	36
3.4	Results and discussion	38
3.4.1	Description of the β -agostic interaction	38
3.4.2	Bare cation	39
3.4.3	Relevant stationary structures along the PEC	41
3.4.4	Chain flipping	46
3.4.5	Inclusion of the counterion	47
3.4.6	Et+[CH ₃ ZrCp ₂] ⁺ /[CH ₃ B(CF ₂ Cl) ₃] ⁻ scan results	47

3.5	Conclusions	64
3.5.1	Bare cation	64
3.5.2	Inclusion of counterion	65
4	Extension to Ti and Hf	67
4.1	Introduction	68
4.2	Methods	69
4.3	Results and discussion	71
4.3.1	PEC scan	71
4.3.2	Stationary points	82
4.4	Conclusions	91
4.5	Acknowledgements	91
I	PECs	93
I.a	Titanocene PECs and FECs	93
I.b	Zirconocene PECs and FECs	95
I.c	Hafniocene PECs and FECs	97
II	Geometries	99
II.a	Titanocene geometries	99
II.b	Zirconocene geometries	104
II.c	Hafnocene geometries	108
	Bibliography	113

Chapter 1

General Introduction

Contents

1.1	From natural rubber to polyolefins	2
1.2	Theoretical introduction	5
1.2.1	DFT methods	8
1.2.2	But there are other methods!	11
1.2.3	What about the building bricks?	14

1.1 From natural rubber to polyolefins

“Begin at the beginning,” the King said, very gravely, “and go on till you come to the end: then stop”

Lewis Carroll

The UPV/EHU Chemistry Faculty at Ibaeta, Donostia, is a leading center in Polymer Science research and teaching. I studied there Macromolecular Chemistry, learning many fascinating facts about this versatile and complex group of molecules.

Polymers¹ are very large molecules that occur in nature (proteins, polysaccharides, DNA, natural rubber, silk, cotton, wool) or may be synthesized in the laboratory (plastics, synthetic fibers, synthetic rubber). Natural rubber samples were introduced in Europe by XVI century Spanish explorers, who brought them from South America.

But the real first step in polymer science was made by Hermann Staudinger (Worms, Germany, 1881-1965), who in 1920 suggested that some of the plastic materials that had been recently developed were actually huge molecules, and not aggregates of smaller ones. He coined the word “macromolecule” to describe them. His postulate generated a terrible controversy, but his merit was finally acknowledged with the 1953 Nobel Prize in Chemistry.

Let us skip the tremendous, and meritable, avalanche of new polymeric material discovered and invented until and during the World Wars, mostly the second one, and fast-forward to the fifties. In 1953, the German chemist Karl Waldemar Ziegler (Helsa, Germany, 1898-1973) developed the polyethylene (PE), and one year later the Italian Giulio Natta (Imperia, Italy, 1903-1979) developed the polypropylene (PP). The discovery of these two polymers (PE and PP), turned out to be a mayor breakthrough. Not only they are the paradigm of an important family of polymers (the polyolefins) but even today they are the most used plastics altogether, growing from a market share of 20% in the 1960s, to around 60% in the beginning of this century. Not surprisingly, they shared the Nobel Prize in Chemistry in 1963.

Ziegler and Natta not only discovered these new molecules, but they also developed a catalytic system to produce them[6, 7, 8, 9, 10]. The titanium trichloride and triethylaluminium mixture Ziegler used for the first time in the early 1950s is still called **Ziegler-Natta catalyst**. In 1980, Walter Kaminsky (Hamburg, Germany, 1941) and coworkers discovered a catalytic system based on metallocenes of Group 4 transition metals and methylaluminumoxane (MAO).

¹A big deal of information in this Thesis, and particularly in this Section, has been gathered from different sites on the Internet, particularly the Wikipedia (<http://en.wikipedia.org/>), but also too many others to be credited.

The first metallocene (ferrocene, see Figure 1.1) had been discovered back in the very early 50s by T.J. Kealy and P.J. Pauson[11] and S.A. Miller *et al.*[12], and Natta and Breslow were the first ones to use them as catalyst in the late 50s[13, 14, 15, 16]. However, it was Kaminsky who first obtained high activities for such systems. It is worth noting, however, that metallocenes have a variety of uses, besides olefin polymerization catalysis. In the **ESPA2006** congress I learned from Prof. Judit E. Šponer (Czech Republic), that some titanocene derivatives are being developed as possible substitutes for cisplatin as anticancer drugs[17, 18].

These metallocenic catalysts are similar to the Ziegler-Natta ones, but they offer two very valuable properties: they are soluble in the polymerization medium (they are homogeneous catalysts) and they are single-site catalysts (all the simultaneous growing polymer chains in the medium are in the same reactive environment, thus giving polymers with more homogeneous properties).

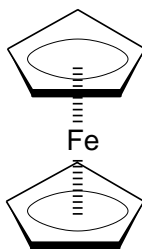


Figure 1.1: Structure of a ferrocene

But this catalyst dependency lead me to one of the surprising facts I mention above, and it is that many polymers are extremely stable compounds, and even though the reactants themselves are not unstable at all, the polymerization reactions are usually very exothermic. Why is, then, a catalyst required to obtain the polymer from the monomer? It is, of course, a naïve question from a chemical point of view, and the answer is quite obvious: the two stable states (reactants and products) are connected through a reaction path which involves intermediate geometries that have a much higher energy than either of them. The highest of such points is called transition state (TS), and this is where catalysts act. A catalyst is merely a molecule that interacts with the reactant through the reaction path, creating a different TS with a lower barrier (See Figure 1.2).

It is of vital importance to rationalize the mechanism by which a catalyst lowers the barrier for the reaction, since this knowledge will help us discover

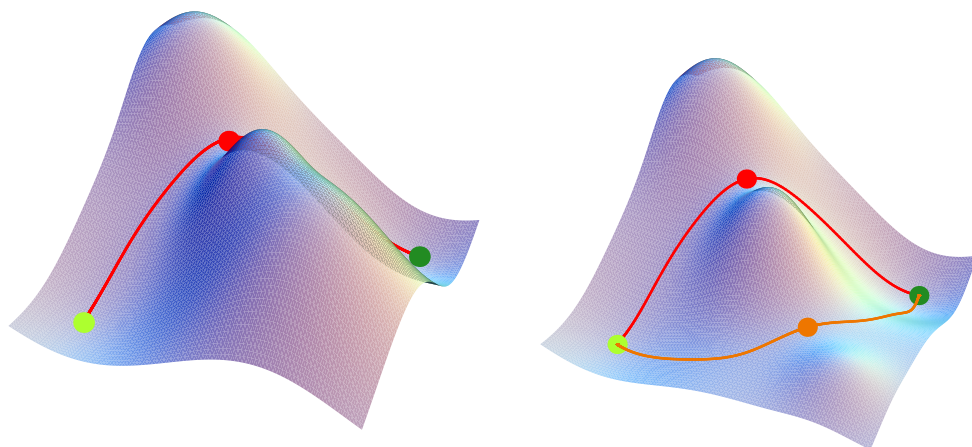


Figure 1.2: Fictional 2-dimensional Potential Energy Surface (PES) (left), where the molecule travels from the reactant state (light green point) to the product state (dark green point), along the path (red line) that crosses a TS (red point). On the right side, the PES has been modified by inclusion of a catalyst, opening a new reactive channel (orange path), that goes through a lower TS (orange point).

better catalysts, and new ways of manipulating the outcome and the rate of the reaction.

In the 1960s[19, 20, 21, 22, 23] Piet Cossée and E.J. Arlman proposed a molecular mechanism by which they inferred the Ziegler-Natta catalysts worked. Later on, after the metallocenic catalysts were discovered by Kaminsky, the **Cossée–Arlman mechanism** (CAM) was translated to them with little, if any, fundamental change, by Walter Kaminsky himself and Paolo Corradini (Rome, 1930)[24, 25]. Figure 1.3 features the reaction as proposed in the CAM, applied to a metallocenic catalyst. Figure 1.3 assumes a total dissociation between the active catalyst cation and its anionic counterpart (which is omitted in the picture). The first step would be the approach and **complexation** of a monomer unit (ethylene in this picture), followed, through the corresponding TS, by an **insertion** into the Zr–R bond. The resulting product happens to be a new R, two carbon atoms longer, and placed at the “other” coordination site of the zirconium (the one that was empty in the reactant).

The CAM, so happily and widely accepted for these metallocenic catalysts, has been virtually unchanged since its proposal, but many questions still remain unanswered, as covered in Chapter 3. As a Theoretical Chemist, the most natural procedure would be, of course, to use Theoretical Chemistry

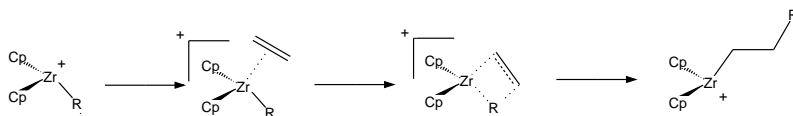


Figure 1.3: Cossée–Arlman mechanism. From left to right: bare cationic reactant, monomer π -complex, insertion TS and product.

(TC) to bring light upon the subject.

The next Section of the Introduction, thus, elaborates on what we mean by TC and QC (Quantum Chemistry).

1.2 Theoretical introduction

“There is no subject, however complex, which, if studied with patience and intelligence will not become more complex”

Gordon Rohman

Almost all of the material in this Thesis has been generated by means of Quantum Chemistry (QC). QC is the hard core of Theoretical Chemistry (TC), a set of methods aimed at discerning chemical (and physical) properties of gas phase atoms and molecules (*in vacuo*) and condensed phases (solutions and bulk solids) by means of pen and paper (or a PC connected to an array of hundreds of parallelized state-of-the-art ultra-powerful computers), rather than performing an experiment with the actual atoms involved.

One can argue endlessly about the many scientific advantages of theoretical investigation, but most of us are working there because we are either too lazy to actually do the hand-work, or too clumsy to be allowed to do so.

However, one can’t help but point out that there *are* advantages leading to a knowledge that is sometimes more profound than, and usually just complementary to, experimental work. One pro is that all the evidence experimentalists gather is indirect. If we make use of TC, we can pick by hand the molecules involved in the reaction we are studying. We can add, at will, solvent molecules, and see their effect. We can do whatever we want, and see how the system reacts directly.

But experiments are still necessary, and the reason is very simple: accuracy. Whenever one carries out a reaction in a test tube, she knows that whatever comes out, is what “really” comes out. One might not know how or why it happened, but it certainly happened, and the experiment will be reproduce-

able, unless errors have been made in the measurements or reactant/product manipulation, or reaction conditions change.

When dealing with TC, the results will typically be quite reproduceable, but not necessarily correct (realist). The sources of inaccuracy are fundamentally two: realism of the model and limitations of the theory. It is evident that, even though dramatic performance developments have been made in computational resources in the last decades, whatever “real” chemical system we would like to study has to be reduced to a relatively small model that we can stuff into the CPU and not burn it out or wait endlessly until our friend digests it and spits the answer out.

And not only the *size* of the model determines its realism, but also how we describe the interactions of the parts we include in the model, or how significant the omitted parts are.

The other side of the accuracy/realism coin are the limitations of the theory used. The complexity and size of the molecular model evidently determines the degree of simplifications done to the theory describing it. At the very top of what has sometimes been called this *Jacob’s ladder*, is Quantum Chemistry, that is, Quantum Theory applied to chemistry.

Quantum Theory is a relatively modern branch of science, and undoubtedly one that has been much heard of, even among laymen. It is well beyond the scope of this Thesis to even summarize its fundamentals. Suffice it to say that, applied to an arrangement of atoms (protons in nuclei, plus some neutrons adding their masses, and some electrons dancing around), QT boils down to saying that such arrangement can be described with a mathematical function called *wavefunction*. The wavefunction of a system is often denoted by the Greek letter Ψ , and it is obtained from the Schrödinger equation (Eq. 1.1) corresponding to that system.

$$\hat{H}\Psi = E\Psi \quad (1.1)$$

In equation 1.1, the symbol \hat{H} denotes the Hamiltonian operator, which, when applied to the wavefunction, outputs the energy of the system, times the wavefunction itself. For an N_e electron and N_N nuclei system, the Hamiltonian would have the form in Eq. 1.2, aside from relativistic effects and spin-orbit coupling.

$$\begin{aligned} \hat{H} &= \hat{T}_e + \hat{T}_N + \hat{V}_{e-e} + \hat{V}_{e-N} + \hat{V}_{N-N} \\ &= -\sum_i^{N_e} \frac{\nabla_i^2}{2} - \sum_A^{N_N} \frac{1}{2M_A} \frac{\nabla_A^2}{2} \end{aligned}$$

$$-\sum_A \sum_i^{N_e} \frac{Z_A}{r_{iA}} + \sum_{i>j}^{N_e} \frac{1}{r_{ij}} + \sum_{A>B}^{N_N} \frac{Z_A Z_B}{R_{AB}} \quad (1.2)$$

Equation 1.2 can be simplified supposing that, since nuclei are so heavy with respect to electrons, their movement will be much slower, and hence the \hat{T}_N , nuclear kinetic term, can be neglected, and the \hat{V}_{N-N} nucleus-nucleus potential energy term can be regarded as constant (because it depends on internuclear distances only, which are fixed in the approximation). This is referred to as the **Born-Oppenheimer approximation**, and gives the approximate Hamiltonian in Eq. 1.3.

$$\begin{aligned} \hat{H}_e &= \hat{T}_e + \hat{V}_{e-e} + \hat{V}_{e-N} \\ &= -\sum_i^{N_e} \frac{\nabla_i^2}{2} - \sum_A \sum_i^{N_e} \frac{Z_A}{r_{iA}} + \sum_{i>j}^{N_e} \frac{1}{r_{ij}} \end{aligned} \quad (1.3)$$

By means of \hat{H}_e we would find Ψ_e and E_e from Schrödinger's equation (Eq. 1.1). E_e would then be the *electronic* energy. The wavefunction Ψ_e thus depends explicitly on the electronic coordinates, and parametrically on the positions of the nuclei.

If we want to solve the other half of the problem, we need to solve the *nuclear* Schrödinger equation, and to do so we need the nuclear Hamiltonian. This Hamiltonian must include the nuclear kinetic energy (\hat{T}_N), plus the nucleus-nucleus interaction potential (\hat{V}_{N-N}), but also the potential energy the nuclei see, caused by being immersed in an electronic cloud. This potential is the electronic energy obtained above, which depends parametrically on the position of the nuclei. The nuclear Hamiltonian is then written down in Eq. 1.4.

$$\hat{H}_N = \hat{T}_N + \hat{V}_{N-N} + E(\{R_A\}) \quad (1.4)$$

The solution wavefunction Ψ_N to the nuclear Schrödinger equation describes the movement of the nuclei, and hence the translation, rotation and vibration of the molecule.

It is worth mentioning that for any R_A arrangement of nuclei (that is, each molecular geometry), one obtains an electronic energy $E_e(\{R_A\})$, and also a nucleus-nucleus interaction given by V_{N-N} . This builds up an effective $3N_N$ -dimensional energy potential (for N_N nuclei), the topology of which will provide us with the energies of different conformations, and the paths through which two energetically local minima structures are connected. This effective potential is often called **Potential Energy Surface** (PES). The PES of a

set of atoms is a vital feature that provides the much needed information to discern the mechanisms of chemical transformations, and their energetics.

Many (mathematical) methods have been devised to provide a way of finding the electronic wavefunction for any given atomic arrangement: Hartree-Fock (HF), n^{th} order Møller-Plesset (MP n), Coupled-Cluster methods (CC), Configuration Interaction methods (CI), Complete Active Space Self Consistent Field (CASSCF), Multi-Referential Configuration Interaction (MRCI)... This methods are called *ab initio* methods, because they calculate the wavefunction from first principles, according to the raw QT.

A more modern approach, and highly promising, is the **Density Functional Theory** (DFT). Although not strictly *ab initio*, it is nonetheless very closely related to the HF method above (simplest of *ab initio* methods), but modified in such a way that its accuracy is substantially improved. Since most, if not all, of the work the reader will find in this book has been carried out making use of one of the many DFT methods, I feel it deserves a section by its own.

1.2.1 DFT methods

I will not cut corners

” ” ” ”
” ” ” ”

Bart Simpson

The *Density Functional Theory* is a formalism that tries to be an alternative to the wavefunction one. As mentioned above, the Quantum Theory proposes that all the properties of an N -electron system can be calculated from a mathematical entity called *wavefunction*, which is obtained solving the famous Schrödinger equation for that given system.

The wavefunction formalism, thus, tries to find (approximate) solutions to that equation. The problem here is that the sought wavefunction Ψ_e is $3N_e$ -dimensional, being N_e the number of electrons in the system, and the mathematical complexity increases exponentially with the number of dimensions.

Wouldn't it be much nicer to have an, at most, 3-dimensional wavefunction? Pierre C. Hohenberg (born 1934) and Walter Kohn (Vienna 1923, Chemistry Nobel Laureate in 1998) asked themselves the same question, and concluded that such “wavefunction” could well be the total electronic density, $\rho(\mathbf{r})$. In 1964 they published the later famous **Hohenberg-Kohn theorem**, stating that there is a one-to-one mapping between the ground state of a

system (the electronic wavefunction Ψ_0 which gives the lowest E_0 electronic energy among all the possible Ψ_i that are a solution to $\hat{H}_e \Psi_i = E_i \Psi_i$), and its total electronic density $\rho(\mathbf{r})$.

Such a mapping might in principle allow us to calculate the ground state energy provided that we have the ground-state electronic density, and also the mathematical functional $E[\rho(\mathbf{r})]$ that gives the electronic energy from the density function. Pity we don't have either.

In a second theorem, Hohenberg and Kohn postulate that if $E[\rho(\mathbf{r})]$ is known, then a variational principle will hold for any trial function $\tilde{\rho}(\mathbf{r})$, as long as $\int \tilde{\rho}(\mathbf{r}) d\mathbf{r} = N$. The variational principle states that $E_0 \leq E[\tilde{\rho}(\mathbf{r})]$, so that if we find the $\tilde{\rho}(\mathbf{r})$ trial density that minimizes the energy functional, then $\tilde{\rho}(\mathbf{r}) = \rho_0(\mathbf{r})$. So now we have a recipe for obtaining the density, and we only need the functional, which is still unknown.

Later Kohn, together with Lu Jeu Sham (Hong Kong, 1938), devised an indirect method to make an approach to this functional. The **Kohn-Sham method** takes advantage of the fact that the exact ground-state electronic energy E_0 of an N-electron system is given by Eq. 1.5

$$E_0 = -\frac{1}{2} \sum_{i=1}^N \langle \psi_i(1) | \nabla_1^2 | \psi_i(1) \rangle + \int v(r) \rho(1) d\mathbf{r}_1 + \frac{1}{2} \int \int \frac{\rho(1)\rho(2)}{r_{12}} d\mathbf{r}_1 d\mathbf{r}_2 + E_{xc}[\rho(\mathbf{r})] \quad (1.5)$$

In Eq. 1.5, $v(r) = \sum_{\alpha} \frac{Z_{\alpha}}{r_{1\alpha}}$ is the *external potential* exerted by the nuclei, ψ_i are the *Kohn-Sham orbitals*, and $E_{xc}[\rho]$ is the *exchange-correlation energy*. The ground-state density $\rho(\mathbf{r})$ can be constructed from the Kohn-Sham orbitals according to Eq. 1.6.

$$\rho(\mathbf{r}) = \sum_{i=1}^N |\psi_i|^2 \quad (1.6)$$

The Kohn-Sham orbitals, in turn, are obtained from the set of one-electron equations 1.7.

$$\hat{F}_{KS}(1)\psi_i(1) = \epsilon_i\psi_i(1) \quad (1.7)$$

The \hat{F}_{KS} in Eq. 1.7 is the Kohn-Sham operator, and in turn depends on a term called the *exchange-correlation potential*, V_{xc} . This V_{xc} is the functional derivative of the exchange-correlation energy with respect to the electronic density, namely $V_{xc} = \frac{\delta E_{xc}[\rho(\mathbf{r})]}{\delta \rho(\mathbf{r})}$.

The procedure for finding out $\rho(\mathbf{r})$ is rather similar to the *self-consistent field* (SCF) employed in the Hartree-Fock method. Here one proposes a trial density $\tilde{\rho}_0(\mathbf{r})$, and uses it to construct a \hat{F}_{KS} , which has two terms that depend on the density. The first one is a term called *Coulomb operator*, and the second one is the aforementioned V_{xc} . The latter is obtained from functional derivation of E_{xc} , which in turn is defined to depend on $\rho(\mathbf{r})$ as given by Eq. 1.8. We can then obtain a set of Kohn-Sham orbitals from Eq. 1.7, and consequently a new density from Eq. 1.6. This new density can be fed into a new \hat{F}_{KS} , and rinse and repeat until self-consistency is found, i.e., the input density is equal to the output one.

$$E_{xc}[\rho] = \int \rho(\mathbf{r})\epsilon_{xc}[\rho(\mathbf{r})]d\mathbf{r} \quad (1.8)$$

In Eq. 1.8, the ϵ_{xc} function corresponds to the exchange-correlation energy per electron, and is an unknown functional of ρ . The last bastion of the unknown is, thus, the form of the ϵ_{xc} functional.

One approach can be made assuming that, if the electronic density fluctuates slowly from one point of the space to another one, the *local* exchange-correlation energy per electron (its value at a given point) is given by the same equation that would rule a constant density (homogeneous) electron gas. This approximation is named **Local Density Approximation** (LDA), and an accurate ϵ_{xc} is given by an expression by Vosko, Wilk and Nussair[26]. When the LDA is applied taking into account different functions for the α and β spin electrons, then it is called *Local Spin Density Approximation* (LSDA).

Since the true molecular electronic densities are far from smoothly-varying, as the LDA assumes, many more sophisticated formulations of ϵ_{xc} have been proposed and tested. One route to increasing the accuracy of the functional is to add to it terms including not only the value of the density in a given point of space, but also the value of its gradient. Since including a gradient gives a touch of non-locality, these modifications are named *non-local gradient corrections*.

A parallel route would be to add a part of the HF exchange (E_x^{HF}), the formula of which is exactly known. This gives rise to *hybrid* methods. These hybrid methods give astonishingly good results, provided that they have been fine-tuned by hand previously. This, however, is a serious drawback, since it breaks the *ab initio* compliance, and makes these methods *semiempirical*, strictly speaking.

Nevertheless, the most used DFT functional by far, and main responsible of the success of DFT, is the one using Axel D. Becke's (Esslingen, Germany, 1953) corrections[27] for the exchange, and Chengteh Lee, Weitao Yang (Chaozhou, China, 1961) and Robert Ghormley Parr's (Chicago, USA, 1921)

correlation formula[28]. The expression for this functional is shown in Eq. 1.9, and, since it depends on three parameters, it is known as Becke’s 3-parameter functional, with Lee, Yang and Parr’s corrections for correlation (B3LYP).

$$E_{xc} = (1 - a_0)E_x^{LSDA} + a_0E_x^{HF} + a_xE_x^{B88} + a_cE_c^{LYP} + (1 - a_0)E_c^{VWN} \quad (1.9)$$

The DFT methods are close to HF when it comes to computational cost, but since they include some sort of corrections for taking into account the exchange and correlation, the accuracy of their results is comparable to MP2, and sometimes better. As the reader will find out later on, most of the results in this Thesis have been obtained by DFT calculations, specifically B3LYP ones.

1.2.2 But there are other methods!

I have to say that I have been kind of unlucky with some aspects of my subject of choice. As I will say ahead in the corresponding Section, I tried to reduce my system to a bare cation, which about halved the size of the system (and consequently much more than halved the computational expense). Unfortunately the anion also happened to be necessarily taken into account.

When it comes to theoretical methods, less expensive ones than DFT do exist. I have mentioned above HF, for example. Descending the accuracy ladder, we can find **Semiempirical** methods, much faster than any *ab initio* or DFT calculation, but less rigorous in their treatment of the underlying physics. At the bottom of the physical slack pit we have the **Molecular Mechanics** (MM), intended for giving insight into molecular systems with thousands of atoms.

The **Semiempirical** methods are a simplification of the HF method, to beef up its performance. Most or all of them make use of the Neglect of Differential Diatomic Overlap (NDDO), a sub-class of the Zero Differential Overlap (ZDO) method, in which all two-electron integrals involving two-center charge distributions are neglected. The “Semiempirical” name comes from the fact that all of these methods make use of parameters fitted from experimental results, or higher level calculations.

Molecular Mechanics is a method suited for systems with thousands of atoms, in which the precise electronic interactions are cumbersome to compute². Its fundamentals[29] consist on describing just the *interatomic* interactions, through some properly fitted functions, instead of the electronic struc-

²In this context, cumbersome means “you have to screw down the top of your head to prevent it from flying away if such a thought even sets foot in the portal of your brain”.

ture. The energy is defined by an *ad hoc* analytic potential surface, where different terms appear for atom–atom distances, 3-atom angles, 4-atom dihedral angles, first-to-third atom distances, improper angles and so on. Evidently, the input consists in predefined constants for these expressions, and the variables are just the atomic positions.

With MM, one can perform Molecular Dynamics calculations to calculate averages of dynamic properties of molecules, but also predict molecular geometries, minimizing the expression of the potential energy with respect to the variables (atomic positions). The main limitation of MM is its inability to describe chemical bond formation and destruction. This is quite understandable, because the electrons of the system, which are responsible for the chemical reactivity, are not explicitly treated.

Although appealing because of their low computational cost, MM methods have an important drawback: the accuracy is very poor for systems not similar to the ones used to parametrize the aforementioned atomic interactions. Metallocenes fall in this category. In these catalysts the central metal has 12 atoms in its coordination sphere, and, as an example, MM methods are parametrized to give Zr up to four covalent bonds, being unable to represent the η -Zr–Cp bonds properly.

Figure 1.4 shows the final geometries for a DFT optimization (B3LYP with the LanL2DZ basis set) and a MM one (UFF force field). It is apparent that the UFF geometry is qualitatively incorrect.

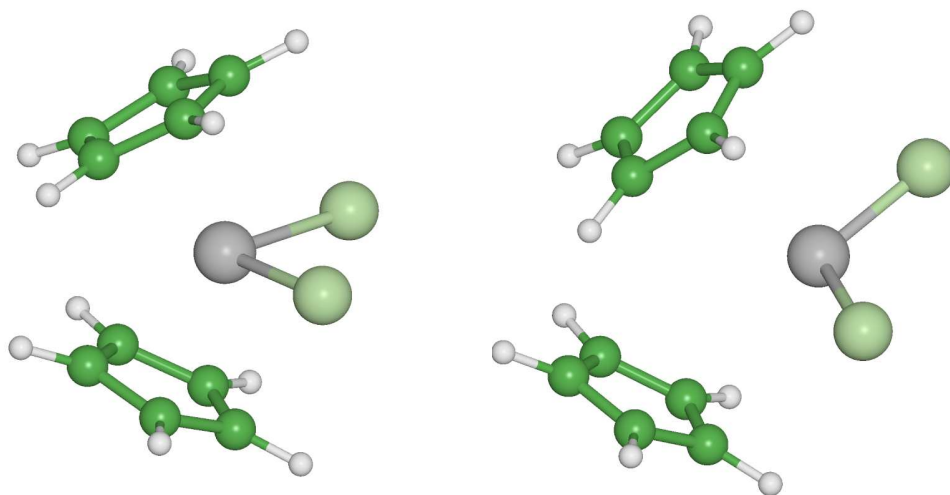


Figure 1.4: Cp_2ZrCl_2 molecule optimized at the B3LYP/LanL2DZ *ab initio* quantum level (left) and with the UFF molecular mechanics force field (right).

The failure to describe the η -Zr-Cp bonds can be seen quite clearly if we plot the Zr-C distance for all the carbon atoms in both cyclopentadienyls, as depicted in Figure 1.5: the Zr-C distances are quite small and constant in the DFT geometry, while in the MM case, not only they are much longer on average, but they also vary over a tremendously wide range (3.15–3.97 Å).

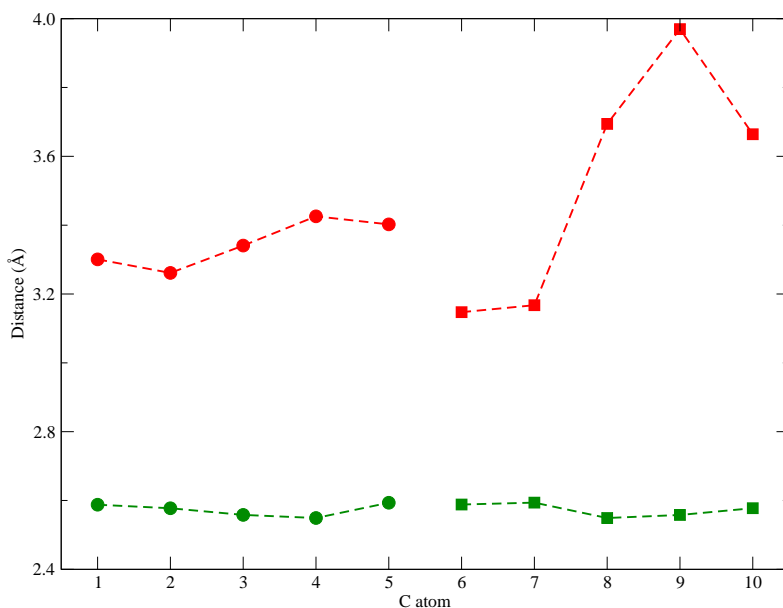


Figure 1.5: Zr-C distances in the Cp_2ZrCl_2 molecule, for the atoms in the “upper” (circles) and “bottom” (squares) Cp rings, for geometries optimized at the B3LYP/LanL2DZ level of theory (green points) and with the UFF MM force field (red points)

On the other hand, although Semiempirical methods as PM3 can allegedly treat Zr and its coordination in a zirconocene, at least in the **Spartan** program, I have found that at least the **Gaussian** implementation is highly unreliable for this system. For a start, the VSTO-3G basis set that PM3 uses assigns 4 basis functions (12 primitives) to the 4 “valence” electrons of Zr, and a calculation on the Zr(0) atom requires at least (according to the **Gaussian 98** output), 9 basis functions to create a simple Hückel guess wavefunction. This could be overcome generating a guess with another method, and then reading it, instead of asking Gaussian to generate it with the Hückel method, but one has to wonder how reliable a method unable to perform a simple *single point* of an atom in gas phase is.

There is, however, an interesting composite method I tried to make use of: **ONIOM**[30, 31]. Within this method, the user divides the subject molecular system into different zones or *shells* (much like an... onion), and applies a different theory level to each one of them. Figure 1.6 shows an ONIOM system, in which the “interesting” reactive part (Part I) is calculated at a high quantum level (e.g. DFT with high quality basis set), the cyclopentadienyl ligands (Part II) at an intermediate level (e.g. DFT with an small basis set), and a big part of the counterion (Part III) with the cheapest method available (e.g. MM). The problem with this setup is that the highest level will be applied only to Part I, but the intermediate one will be applied to both Parts I and II, and the lowest theory level to the whole molecule. From this, it follows that the intermediate and lowest levels of theory must be able to describe the η -Zr-Cp bonds, which leaves the search for a low-cost method capable of handling the whole system correctly unanswered.

1.2.3 What about the building bricks?

OK, all this chatter about “methods” and “theories” to solve the Schrödinger equations sounds reasonable and fine, but how exactly does one represent the wavefunctions and densities mathematically? It turns out that only the simplest of atoms, the hydrogen-like ones (H, He⁺, Li²⁺, etc.), can have their Schrödinger equation analytically solved, because they have a single electron under the influence of a central external potential (the nuclear charge). The resulting hydrogen-like wavefunctions all consist on a spherical harmonic angular part and a radial part of the **Slater** type. Slater type functions are of the kind $f_{Slater} = Ar^l e^{-\alpha(\mathbf{r}-\mathbf{R})}$, where \mathbf{r} is the position of the electron, \mathbf{R} the position of the nucleus, α a constant that depends on the nuclear charge, l an integer number accounting for the angular momentum, and A a *normalization* constant, which makes $\int f^2 d\mathbf{r} = 1$. Each such Slater type function that describes the state of an electron, is said to describe an **orbital**. Electrons were

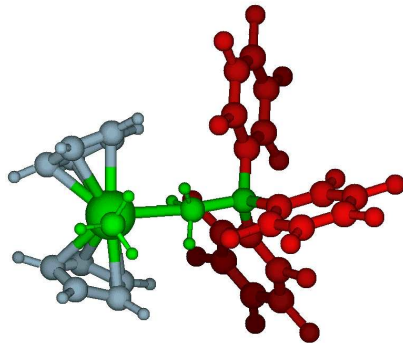


Figure 1.6: Example of ONIOM system. Green atoms would belong to Part I (described with the highest level of accuracy), light blue ones to Part II (intermediate accuracy), and red ones to Part III (most modest accuracy).

thought to describe *orbits* around the nucleus, much like planets around stars. Now we know they more closely resemble (huge) atmospheres around (tiny) planets, and the term “*orbit*” was dumped for “*orbital*”.

Making the optimistic guess that in multi-electronic systems, each electron will dwell an orbital that will resemble one of those hydrogen-like wavefunctions, we could use discrete sets of different hydrogen-like wavefunctions as **basis sets**, that is, elements whose proper combination gives rise to a good approximation of the actual total wavefunction. Such basis sets are called STOs (Slater-Type Orbitals).

In practice, the mathematical operations required to find the coefficients of this “proper” combination are much more efficiently carried out if instead of STOs one makes use of GTOs (Gaussian-Type Orbitals). These functions are similar to Slater-type functions, except their exponents are squared: $f_{Gauss} = Ar^l e^{-\alpha(\mathbf{r}-\mathbf{R})^2}$.

Since a single GTO is a much worse fit to a hydrogen-like wavefunction (and hence, also to a multi-electron wavefunction orbital), modern basis sets consist of functions that are formed, each of them, by Gaussian-type function combinations (typically 3-6 of them) that resemble single STOs (See Eq. 1.10).

$$f_{GTO} = \sum_i^N c_i f_{Gauss}(\alpha_i) \quad (1.10)$$

All-electron basis sets and Pseudopotentials

All-electron basis sets are defined as basis sets in which all the electrons of our system have their orbital described by one or more GTO of the set. As an example, the 3-21G all-electron basis set for carbon follows, as obtained from the EMSL Basis Set Library[32]:

$$\begin{aligned}
 f_1(S) &\rightarrow c_i = (0.0617669, 0.358794, 0.700713) \\
 &\quad \alpha_i = (172.256, 25.9109, 5.53335) \\
 f_2(S) &\rightarrow c_i = (-0.395897, 1.21584) \\
 &\quad \alpha_i = (3.66498, 0.770545) \\
 f_3(S) &\rightarrow c_1 = 1.0 \\
 &\quad \alpha_1 = 0.195857 \\
 f_1(P) &\rightarrow c_i = (0.23646, 0.860619) \\
 &\quad \alpha_i = (3.66498, 0.770545) \\
 f_2(P) &\rightarrow c_1 = 1.0 \\
 &\quad \alpha_1 = 0.195857
 \end{aligned}$$

Since each P function consists actually of three functions (P_x , P_y and P_z), the 3-21G basis set (as the name implies in a cryptic nomenclature), devotes 3 Gaussian-type functions for the orbitals in the core of the atom (just the 1s orbital in the case of carbon), that is $f_1(S)$, which is built by the linear combination of three Gaussians.

The valence orbitals are described by two functions each: $f_2(S)$ and $f_3(S)$ for the 2s, a $f_1(P)$ and a $f_2(P)$ for each of the 2p. The accuracy loss caused by the construction of the GTOs with less than three Gaussians is more than compensated by the fact that each orbital in the valence can be described by the arbitrary linear combination of two GTOs.

In the case of **pseudopotentials**, the *core* electrons are replaced by model potentials, and the valence electrons are treated by regular GTOs. Because of this, they are also called Effective Core Potentials (ECPs). This way, the chemically active valence electrons are considered to move in the potential caused by the chemically inactive core electrons. The fact that a whole lot of electrons is not considered into the wavefunction coefficient optimization makes that much less GTOs are required into the basis set, and thus the calculations are sped up a big deal.

These advantages of the basis sets that include ECPs made me use two of them across this Thesis. They will be described in the corresponding sections.

Chapter 2

Model Validation

“Everything should be made as simple as possible, but not simpler”

Albert Einstein

Contents

2.1	Know thy enemy. Then strawman her	18
2.1.1	Dances with MAOs	18
2.1.2	Users of a lesser CPU	20
2.1.3	Beautiful models	21
2.1.4	If the shoe fits	23

2.1 Know thy enemy. Then strawman her

In rhetoric and philosophic discussions it is, sadly, common practice to use the “straw man argument” (SMA, no text is scientific without acronyms) in more than a healthy dose. Politicians, in particular, (ab)use it in more than a *deadly* dose.

Simply put, the SMA consists in building up a (preferably laughable) fake representation of our adversary or her line of thought, and then direct our attacks to that straw man. These attacks will, of course, find a much easier target on the mock up construction we made ourselves, and our adversary will hopefully be blown away along with the bits of the shattered straw man¹.

The reader might be asking herself where in the world I am heading with this chatter, and probably not for the last time in this Thesis. Patience is the mother of science².

I realize the above is not a very kind introduction to a scientific technique, but unfortunately I haven’t read Shun Tzu’s *Art of War*, and could not come up with a witty parallelism from therein. For the first part of this work, I might say I have tried to strawman my problem away, although in a hopefully rigorous way.

2.1.1 Dances with MAOs

They say stating your problem clearly is half of its solution, and this is one of the biggest truths the reader will find in this book.

As I have said in the Introduction, my most basic motivation was to understand how a two-step reaction, of the kind I thought the propagation step of the olefin polymerization was, could follow the reaction rate order I thought it did.

For me, of course, it meant opening up **Molden**[33], creating some sort of ball-and-stick construction out of atoms in a *Z*-matrix, and then feeding it to **Gaussian**[34, 35]³, to minimize its geometry and calculate its energy. In other words: I was eager to give it a go with Quantum Chemical methods.

The first problem I encountered was the chemical species known as **methylaluminumoxane** (MAO). It gave me some bad headaches, or would have,

¹So, watch out for this trick, kids. It is usually paired with *ad hominem* attacks (AHA). Needless to say, whoever is using SMA or AHA in an argument is trying to fool you, don’t fall for it!

²A quotation sometimes attributed to W. Shakespeare, but which I think belongs to Spanish popular sayings, chiefly because in Spanish it rhymes, and in English it doesn’t.

³Note for my grandchildren: I have known this program as far back as **Gaussian 94**. Back then mice were not USB, the DVDs were read-only, and **Slackware** did not have a graphical installer. Wait, it still hasn’t!

had I not quickly decided to dump it for good.

It might be pertinent, at this point, to outline the activity and structure of MAO. In the beginning of the metallocenic olefin polymerization development, it was seen that the active center, quite logically, was the transition metal cation. When dealing with Group 4 transition metals (titanium, zirconium and hafnium), their active form is the IV oxidation state, that is, a tetracoordinated metal, with a pyramidal ligand arrangement. Two vertices would be occupied by the cyclopentadienyl (Cp) ligands, and the other two by chloride or methyl substituents in the “inactive” metallocene (the one “that comes in the jar”).

The way to activate the metallocene consisted, and still does, in adding some “co-catalyst” to the reaction medium, so that it would deprive the metal of one of its methyl groups, or rather from a *methide* group, leaving a +1 cation behind. An example of such a reaction is displayed in Figure 2.1, where a triethylaluminum abstracts a methide group from a zirconocenic pre-catalyst.

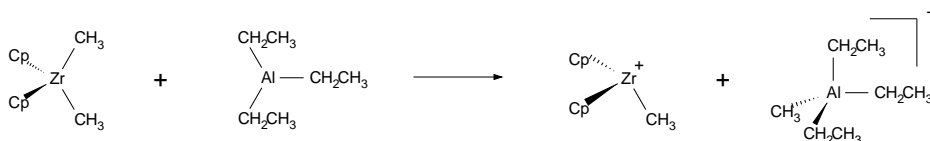


Figure 2.1: Example of Lewis acid attack unto metallocenic pre-catalyst.

In the mid-1970s Kaminsky discovered that the aforementioned MAO performed the co-catalyst task remarkably well. Adding MAO in the orders of hundreds or even thousands of aluminum atoms per zirconium atom (in zirconated metallocenes. Similarly for other transition metals), would increase immensely the reaction rate, with respect to more primitive activation techniques as the addition of triethylaluminum.

So, for the industry, everything was fine... but, how about the academic chemists? I have mentioned that MAO is added in so and so Al/Zr ratio, and this may make the reader suspicious: why not say “in such and such molar ratios” or “such and such times the stoichiometry”? Well, fact is the molecular structure of MAO is not known[36, 37, 38]. MAO is defined as some sort of reactant by the general formula $(-Al_{na}(CH_3)_{nm}O_{no-})_n$, where usually $na = 1$, $nm = 2$, $no = 1$ [39, 40, 41].

Also unknown is the exact mechanism by which the activation of the metallocenes is performed by MAO, beyond the aforementioned methide abstraction.

The academic study of the chemical systems created in the polymeriza-

tion media cried for a suitable species to lay its hands on, and so different molecularly well-defined Lewis acids were tried. Among the successful ones, the tri(perfluorophenyl)borate (TFPB) became one of the most popular ones[42, 43].

TFPB was seen to be able to abstract a methide from the metallocene dimethyl (see Figure 2.2), and thus activate it for olefin polymerization, in a very convenient and efficient way. Replacing MAO with TFPB as olefin polymerization co-catalyst finally provided experimentalists a straw man they could cope with.

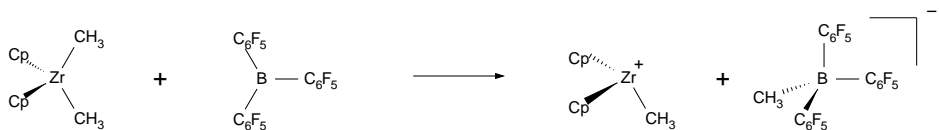


Figure 2.2: Methide abstraction by TFPB on a metallocenic pre-catalyst.

2.1.2 Users of a lesser CPU

Literature on the subject would, then, provide me with a properly defined chemical system I could fill my **Gaussian** inputs with. Unfortunately, as is well known among the Theoretical Chemists, the size of the system fed to a Quantum Calculation dramatically determines the time (and RAM, and hard disk space) needed by a given computer to carry it out.

In order to cut down the “weight” of my calculations, I decided to use as small a basis set as possible, and reduce the number of active electrons by making use of ECPs. I also decided to go for DFT calculations, which have exceptionally low memory and disk requirements, and have a very good accuracy/CPU load ratio. The bare fundamentals of DFT and ECP basis sets are described in the Introduction.

However, one always ends up stumbling upon the same obstacle: the number of atoms in the system to be calculated. Being a humble group in a humble University of a humble... well, the reader gets the picture. Our computational resources have always been limited, and so I boldly proceeded to mangle my molecules as much as possible.

My first move consisted in considering only the cationic part of the catalyst, plus a monomer unit. After all, if the TFPB simply abstracts a methide group, the TFPB-Me⁻ counterion should be safely dismissable. But, after getting a severe warning from one referee of a paper for such a sacrilege, I saw the light, and realized the counterion (CI) should be included.

Stubborn is as stubborn does, as Forrest Gump would say, so I did not settle for the inclusion of the full CI. A minimal metallocene by the formula $[\text{Cp}_2\text{MCH}_3]^+$ accounts for 25 atoms and 78 electrons, plus the ones on the metal (Ti: 22, Zr: 40, Hf: 72). The TFPB counterion, $[\text{CH}_3\text{B}(\text{C}_6\text{F}_5)_3]^-$, would add 38 atoms and 258 electrons! The use of ECPs instead of all-electron basis sets would cut these figures down by quite a bit, since not all of the electrons in the atoms are treated explicitly, but they would still be too many.

Now, if TFPB was the straw man of the experimentalists, I decided to build my own straw man of the straw man. And here is where the knowledge of my enemy would make me some good. If my straw man was to be of any use, it had to mimic as closely as possible the properties of the original CI.

2.1.3 Beautiful models

Some time ago, Prof. Xabier López ordered online a book by the same title as this section. I distinctly remember my disappointment when I perused the first few pages, only to discover that it dealt with some mathematical models to describe Quantum phenomena.

But models (besides those skinny hangers for the weird creations of sadistic fashion tailors), in the context of that book, are beautiful things, indeed.

In general a model is some sort of theory or idea, that, being much more simple and easy to handle than the original subject of study, still retains enough of its complexity as to enable one to use it to discover its features. Since a model is not the modeled thing itself, some characteristics will be different, some missing, and some will even be new, and pertain only to the model, not the modeled (artifacts). One has to make sure that the missing characteristics are not vital for the study one is making, and that the artifacts do not generate anomalous results. A sphere of constant density can be a good model for the Earth, in astronomical matters. However, when it comes to topography, the perfect sphere model crumbles down, as it does the constant density assumption when dealing with seismography.

I once attended a symposium⁴ where I heard Odile Eisenstein (Montpelier, France), complain about the tendency to overdo models. She regretted that sometimes models could miss critical features of the modeled, and hence be utterly useless.

In the same symposium, Christopher J. Cramer (Minnesota, USA) talked about the limitations of “lesser” Quantum Mechanical methods such as HF, MP2, and probably to Axel Becke’s dismay, who was in the audience, DFT methods such as B3LYP.

⁴ESPA2004 at Valladolid, Spain

So, to be a purist, one should perform high level coupled cluster calculations on the full system under study, be it a methane molecule in gas phase, or a fully solvated protein. To be a purist, then, one would have to either have access to exorbitant CPU power or refrain from working on the Quantum Chemistry field at all.

In order to follow as much as possible Prof. Eissestein's directives on model suitability⁵, I took my first step towards a smaller model for my system: feature definition.

The borate I was trying to model consisted, put bluntly, in a tricoordinated boron atom whose electron deficiency (Lewis acidity) would allow it to abstract a methide group from a transition metal cation such as zirconium in a zirconocene. The anion thus generated would stay loosely bound to the metallocenic cation left behind, through a methyl-bridge.

It was, thus, apparent to me that the main "backbone" of my methylborate model should consist on a CH_3B structure; that had to stay unchanged. However, the three perfluorophenyl groups could, and should, be substituted. I was under the impression that their main function would be to stabilize the charge excess of the anion, so I decided to build my model as a $[\text{CH}_3\text{BZ}_3]^-$ anion such that some of its properties would be as close as possible to the TFPB.

At this point I should recognize that the perfluorophenyl groups could play some steric role as well, but this role can not be taken into account with any model that, by definition, tries to reduce the size of the moiety included in the calculation. To include the full system I would be forced to use lower-level methods, and this has already been discussed in Section 1.2.2.

⁵although decided to pay little attention to the sensible, but definitely wing-cutting remarks by Prof. Cramer

2.1.4 If the shoe fits

“Social psychology shows that, whatever their own good or bad choices, most people believe that others would do whatever they personally chose to do, a phenomenon termed false consensus.”

Susan T. Fiske *et al.* in *Science*[44]

The first task for finding appropriate groups Z for my BZ_3 model Lewis acid, consisted in defining what kind of Z groups I would deal with. Recall that I am trying to mimic TFPB (see Figure 2.3), in which $Z = C_6F_5$. For my trial, apart from Z = methyl (which is a ubiquitous first choice, even if it has nothing to do with the original group to be substituted), I decided to test the following species: $Z = X$, CX_nY_{3-n} and $CXCX_mY_{2-m}$, where X, Y = F and Cl, and $n = 0-3$, $m = 0-2$. In other words, fluorine, chlorine and perfluoro/perchloro derivatives of the methyl and vinyl groups. Example compounds are depicted in Figure 2.4.

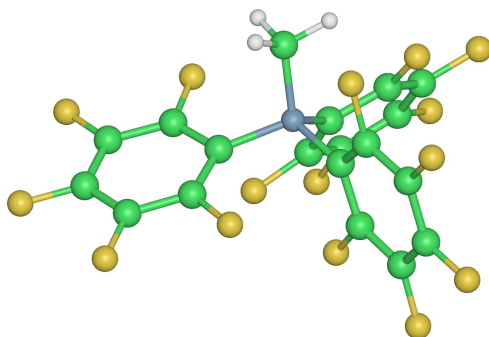


Figure 2.3: Molecule I try to modelize (TFPB).

The second step would be to choose the properties of the original compound, that we would like the model to mimic. The choice had to have some level of arbitrariness, so I opted for making it as broad as possible. With this aim, I chose to take into account atomic charges, because these are somehow connected to the shape of the electronic cloud around a molecule. A word or two should be spared on the subject of atomic charges. There are different ways of defining the amount of electronic density assignable to each of the atoms in a molecular system. The choice really depends on what we are looking for. Since my only concern at this point consisted in comparing numbers, I decided to take the simplest of methods, i.e. the Mulliken charges.

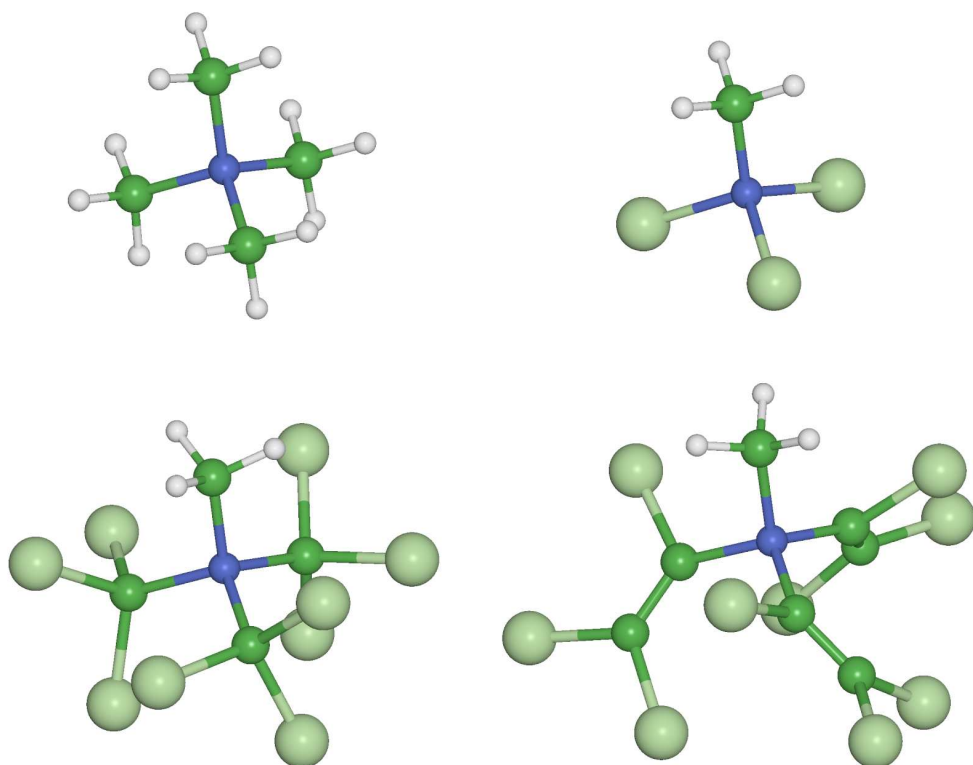


Figure 2.4: Example compounds for the proposed CI models, where X,Y = Cl. From left to right, top to bottom: Z = $-\text{CH}_3$, $-\text{Cl}$, $-\text{CCl}_3$ and $-\text{C}_2\text{Cl}_3$.

I also included some interatomic distances, to have some reflection of the geometry of the original molecule(s). Finally, I added a binding energy, as defined by the reaction in Eq. 2.1, because this tells us how strongly our model CI binds to the cationic metallocene, and this is an important measure indeed.



The atoms having their charges and interatomic distances measured are depicted in Figure 2.5. Notice that not only properties of $[\text{CH}_3\text{B}(\text{C}_6\text{F}_5)_3]^-$ have been mimicked, but also those of the $[\text{CH}_3\text{Cp}_2\text{Zr}]^+ / [\text{CH}_3\text{B}(\text{C}_6\text{F}_5)_3]^-$ complex.

The values of the aforementioned properties for each and every considered model have been summarized in Table 2.1, along with the number of electrons

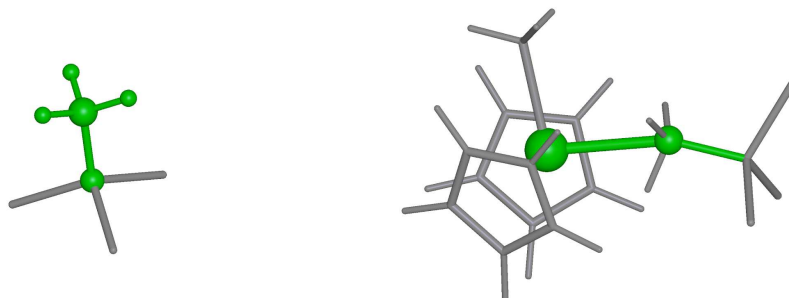


Figure 2.5: General forms of Cl^- (left) and $[\text{Cp}_2\text{ZrCH}_3]^+/\text{Cl}^-$ (right). Atoms in green have had their electronic charges taken into account for the CI choice. The interatomic distances taken into account are also green-colored.

of each fragment Z , to give an idea of their relative computational “weight”.

Z	n_e	$[\text{CH}_3\text{BZ}_3]^-$					$[\text{CH}_3\text{Cp}_2\text{Zr}]^+ / [\text{CH}_3\text{BZ}_3]^-$			
		q_B	q_C	$\langle q_H \rangle$	d_{B-C}	$\langle d_{C-H} \rangle$	q_{Zr}	d_{Zr-C}	d_{B-C}	BE
-C ₆ F ₅	81	0.147	-0.434	0.109	1.647	1.099	0.590	2.528	1.689	-81.208
-Cl	17	0.172	-0.312	0.094	1.599	1.104	0.670	2.535	1.639	-86.824
-F	9	0.716	-0.482	0.069	1.615	1.103	0.751	2.519	1.675	-97.456
-CH ₃	9	0.285	-0.446	0.041	1.661	1.108	1.273	2.292	4.451	-125.885
-CCl ₃	57	0.816	-0.358	0.118	1.628	1.098	0.536	2.563	1.660	-81.020
-CCl ₂ F	49	0.587	-0.413	0.125	1.635	1.098	0.621	2.550	1.667	-81.487
-CClF ₂	41	0.333	-0.440	0.121	1.644	1.100	0.602	2.533	1.650	-84.418
-CF ₃	33	0.142	-0.469	0.111	1.632	1.100	0.615	2.532	1.657	-85.220
-C ₂ Cl ₃	63	0.384	-0.473	0.128	1.656	1.098	0.541	2.530	1.702	-83.293
-C ₂ Cl ₂ F	55	0.360	-0.477	0.120	1.647	1.099	0.582	2.512	1.691	-85.319
-C ₂ ClFCl	55	0.319	-0.456	0.124	1.653	1.099	0.549	2.518	1.698	-85.489
-C ₂ FCl ₂	55	0.057	-0.450	0.117	1.659	1.099	0.619	2.518	1.702	-84.639
-C ₂ ClF ₂	47	0.340	-0.461	0.114	1.645	1.100	0.572	2.508	1.691	-87.630
-C ₂ FClF	47	0.042	-0.473	0.111	1.651	1.100	0.643	2.513	1.696	-86.058
-C ₂ F ₂ Cl	47	0.014	-0.446	0.112	1.657	1.100	0.623	2.511	1.702	-87.157
-C ₂ F ₃	39	0.037	-0.468	0.104	1.651	1.101	0.639	2.509	1.698	-88.865

Table 2.1: Selected properties of some $[\text{CH}_3\text{BZ}_3]^-$ models for the $[\text{CH}_3\text{B}(\text{C}_6\text{F}_5)_3]^-$ counterion, at the B3LYP/LanL2DZdp level. Charges are given in electron units, distances in Å and energies in kcal/mol. n_e stands for number of electrons in fragment Z. q_i stands for Mulliken atomic charge for atom i, where $i = \text{H}, \text{B}, \text{C}$ and Zr. d_{i-j} stands for interatomic distance between atoms i and j, where $i, j = \text{H}, \text{C}, \text{B}$ and Zr. BE stands for Binding Energy, as defined by $\text{BE} = E_{\text{complex}} - E_{\text{cation}} - E_{\text{anion}}$. $\langle q_H \rangle$ and $\langle d_{C-H} \rangle$ stand for the average values of both properties for the three quasi-equivalent hydrogen atoms in the methyl group of the CH_3B core.

Z	n_e	ϵ_q	ϵ_d	ϵ_{BE}
-CCl ₃	57	0.302	0.025	0.188
-CCl ₂ F	49	0.197	0.017	0.279
-C ₂ Cl ₃	63	0.110	0.008	2.084
-CClF ₂	41	0.083	0.020	3.210
-C ₂ FCl ₂	55	0.043	0.010	3.431
-CF ₃	33	0.019	0.018	4.012
-C ₂ Cl ₂ F	55	0.097	0.008	4.110
-C ₂ ClFCl	55	0.080	0.007	4.281
-C ₂ FClF	47	0.056	0.008	4.849
-Cl	17	0.067	0.035	5.615
-C ₂ F ₂ Cl	47	0.062	0.012	5.949
-C ₂ ClF ₂	47	0.087	0.010	6.422
-C ₂ F ₃	39	0.056	0.010	7.656
-F	9	0.266	0.018	16.247
-CH ₃	9	0.313	1.386	44.677

Table 2.2: Relative errors for the different models of counterion, according to data from Table 2.1 and formulae at Eqs. 2.2, 2.3 and 2.4. Entries have been ordered by increasing ϵ_{BE} for convenience.

In order to be able to make a clear comparison, some errors ϵ have been defined in Eqs. 2.2, 2.3 and 2.4, and tabulated in Table 2.2. Each Δx there refers to the difference, for property x , between the given model and the modeled species. As can be seen, charge, distance and energy errors have been grouped each in a bundle.

$$5\epsilon_q^2 = (\Delta q_B)^2 + (\Delta q_{C_{CI}})^2 + (\Delta q_{C_\alpha})^2 + (\Delta q_H)^2 + (\Delta q_{Zr})^2 \quad (2.2)$$

$$4\epsilon_d^2 = (\Delta d_{B-C,anion})^2 + (\Delta \langle d_{C-H} \rangle)^2 + (\Delta d_{Zr-C})^2 + (\Delta d_{B-C,complex})^2 \quad (2.3)$$

$$\epsilon_{BE} = |\Delta BE| \quad (2.4)$$

A glance at Table 2.2 quickly reveals that there is no *perfect* model, and the final choice must definitely depend on what properties we regard most important, and how much so.

The first step to trim the list was to look at the ϵ_{BE} ⁶. I discarded all but the five models with smallest ϵ_{BE} , all of them below 3.5 kcal/mol.

I then rejected $Z = -\text{CCl}_3$ and $-\text{CCl}_2\text{F}$, despite their very good binding energies ($\epsilon_{BE} = 0.188$ and 0.279 , respectively), on account of their slightly too high discrepancies in atomic charge: $\epsilon_q = 0.302$ and 0.197 , respectively.

Finally, from the remaining $Z = -\text{C}_2\text{Cl}_3$, $-\text{C}_2\text{FCl}_2$ and $-\text{CF}_2\text{Cl}$, I chose the latter. Although the ϵ values of the former two were quite good, they would not justify their increased size, and associated higher computational expense (61 and 55 electrons versus 41, respectively).

All in all, $Z = -\text{CF}_2\text{Cl}$ was regarded as sufficiently accurate, and conveniently small. It is depicted in Figure 2.6. Nevertheless, it would not be fair to not to stress the fact that there always is some degree of arbitrariness in such selections. In this case, $Z = -\text{CF}_3$ could have been selected, for example, on account of its tiny ϵ_q and ϵ_d , had it not been eliminated in the first cut because of its ϵ_{BE} . When all is said and done, though, its ϵ_{BE} is only about 0.8 kcal/mol higher than my final choice.

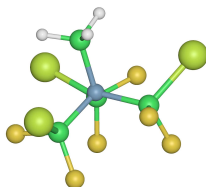


Figure 2.6: Final choice on CI model.

⁶Which might come as a huge surprise, given that I have ordered the errors in Table 2.2 by ϵ_{BE}

Chapter 3

Mechanism Elucidation

Contents

3.1	Introduction	30
3.2	Selected characteristics of metallocene catalyzed α-olefins	33
3.2.1	The reaction rate order of the monomer predicted by theory does not match experiment	33
3.2.2	The effect of Lewis bases (including MAO ⁻ counterion) is controversial	34
3.2.3	The growing chain flipping behavior is still unexplained	34
3.3	Methods	36
3.4	Results and discussion	38
3.4.1	Description of the β -agostic interaction	38
3.4.2	Bare cation	39
3.4.3	Relevant stationary structures along the PEC	41
3.4.4	Chain flipping	46
3.4.5	Inclusion of the counterion	47
3.4.6	Et+[CH ₃ ZrCp ₂] ⁺ /[CH ₃ B(CF ₂ Cl) ₃] ⁻ scan results	47
3.5	Conclusions	64
3.5.1	Bare cation	64
3.5.2	Inclusion of counterion	65

3.1 Introduction

“He was determined to discover the underlying logic behind the universe. Which was going to be hard, because there wasn’t one. The Creator had a lot of remarkably good ideas when He put the world together, but making it understandable hadn’t been one of them.”

Mort, Terry Pratchett

More than 45 years after the first olefin polymerizations by Ziegler-Natta type catalysts[6, 7], and 40 after Cossée and Arlman formulated their widely-accepted two-step mechanism (see Figure 3.1) for the propagation step of this kind of reactions[19, 20, 21, 22, 23], there still remain some unanswered questions.

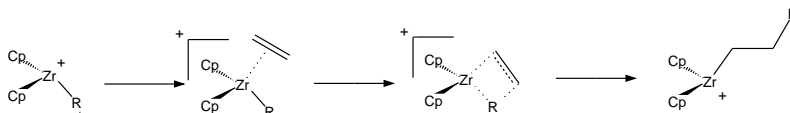


Figure 3.1: Cossée-Arlman mechanism

A very important one is whether the π -complex exists, i.e. whether the complexation of the vinyl monomer to the catalyst fragment is a true minimum in the reaction potential energy surface (PES). Related to this, the presence of an complexation barrier is also under debate.

Early work by Morokuma (who has been very active on the field[45, 46, 47, 48, 49, 50]) *et al.* on the ethylene + [Cl₂TiCH₃]⁺ system[45] predicted a π -complex optimized at Hartree-Fock (HF) level of theory. *Single point* energy calculations at second order Møller-Plesset (MP2) theory level on the HF geometry gave a binding energy of 56.6 kcal/mol.

They also studied the silylene-bridged [H₂SiCp₂ZrCH₃]⁺ + ethylene system[46], and predicted a π -complex with a restricted Hartree-Fock (RHF) binding energy of 19.1 kcal/mol and 33.5 kcal/mol at the restricted MP2 (RMP2) level of theory. An insertion transition state (TS) was also found, giving rise to an insertion barrier of 16.7 kcal/mol at RHF level and 6.0 kcal/mol at RMP2 level.

Similar results were obtained by Ziegler *et al.*[51], using DFT methods. They came up with a π -complex with a 23 kcal/mol binding energy for ethylene + [Cp₂TiCH₃]⁺ and around 26 kcal/mol for ethylene + [H₂SiCp₂ZrCH₃]⁺. However their insertion barriers were tiny, namely less than 1 kcal/mol for both of them.

Later work by Ahlrichs *et al.*[52] on both ethylene + $[\text{Cp}_2\text{TiCH}_3]^+$ and ethylene + $[\text{Cl}_2\text{TiCH}_3]^+$ stressed the importance of including electron correlation even in the geometry optimization step, lest *qualitatively* incorrect results be obtained. They claimed having avoided this problem by optimizing the geometries with the MP2 method, at which level they predicted a strictly downhill insertion of ethylene in the Ti–C bond (i.e., no π -complex nor insertion TS) for the ethylene + $[\text{Cp}_2\text{TiCH}_3]^+$ system. This result was rationalized by stressing how efficiently α -H agostic interactions reduce the steric hindrance to ethylene approach. For $[\text{Cl}_2\text{TiCH}_3]^+$ agostic interactions seemed to be weaker (or absent), and thus a π -complex and an insertion TS were indeed found.

In a pioneering paper, Buda *et al.*[53] treated the insertion of ethylene into $[\text{H}_2\text{SiCp}_2\text{ZrCH}_3]^+$ (same system as in one of the articles by Morokuma *et al.*[45]), by Car-Parrinello *ab-initio* molecular dynamics (AIMD). This approach has the interesting advantage that it is not the electronic energy space that is analyzed, but the free energy one, that is, the actual hypersurface in which chemical reactions take place. The remarkably short reaction time span they obtained (~ 150 fs) led them to conclude that a very low or no energy barrier at all was present in the monomer insertion. A second study on the same system[54], but at different temperatures, further supported this idea, since the reaction time span turned out to be quite independent of the temperature.

Nevertheless, another paper by Morokuma *et al.*[47] questioned the aforementioned ones. Although RMP2//RHF (RMP2 single point energy at RHF-optimized geometries) made Ahlrichs *et al.*[52] consider a downhill PES, similar calculations with the much more sophisticated restricted singlets and doublets configuration interaction with correction for quartets (RQCISD) level of theory for calculating the energy of geometries optimized at the RHF level (that is, RQCISD//RHF energies), applied to $[\text{H}_2\text{SiCp}_2\text{MCH}_3]^+$ (M=Ti, Zr, Hf) led Morokuma *et al.* to conclude that there actually exists a π -complex (with a RQCISD//RHF binding energy of 29.1 kcal/mol for M=Zr), and also a subsequent insertion TS, although with a low activation energy (9.4 kcal/mol in the case of M=Zr, at RCISD//RHF level). They regarded the MP2 results by Ahlrichs *et al.* as “an artifact”, and blamed the absence of barrier in the AIMD simulations by Buda *et al.* on an overestimation of the correlation energy by the LDA method, thus (they hypothesized) the TS disappeared because it was unrealistically stabilized at that theory level. While this artificial stabilization effect may well be present, I would like to emphasize that the AIMD calculations explore the reaction free energy, not the electronic energy. Thus there would be no contradiction in the prediction of the existence of an electronic energy insertion barrier and none in the free energy surface.

Some questions related to the Cossée-Arlman mechanism have been addressed by Martin Ystenes. He proposed an alternative mechanism referred to as *Trigger* mechanism (TM)[55, 56], and references therein, although in more recent papers Ystenes seems to get back to giving credit to the model by Cossée and Arlman[57].

The main change the *Trigger* model introduces in the CAM is to propose the catalytic action of a second monomer unit for the insertion of a given monomer in the growing chain attached to the metallic center (see Figure 3.2). The idea is not new, as Ystenes himself makes clear (see refs [21-24] in ref [55]), but it is in his papers where the idea has been properly placed into perspective for the first time.

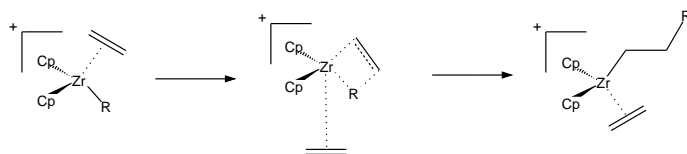


Figure 3.2: *Trigger* mechanism

I would like to emphasize that both the model by Cossée and Arlman and that by Ystenes were developed for Ziegler-Natta catalysts. Both Kaminsky[24, 36] and Corradini[25, 36] have translated the CAM to metallocenic catalysts, with little, if any, fundamental change. While some details may vary, the problems I will discuss here are essentially equivalent for both the heterogeneous and the homogeneous branch of these metallic catalyst family. Moreover, many more recently discovered post-metallocenic catalysts[48, 58, 59] possibly follow similar reaction steps.

The calculations presented in the first section have been carried out for the “bare” metallocene cation, without any explicit effect of the counterion (e.g. methylaluminoxane anion, MAO⁻), beyond the implicit activation of the metallocene itself. The hypothesis that the primary effect of the MAO is to activate a metallocene precursor (usually a dichloride), giving rise to a cationic molecule, which is the active species, is assumed in many papers, and was experimentally confirmed by Yang *et al.*[60] for zirconocenes and Eish *et al.*[61] for titanocenes.

Nevertheless the effect of the counterion is still under debate, thus while some authors[62, 63] suggest that the effect of the complexation of the cocatalyst anion to the metal is not negligible, and should be included explicitly in the calculations (for example in the form of boron compounds), others[64] justify the neglect of counterions in simulations. Consequently, I have de-

voted a second part of this chapter to include a model for $[\text{CH}_3\text{B}(\text{C}_6\text{F}_5)_3]^-$, a moiety that has been widely used as molecularly well-defined counterion (as opposed to the structurally unknown MAO) in olefin polymerization, both experimentally[60, 65, 66, 67] and theoretically[62, 68, 69, 70].

It is also worth noting that there are many side reactions relevant for the propagation reaction (e.g. production of “dormant” bimolecular species[71], and, of course chain termination by β -hydrogen transfer to the monomer[72, 73] or β -hydrogen elimination[74]), and that the whole polymerization process is much more complex than what I outline here. My concern, though, is to model the propagation reaction of active catalytic centers.

3.2 Selected characteristics of metallocene catalyzed α -olefins

I will refer here only to the three issues I consider most important about the reactions under consideration. These issues have already been put forward by Ystenes in his papers[55, 56], among a couple of others, being regarded as conflictive points for the CAM for Ziegler-Natta catalysts, and I extend them to metallocenic catalysts.

3.2.1 The reaction rate order of the monomer predicted by theory does not match experiment

It is widely accepted that most metallocene-catalyzed polymerizations have reaction rates proportional to the monomer and catalyst concentrations, i.e. are of first order with respect to both the monomer and the catalyst[71, 75, 76], even though non-integer pseudo reaction orders have been reported[55, 74]. The problem here is that the CAM suggests that the propagation reaction takes place in two steps (complexation and insertion of the monomer), and chemical intuition indicates that the second one is most likely the slowest one, if the first one has no barrier and so it is expected to be very fast. If it were the case, then a comparison with a typical *Michaelis-Menten* reaction mechanism (Eq. 3.1) would show that the reaction rate would be of first order with respect to the catalysts, but of zeroth order (i.e., independent) with respect to monomer. This is illustrated in the *Michaelis-Menten* kinetic equation (Eq. 3.2), where $v = k_2[\text{Catalyst}]$ if $k_1 \gg \gg k_2$. Linear proportionality for monomer seems to be reasonable only if the first step (complexation) is much slower than the second one (insertion). Following Eq. 3.2, $v = k[\text{Catalyst}][\text{Substrate}]$ if $k_1 \ll \ll k_2$. The latter is highly counterintuitive.



$$v = \frac{k_2[Catalyst]}{1 + \frac{k_{-1} + k_2}{k_1[Substrate]}} \quad (3.2)$$

3.2.2 The effect of Lewis bases (including MAO⁻ counterion) is controversial

It is quite straightforward that Lewis bases that may be present in the medium (one of them being the MAO⁻ counterion for the catalyst cation), should compete for the empty site in the coordination sphere of the metal formed in various steps of the CAM. Vanka and Ziegler[68] studied this scenario by computational means (DFT calculations). They calculated the formation enthalpies of the complexes formed by the bare catalyst cation and some other Lewis bases, namely zirconocenic precatalyst itself (Cp₂Zr(CH₃)₂), solvent (toluene), co-catalyst (B(C₆F₅)₃) and Al(CH₃)₃. Although all of them produced stable complexes, none would bind stronger than the counterion [B(C₆F₅)₃CH₃]⁻, so they also studied the possibility of forming “sandwich” species, that is, the Lewis base inserted between the aforementioned cation and counterion.

Comparing the results with the ones obtained with the monomer (ethylene) for Lewis base, they concluded that dormant species formed by complexation of these Lewis bases with the catalyst could compete successfully with ethylene complexes, but for longer growing polymer chains (modeled by a propyl instead of a methyl attached to the zirconium atom), the complexation of the monomer was deemed closer in energy (probably due to steric effects) to that of Lewis bases. It should be noted that this would agree with the experimental results, where usually the propagation rate is smaller at the beginning of the polymerization (presumably due to greater abundance of dormant species. Increasing the growing polymer chain length would make the monomer more and more favored over other Lewis bases). In the case of sandwiched species, ethylene seemed to bind more strongly in its corresponding sandwich than the solvent, but not more than Al(CH₃)₃, therefore the latter could well inhibit the catalysis process (anyway its concentration, when used as scavenging agent, should be significantly lower than that of the monomer).

3.2.3 The growing chain flipping behavior is still unexplained

It is widely accepted that in metallocenic catalytic systems each metallic center has two coordination positions active for the polymerization reaction. Every

insertion step, the growing polymer chain is attached to one of them, and the incoming monomer binds to the other one. The possibility of obtaining isotactic or syndiotactic polymer is explained by how the monomers tend to bind to these coordination sites. Given that these two coordination sites will favor the complexation (and subsequent insertion) of the monomer with either equivalent or opposite side group (e.g. methyl group in propylene) arrangement, one can assume that the first case will produce an isotactic polymer (Figure 3.3), and the second one a syndiotactic one (Figure 3.4), provided that the monomer complexations happen in a coordination-site alternating fashion[77, 78]. Of course, if neither of them favors a given orientation of the monomer, the product will be atactic.

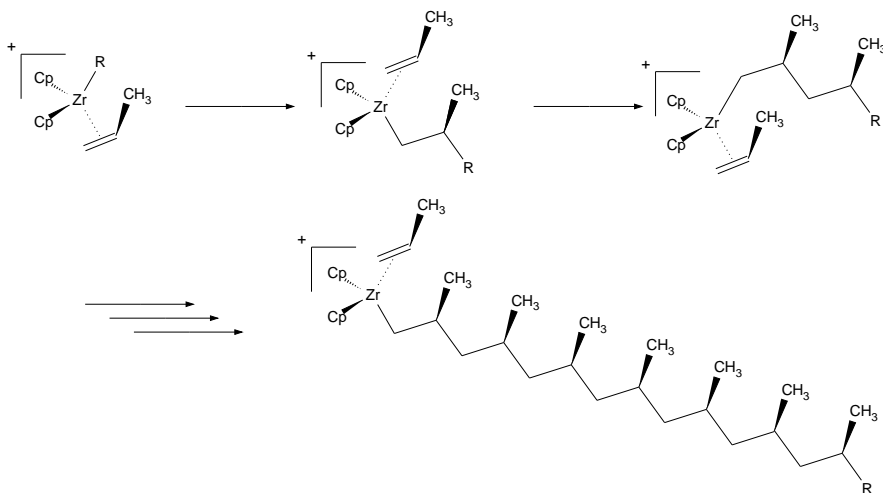


Figure 3.3: Isotactic growth

It is important to note that the growing chain has to flip once (or an odd number of times) per monomer insertion. A successful theoretical mechanism has to be able to account for this fact, and explain not only how the flip happens when the monomer inserts itself, but also why the chain stays in place between two successive insertions (or flips exactly an even number of times). If the growing chain stays in the same coordination site all the time, then both isotactic and atactic products can be rationalized, but no easy explanation can be given to the formation of syndiotactic polymers with a static growing chain, nor with an uncontrolled flipping of the chain. Anyway, some authors[79] have taken into account the possibility of chain flipping between successive insertions, and have come up with the conclusion that for some catalytic systems the inversion (flip) rate can even be much higher than the

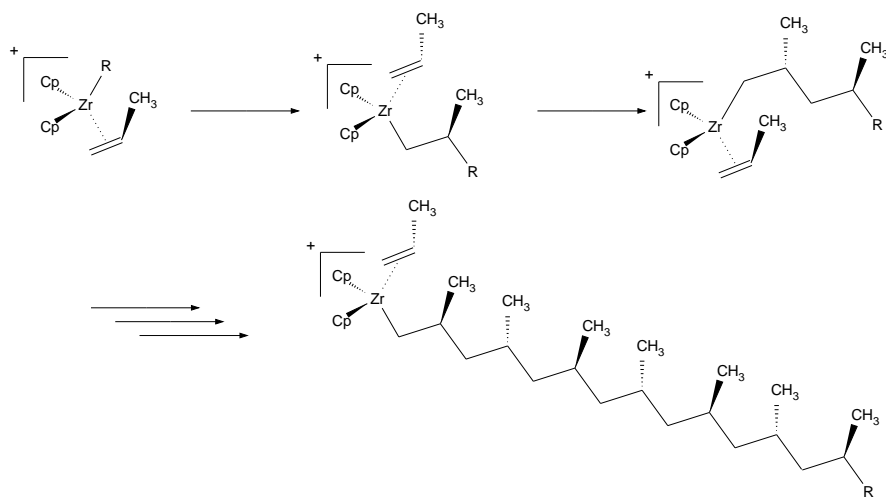


Figure 3.4: Syndiotactic growth

monomer insertion rate.

3.3 Methods

My first step is to use quantum calculations to sketch a potential energy curve (PEC) for the approach of the monomer to the metal. Then more accurate calculations will be done on the stationary points, so that I can compare the heights of the energetic barriers for the propagation reaction.

For my calculations I have chosen $[Cp_2ZrCH_3]^+$ as the active catalyst, and ethylene as the monomer, provided that they are the simplest species that can model the reaction, and thus the less computationally demanding. The counterion $[CH_3B(C_6F_5)_3]^-$, when used, has been modelled by a $[CH_3B(CF_2Cl)_3]^-$ unit. The suitability of such a model was discussed in Chapter 2.

All the calculations have been carried out using the GAUSSIAN 98 package[34] and the B3LYP density functional (DFT) method therein.

I have used 4 basis sets throughout this work. Firstly, for the relaxed PEC scans I chose SKBJ effective core potential (ECP) basis set[80, 81, 82], as defined in the Extensible Computational Chemistry Environment Basis Set Database[32]. I chose such basis set for performance considerations, since it has all of the core electrons described by pseudopotential functions, and only the valence shell of each element is described with Gaussian basis functions, thus reducing the computational expense considerably.

Secondly, for the geometry optimizations and subsequent frequency calculations I have made use of the LanL2DZdp basis set, which is an extension of the LanL2DZ basis set[83, 84, 85], supplemented with diffuse and polarization functions[86]. Unfortunately there is no such extension for beryllium or zirconium, so I have used the bare LanL2DZ basis set for these elements. However, the diffuse functions are expected to be of little importance for both boron and zirconium, because they have a substantial cationic nature in the compounds under study. The LanL2DZ basis set is a pseudopotential one, as it is SKBJ, but with a smaller core described with ECPs, so that an expected increase in accuracy is achieved at the expense of an actual increase in computational cost.

Thirdly, for the *single point* energy calculations I used the widely known 6-311++G(3df,3pd) basis set, as implemented in Gaussian, for all the elements except for the zirconium, for which the SDD basis set was used, as implemented in Gaussian. I have called this basis set TZ basis set throughout this paper.

Lastly, when testing for the relevance of diffuse functions for the description of a potential β -agostic interaction on the zirconium atom, I used both the LanL2DZ basis set and an extension to it consisting in the inclusion of a diffuse function in the β carbon and its three hydrogens (a total of four extra s functions). I will refer to the latter as LanL2DZ β . Additionally, SKBJ and LanL2DZdp basis sets have also been used, the latter only in the simplest of the two cases studied in this test.

These computational details and the species taken into account are not so different from those studied by Thorsaug *et al.*[57], but additionally I have performed frequency calculations in order to obtain reaction Gibbs free energies, something they did not do due to computational limitations. Of course, temperature is a factor in the entropic part of ΔG . The numbers I give here are calculated at 298K, which is a reasonable temperature for this kind of polymerizations.

It is also noteworthy that I have performed such frequency calculations on all the stationary points, coming up successfully with real frequencies for all the normal modes in the case of local minima, and one and only one imaginary frequency for the transition states. I have also confirmed that in every case the imaginary frequency corresponded to the desired normal mode.

With regard to the flipping of the growing chain, I have modelled it with a typical bridged zirconocene, namely ansa-ethylene-bis(indenyl) methyl zirconium cation, whilst the oscillating chain has been reduced to a simple methyl group.

For the ball-and-stick graphical representation of molecules, the Raster3D software[3] has been extensively used throughout this chapter. The schematic

molecular representations have been produced with ChemTool[87]. Various graphs and schematic figures have been produced with Grace[88] and Xfig[89].

3.4 Results and discussion

3.4.1 Description of the β -agostic interaction

It has been argued that an agostic interaction between the β -hydrogen and the zirconium is formed, and that its description is crucial. Although my calculations with ethyl chains in bare cations suggest that this agostic interaction does exist, when introducing the counterion in the system its importance seems to decrease drastically (see Figure 3.6).

The underlying question is not only whether the length of the growing polymer chain affects the insertion of subsequent monomers (which sounds reasonable for very short chains, and is probably irrelevant for longer chains), but also whether one should add diffuse functions in order to properly describe the possible agostic interactions by means of theoretical calculations, even in a *qualitative* way.

I have tested for the stability of these β -agostic interactions by performing a relaxed potential energy scan along the H-C-C-Zr dihedral angle, D, giving to it values from 0° to 60° . The two limiting structures are depicted in Figure 3.5.

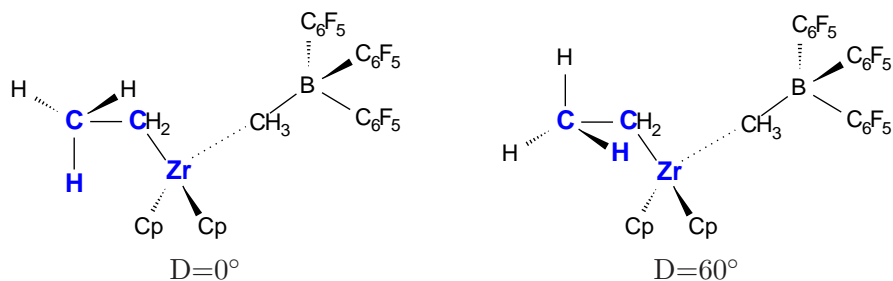


Figure 3.5: Two limit structures in the β -agostic interaction test scan. Atoms defining dihedral angle D highlighted.

This PEC scan was carried out on the bare catalyst cation and on the catalyst/counterion system, using three basis sets, namely SKBJ, LanL2DZ and LanL2DZ β , plus also the bigger LanL2DZdp basis set for the bare catalyst. Figure 3.6 shows the result of the seven scans.

Although the inclusion of diffuse functions on the subject atoms (LanL2DZ β basis set) increases very slightly the relative stability of the geometry with a planar H-C-C-Zr dihedral angle (either for the cation and the

neutral system), it is clear that all basis sets regard the $D=60^\circ$ moiety as the most stable one for the neutral system, and the $D=0^\circ$ geometry for the cation. When the bigger LanL2DZdp basis set is used the β -agostic geometry seems to be even more favored, and it seems reasonable to think that when including the counterion the $D=0^\circ$ and $D=60^\circ$ geometries will be closer in energy. The basis set I use in the bulk of the thesis to calculate the different relaxed scans, that is the small SKBJ, gives figures very close to the bigger LanL2DZdp.

I can therefore conclude that the PEC is quite flat for the rotation of the methyl end of the ethyl group, so that the possible β -agostic interaction cannot be considered too tightly-binding for the cation, and much less so for the neutral system. It is also apparent that the SKBJ basis set is suitable for a qualitative sketch of the PEC along the monomer approach.

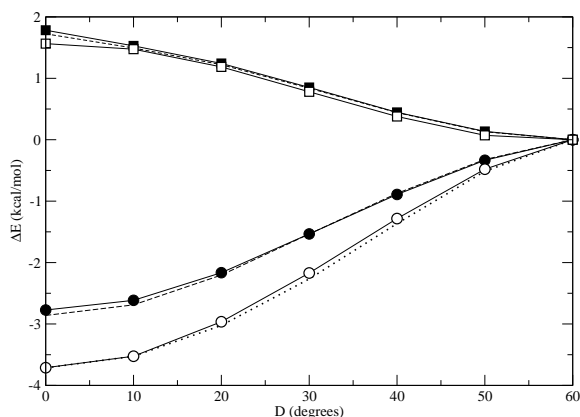


Figure 3.6: PEC along the H-C-C-Zr dihedral angle for the bare catalyst cation (circles) and catalyst/counterion (squares) systems. LanL2DZ basis set results are represented by solid symbols, and SKBJ results by white ones. The dashed lines below each continuous line draw the corresponding LanL2DZ β results. The dotted line corresponds to LanL2DZdp values for bare catalyst. ΔE s are given with respect to the $D = 60^\circ$ moiety.

3.4.2 Bare cation

Monomer approach PEC scan

I have performed some fully relaxed PEC scans in the ethylene + $[\text{ZrCp}_2\text{CH}_3]^+$ system, that is, some internal variables (interatomic distances) were fixed at

selected values, while all the remaining variables were freely optimized. The distances that were fixed in each scan are henceforth labeled as pseudo-reaction coordinates.

Firstly, I wanted to check whether a π -complex exists, that is, if there is a minimum in the PEC corresponding to the approach of the monomer to the cation, *before* it inserts into the Zr–C $_{\alpha}$ bond. I chose the Zr–C $_1$ C $_2$ distance as the pseudo-reaction coordinate to scan, where C $_1$ and C $_2$ are the carbon atoms of the ethylene. The X–YZ notation is used to indicate that both X–Y and X–Z are fixed and equal. I made this variable evolve from a far away distance (6 Å), where the binding energy (defined as the electronic energy of the complex minus the sum of those of the monomer and cation evaluated separately) is small (around 2.0 kcal/mol), and up to a little closer than the minimum energy point, $d(\text{Zr–C}_1\text{C}_2) = 2.4$ Å (see r.h.s. of Figure 3.7).

Secondly, once the monomer is close to the metallic center, one would expect to observe a maximum in the PEC corresponding to the approach of one of the carbon atoms of the monomer to the carbon of the methyl group of the cation (α carbon of the growing polymer chain). In this case I have selected the C $_2$ –C $_{\alpha}$ distance as pseudo-reaction coordinate, and calculated the resulting PEC ranging from carbon–carbon distances closer than the equilibrium C–C single bond (around 1.54 Å), up to where the energy starts decreasing after a maximum, namely the insertion TS (see l.h.s. of Figure 3.7).

Inspection of Figure 3.7 confirms that there exists a π -complex when the olefin is at around 2.9 Å from the zirconium atom. It is also evident, that an insertion TS must exist somewhere near $d(\text{C}_2\text{–C}_{\alpha}) = 2.2$ Å, and of course the product appears close to $d(\text{C}_2\text{–C}_{\alpha}) = 1.55$ Å.

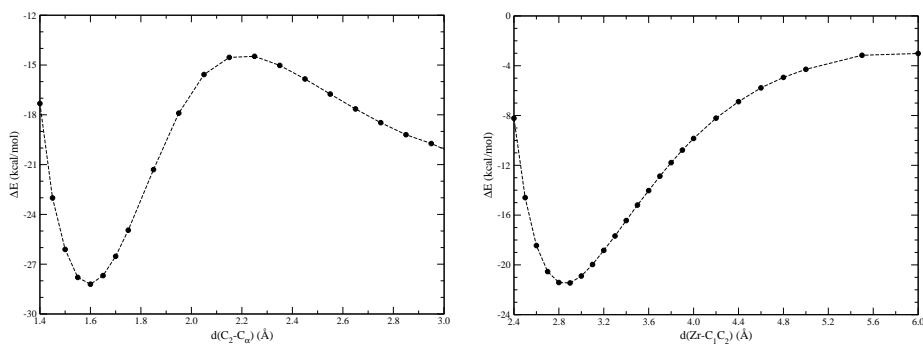


Figure 3.7: PEC corresponding to varying the C $_2$ –C $_{\alpha}$ (left) and Zr–C $_1$ C $_2$ (right) distances for the bare zirconocene cation + ethylene system. Distances in Å and energies in kcal/mol.

In the case of the TM, I did not perform such a PEC scan, but rather directly optimize the corresponding stationary points.

3.4.3 Relevant stationary structures along the PEC

I picked the relevant points of the PEC scans in Section 3.4.2, and optimized their geometries with the LanL2DZdp basis set. I regarded as “relevant” the minimum of the d(Zr–C₁C₂) scan (π -complex, CAM_{comp}) and the maximum (insertion TS, CAM_{TS}) and minimum (product, CAM_{prod}) of the d(C₂–C _{α}) scan, as well as the ethylene and zirconocene moieties infinitely separated (reactants, Et and CAM_{reac}), and their energies were refined by means of *single point* energy calculations with the TZ basis set. These geometries and the Cossée-Arlman mechanism energy profile are depicted in Figure 3.8. The energies are summarized in Table 3.1.

A summary of the geometrical features of the CAM reaction path follows. The nomenclature can be readily made clear by inspection of Figure 3.16 of the following Section, which depicts one of the optimized geometries that include the counterion.

An ethylene monomer unit approaches the CAM_{reac} catalyst cation, forming the CAM_{comp} π -complex without any intermediate TS to be found. In the π -complex the Zr–C distances for the monomer carbons are 2.862 and 2.855 Å, which means that both carbon atoms are similarly bound to the central metal. At this stage the C₁–C₂ double bond is only slightly affected, with a C₁–C₂ distance of 1.353 Å, whereas d(C₁–C₂) = 1.340 Å in the isolated monomer. It is noteworthy that in the complex the three C _{α} –H _{α} distances are in the 1.100–1.101 Å range, while in the case of the CAM_{reac} reactant one of the hydrogen atoms displays a clear α -agostic interaction with the zirconium metal, having its C _{α} –H _{α} distance elongated to 1.133 Å, and a Zr–H _{α} distance of merely 2.394 Å, only 0.18 Å further from the metal than the α carbon itself (Zr–C _{α} –H _{α} angle of 84.6°).

The π -complex evolves to the insertion product through the TS labeled CAM_{TS}. In this TS the Zr–C _{α} bond breaks, the C₁–C₂ double bond turns into a single bond and simultaneously two new bonds are formed: the Zr–C₁ one, and the C₂–C _{α} one. The corresponding distances are: d(Zr–C _{α}) = 2.315 Å, d(Zr–C₁) = 2.405 Å, d(C₁–C₂) = 1.417 Å and d(C₂–C _{α}) = 2.175 Å. In this TS, one of the hydrogens on the α carbon interacts again with the metallic center through an agostic effect, showing an elongation to 1.139 Å, and a Zr–H _{α} distance of only 2.167 Å (Zr–C _{α} –H _{α} angle of 68.2°).

The final product of this reaction features single Zr–C₁ (2.235 Å), C₁–C₂

(1.566 Å) and C₂-C_α¹ (1.561 Å) bonds, with a γ-H agostic interaction accounting for an elongation of the C_α-H_α distance up to 1.127 Å, and a Zr-H_α distance of only 2.262 Å.

For the TM, the reactants consist on an ethylene molecule plus the CAM_{comp} π-complex already calculated for the CAM reaction path, and the corresponding TS (TM_{TS}) and product (TM_{prod}). These two species were also fully optimized at the B3LYP/LanL2DZdp theory level, and the corresponding geometries used for *single point* calculations at the B3LYP/TZ level.

These geometries and the *Trigger* mechanism energy profile are depicted in Figure 3.9. The energies are displayed in Table 3.2.

A summary of the geometrical features of the TM reaction path follows. An ethylene monomer unit approaches the CAM_{comp} π-complex to form the insertion TS, without any intermediate complex to be found. In this TS, labeled TM_{TS}, the same bonds as in the CAM_{TS} case are broken and formed. Here the corresponding distances are: d(Zr-C_α) = 2.317 Å, d(Zr-C₁) = 2.405 Å, d(C₁-C₂) = 1.417 Å, and d(C₂-C_α) = 2.174 Å. In this TS, one of the hydrogens on the α carbon interacts again with the metallic center through an agostic interaction, showing an elongation to 1.139 Å, and a Zr-H_α distance of only 2.167 Å (Zr-C_α-H_α angle of 68.1°). As a matter of fact, the α hydrogen is 0.15 Å closer to the zirconium cation than the α carbon itself.

The final product of this reaction features single Zr-C₁ (2.239 Å), C₁-C₂ (1.564 Å), and C₂-C_α (1.559 Å) bonds, with a γ-H agostic interaction accounting for an elongation of the C_α-H_α distance up to 1.125 Å, and a Zr-H_α distance of 2.272 Å.

The reaction energetics in tables 3.1 and 3.2 are given with respect to the CAM_{comp}+Et reactants in the TM, but with respect to the CAM_{comp} complex in the CAM (and not the CAM_{reac}+Et reactants) for I want to compare barrier heights in both mechanisms. All energies are given in kcal/mol units.

¹Recall that I keep calling C_α to the carbon atom that now occupies a γ position

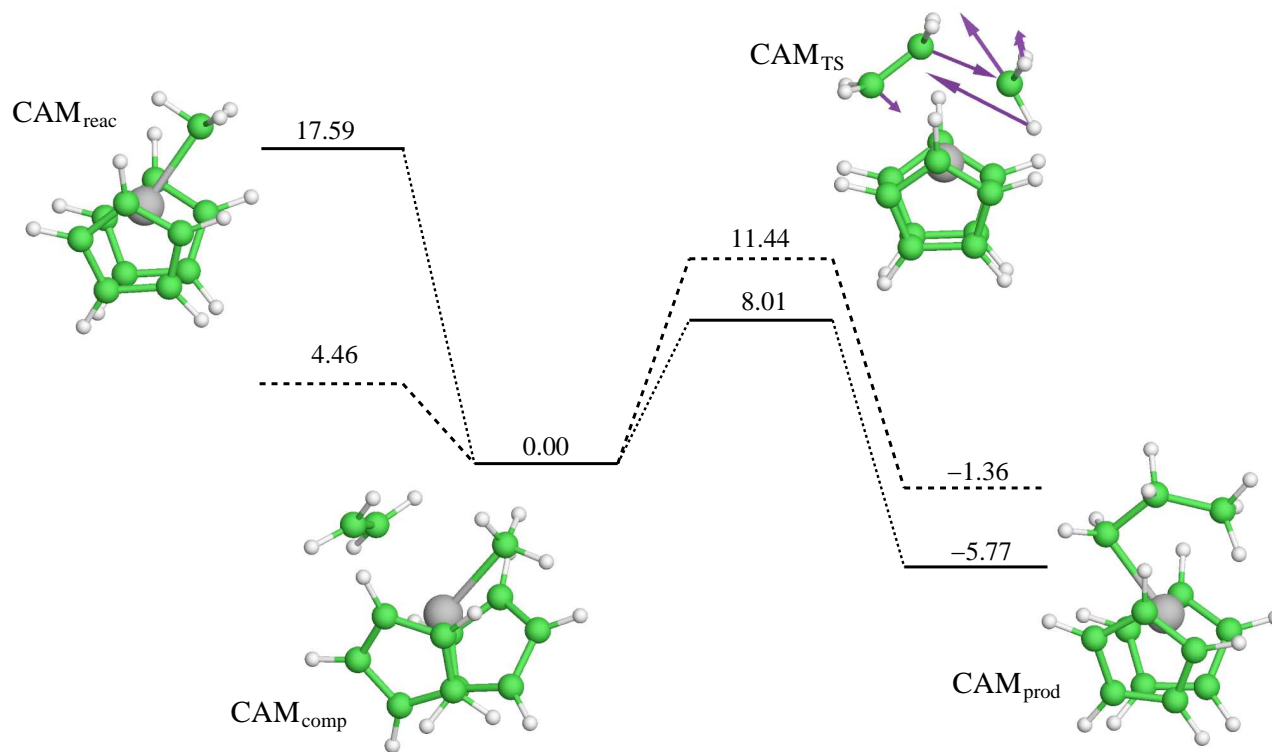


Figure 3.8: Stationary points along the $\text{Et} + [\text{CH}_3\text{ZrCp}_2]^+$ Cossée-Arlman reaction PEC. Solid lines correspond to electronic energies, and dashed lines to Gibbs free energies, both values in kcal/mol at the B3LYP/TZ//B3LYP/LanL2DZdp level. The arrows in CAM_{TS} correspond to the motion of the atoms according to the normal mode with an imaginary frequency. The scale is arbitrary, but the relative moduli of the vectors match those of the Gaussian output.

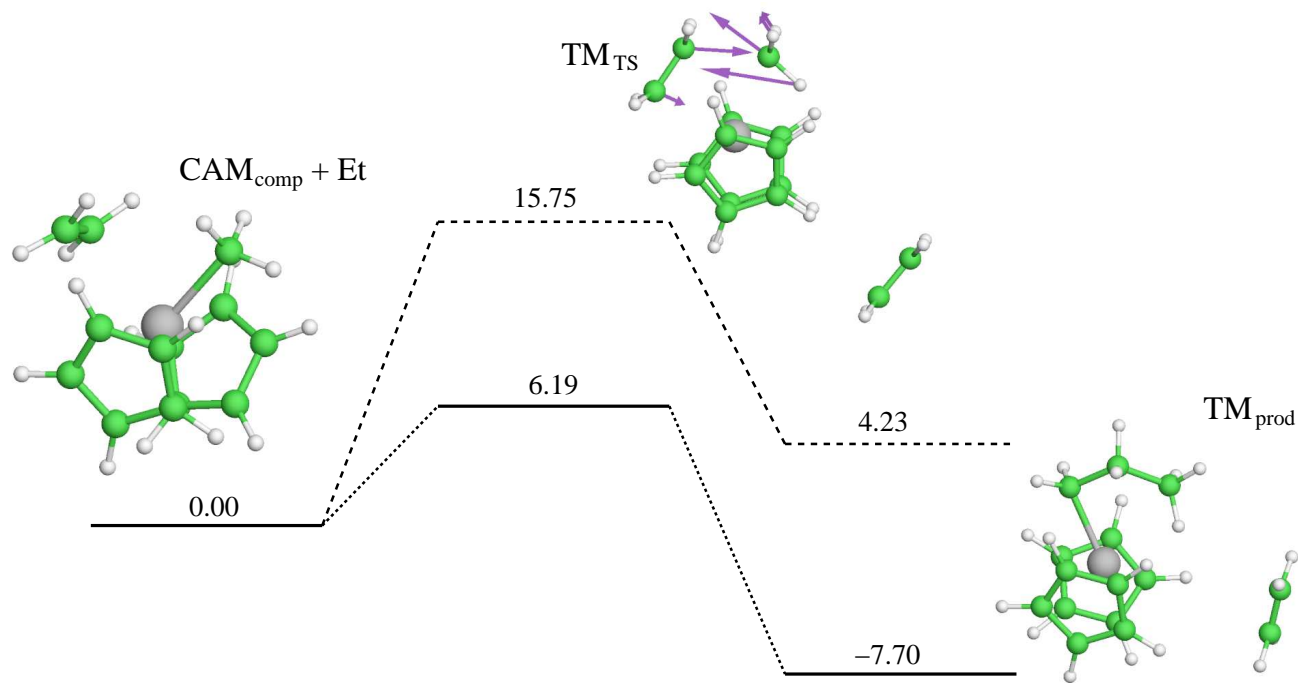


Figure 3.9: Stationary points along the $\text{Et} + [\text{CH}_3\text{ZrCp}_2]^+$ *Trigger* reaction PEC. Solid lines correspond to electronic energies, and dashed lines to Gibbs free energies, both values in kcal/mol at the B3LYP/TZ//B3LYP/LanL2DZdp level. The arrows in TM_{TS} correspond to the motion of the atoms according to the normal mode with an imaginary frequency. The scale is arbitrary, but the relative moduli of the vectors match those of the Gaussian output.

Species	LanL2DZdp		TZ	
	ΔE	ΔG	ΔE	ΔG
$CAM_{reac} + Et$	17.59	5.32	16.73	4.46
CAM_{comp}	0.00	0.00	0.00	0.00
CAM_{TS}	7.12	10.55	8.01	11.44
CAM_{prod}	-8.44	-4.03	-5.77	-1.36

Table 3.1: Energy differences and Gibbs free energy differences (in kcal/mol) at selected stationary points along the Cossée-Arlman reaction path. Values obtained by *single point* calculations with the basis sets shown, on geometries optimized at the B3LYP/LanL2DZdp theory level.

The values for ΔE and ΔG are conveniently plotted in Figure 3.10.

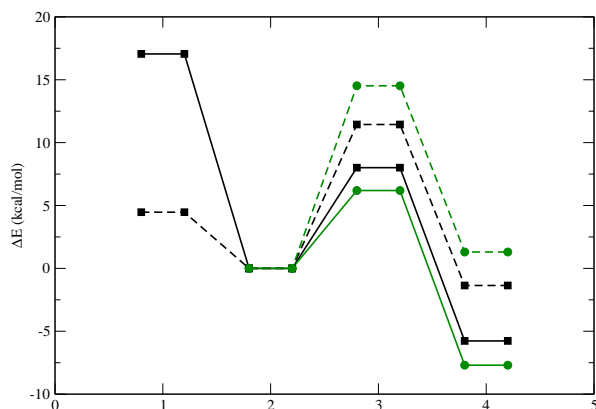


Figure 3.10: CAM (squares) and TM (circles) energy (continuous line) and Gibbs free energy (dashed lines) profiles.

Even if the TM is favored from an enthalpic point of view, the entropic effects of having a second monomer present in the transition state structure, instead of only one, make the system pay a high entropic toll. It is so high that the CAM turns out to be the mechanism with a lower Gibbs free energy barrier in gas phase (4 kcal/mol lower).

Since the entropic contribution has been calculated *via* a harmonic approximation for the vibrational modes, doubt rises whether it has been overestimated, particularly due to many low frequency normal modes present in the species of such a floppy system. These modes can hardly be well described

Species	LanL2DZdp		TZ	
	ΔE	ΔG^{gas}	ΔE	ΔG^{gas}
$CAM_{comp} + Et$	0.00	0.00	0.00	0.00
TM_{TS}	4.97	14.52	6.19	15.75
TM_{prod}	-10.63	1.30	-7.70	4.23

Table 3.2: Energy differences and Gibbs free energy differences (in kcal/mol) at selected stationary points along the *Trigger* reaction path. Values obtained by *single point* calculations with the basis sets shown, on geometries optimized at the B3LYP/LanL2DZdp theory level.

under the harmonic approximation used in the present investigation. Regardless of it, the numbers are solid enough to make the point clear that there is some kind of trade off between the positive catalytic effect of the second monomer, and the negative effect of the increased order of placing a second monomer molecule in the coordination sphere of the metal, or at least weakly bound to it.

3.4.4 Chain flipping

This issue has been recently addressed from an experimental point of view[90, 91], as well as theoretically [77, 79]. In my case, I have found a transition state ind-Zc^{TS} between two equivalent ind-Zc₁ minima, as depicted in Figure 3.11. This TS had a single imaginary frequency of 71i cm⁻¹. The low inversion barrier (*vide infra*), gives an idea of the flatness of the PEC for the inversion. Visual inspection of the corresponding normal mode confirmed that it corresponds to the motion of the methyl group in the expected pseudo-equatorial plane.

The calculated energetic barrier turned out to be 3.0 kcal/mol in electronic energy, and 2.3 kcal/mol in Gibbs free energy, so with this model I would predict a very facile oscillation of the growing chain, if there is no other factor preventing it. The results in the paper by Goddard *et al.*[77] basically agree with mine: the geometrical minima are tetrahedral, not triangular planar (it would be a TS according to my calculations), but the energy difference is almost negligible.

Solvent effects are not expected to be important, since the charge arrangement is not significantly altered in the process, and the shape of the whole molecule is not drastically changed. Regarding this, one could think that, for the long alkyl chain that is formed in the polymerization a huge volume of solvent is displaced by this flipping. But the important point is the move-

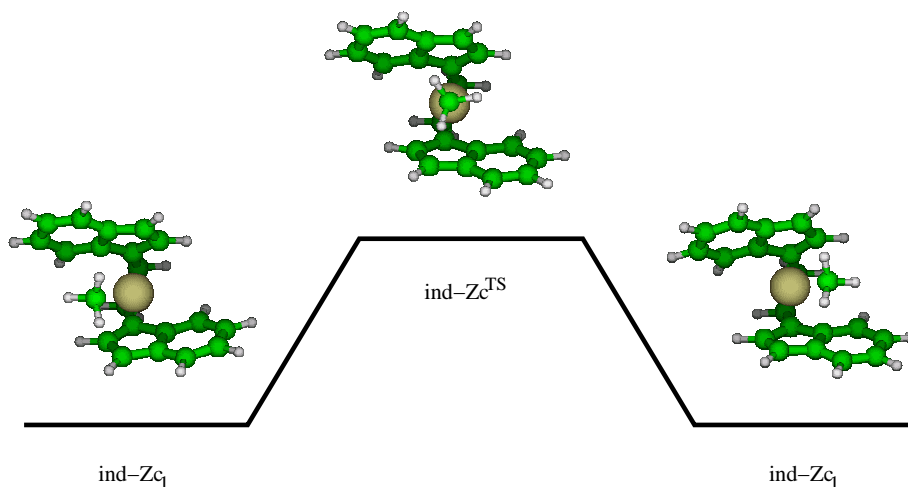


Figure 3.11: PEC scheme for methyl flipping in ansa-ethylene-bis(indenyl) methyl zirconium.

ment of the chain “body” relative to the catalyst “head”, so equivalently one could say that it is the zirconocene that is moving. The latter requires only minor solvent cavity distortion to occur, hence the relative energies within the solvent are expected to be similar to the vacuum.

3.4.5 Inclusion of the counterion

In Chapter 2 it has been extensively discussed the choice of a model CI to represent the tri(perfluorophenyl)borate, and, hence, I will proceed to use that model, namely $\text{B}(\text{CF}_2\text{Cl})_3$.

3.4.6 $\text{Et}^+[\text{CH}_3\text{ZrCp}_2]^+ / [\text{CH}_3\text{B}(\text{CF}_2\text{Cl})_3]^-$ scan results

I have followed the same procedure as in Section 3.4.2, now including an explicit counterion, in the form of a $[\text{CH}_3\text{B}(\text{CF}_2\text{Cl})_3]^-$ anion. The resulting PEC scans, at the B3LYP/SKBJ level, are displayed in Figure 3.12.

The first difference with respect to the bare cation case is that, for $\text{Zr}-\text{C}_1\text{C}_2$ distances ranging from 6.0 Å to 3.55 Å (see right side of Figure 3.12, the potential energy increases monotonically. Although there seems to be a π -complex formation at around $d(\text{Zr}-\text{C}_1\text{C}_2) = 2.9$ Å (as in the bare cation case), the monomer has to overcome an energetic barrier in order to reach it.

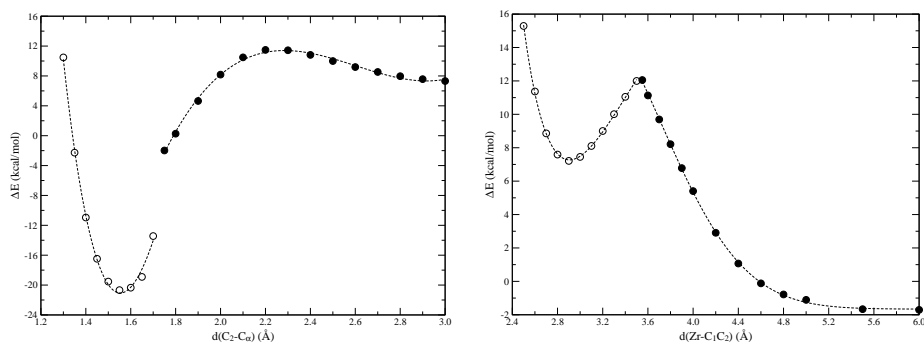


Figure 3.12: PEC corresponding to varying the C_2-C_α (left) and $Zr-C_1C_2$ (right) distances for the ethylene + $[CH_3ZrCp_2]^+/[CH_3B(CF_2Cl)_3]^-$ system. In each plot white and solid black circles have been used to distinguish the two surfaces (see text), and the corresponding fitted functions are represented by dashed lines. Distances in Å and energies in kcal/mol.

This energy maximum seems to be the crossing point of two different energy surfaces, namely the one corresponding to the π -complex basin from 2.50 Å to 3.50 Å, and the monomer approach basin, from 3.55 Å on. The different nature of the two surfaces is evident upon inspection of the $Zr-C_{CI}$ distance, where C_{CI} refers to the carbon atom in the methyl group of the counterion. The evolution of such distance is depicted in Figure 3.13. In the complex basin, $d(Zr-C_{CI})$ has a moderated decrease, from 4.57 Å at $d(Zr-C_1C_2) = 2.50$ Å, to 4.24 Å at $d(Zr-C_1C_2) = 3.50$ Å. However, at $d(Zr-C_1C_2) = 3.55$ Å, $d(Zr-C_{CI})$ jumps to a much shorter value of 3.22 Å, which quickly evolves, as $d(Zr-C_1C_2)$ increases, to a constant $d(Zr-C_{CI}) = 2.58$ Å from $d(Zr-C_1C_2) = 4.80$ Å on.

Recall that Figure 3.13 displays the Fermi-Dirac function that best fits the calculated points. The general form of a Fermi-Dirac function is displayed in Eq. 3.3.

$$f_{Fermi-Dirac} = Y_0 + \frac{Y_1}{1 + e^{\frac{x-x_0}{\lambda}}} \quad (3.3)$$

It is not the author's aim to find any fundamental relationship between the calculated values and the function, but rather extract the information from the similarities and dissimilarities the calculated points and the fitted function may have. A Fermi-Dirac function is best suited to describe a property, $f(x)$, that is almost constant at $f(x) = Y_0$ for large values of variable x , and also constant at $f(x) = Y_0 + Y_1$ for very small values of x , but with a rapid transition from $Y_0 + Y_1$ to Y_0 at precisely $x = x_0$. The parameter λ gives an

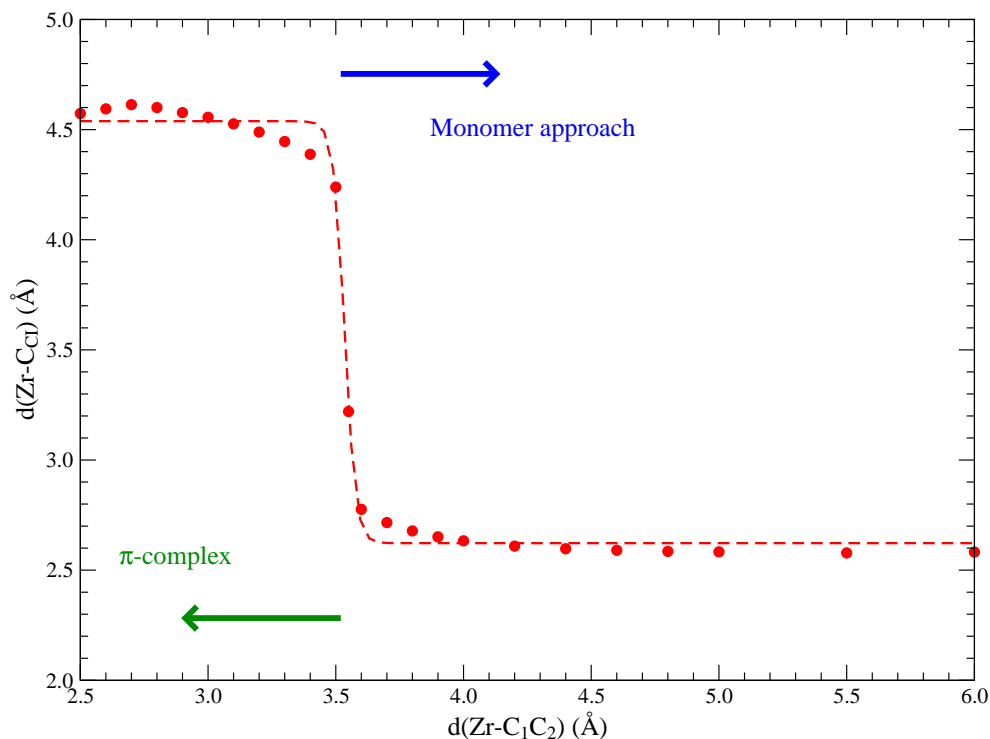


Figure 3.13: Transition between a zone where the ethylene monomer is merely approaching the metallic center of the $[\text{Cp}_2\text{ZrCH}_3]^+ / [\text{CH}_3\text{B}(\text{CF}_2\text{Cl})_3]^-$ complex, and the region where it is already complexated. The dots correspond to calculated points, and the dashed line is a fit to a Fermi-Dirac function (see Eq. 3.3). The fitting parameters are given in Table 3.3, with the label FD-1M in Table 3.3.

idea of the width of the transition. A little algebra can show that the Δx (or $-\Delta x$) displacement from x_0 required to have $f(x)$ differ from Y_0 (or $Y_0 + Y_1$) by only δY_1 (or $-\delta Y_1$) would be $\Delta x = -\lambda \ln(\delta)$. This means that one would have a value over 99% close to the asymptotic one ($\delta = 0.01$), by displacing merely 4.6λ distance units from x_0 .

The values for the constants in the Fermi-Dirac fit in Figure 3.13 are given in Table 3.3. Recall the good overall quality of the fit (R close to unity), despite the fact that some points consistently deviate from the fit. This tells us that the “general” shape of the calculated curve is, at least qualitatively, well grasped by the function. The fit is not quantitative (this was not expected), and, for example, for $x < x_0$ ($x_0 = 3.53$ Å), the calculated points do not lie

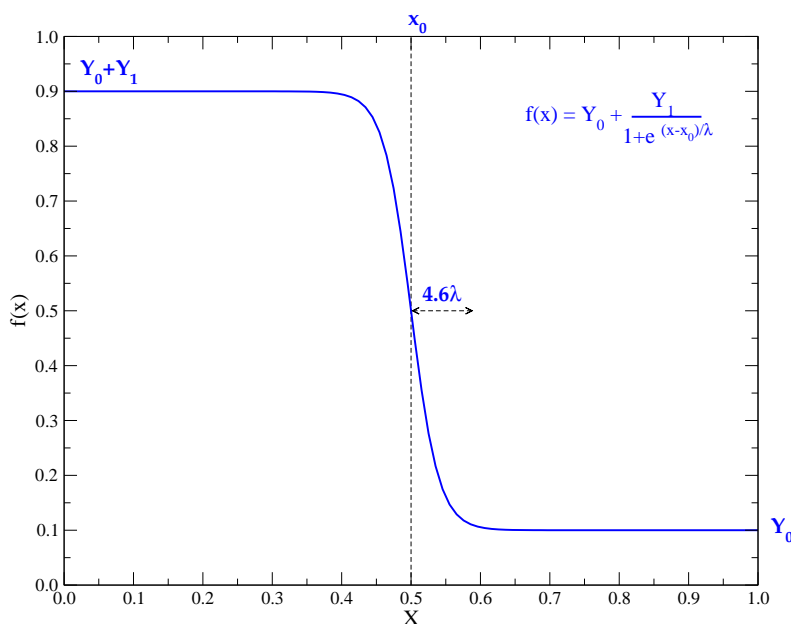


Figure 3.14: Plot of the Fermi-Dirac function (see Eq. 3.3), for parameters $Y_0 = 0.1$, $Y_1 = 0.8$, $x_0 = 0.5$, $\lambda = 0.02$.

on a horizontal line.

A second difference would be that, for $x > x_0$, the increase in $d(\text{Zr}-\text{C}_1\text{C}_2)$ as x decreases (that is, how displaced the CI is as the monomer approaches the metal), is not nearly as abrupt as it would have been had it obeyed the Fermi-Dirac function. In fact, the CI starts to move away from the metal when the monomer is still 4.2 \AA apart, although the transition point where its bond to the metal is completely broken is at around $x = x_0$ (3.53 \AA).

However, the Fermi-Dirac fit gives us an interesting summary of the features of the evolution of $d(\text{Zr}-\text{C}_{CI})$ with $d(\text{Zr}-\text{C}_1\text{C}_2)$: it jumps from around 4.54 \AA ($Y_0 + Y_1$ in first column of Table 3.3), to around 2.62 \AA (Y_0), within a region of approximate width 0.1 \AA (4.6λ) around $d(\text{Zr}-\text{C}_1\text{C}_2) \simeq 3.53 \text{ \AA}$ (x_0).

Once accepted that these two curve fragments are of different nature, each half can be fitted to a relatively simple equation: a Morse-type potential for the π -complex basin and a Gaussian-type one for the approach channel, as displayed in Eqs. 3.4 and 3.5. The values of the constants for such equations are given in Table 3.4.

$$V_{Morse} = A + B(1 - e^{-C(x-D)})^2 \quad (3.4)$$

FD-1		FD-2		FD-3	
Y_0	2.6622	Y_0	2.3272	Y_0	4.4799
Y_1	1.9158	Y_1	2.3347	Y_1	-1.8983
x_0	3.5344	x_0	1.7299	x_0	1.7454
λ	0.021723	λ	0.017434	λ	0.0059523
R	0.99817	R	0.99349	R	0.99275

Table 3.3: Constants for the Fermi-Dirac fits to $d(\text{Zr}-C_{CI})$ vs. $d(\text{Zr}-C_1C_2)$ (first column) and $d(\text{Zr}-C_\alpha)$ and $d(\text{Zr}-C_{CI})$ vs. $d(C_2-C_\alpha)$ (second and third columns). The last value, labeled R, gives the correlation coefficient between the fit and the calculated points.

ZrCC Basin		ZrCC Approach		CC Basin		CC Approach	
A	7.2714	α	-1.66246	A	-21.0658	c_0	-532.441
B	16.4908	β	18.2988	B	391.384	c_1	644.126
C	1.30715	γ	0.944548	C	0.9823	c_2	-251.314
D	2.90584	δ	2.9915	D	1.5535	c_3	32.2016
R	0.99968	R	0.99990	R	0.99883	R	0.99785

Table 3.4: Fitted constants for the Morse (first and third columns), Gaussian (second column), and third order polynomial (fourth column) fits corresponding, respectively, to the π -complex basin, monomer approach to Zr, C_1-C_α binding and C_1-C_α approach before binding, for the case of $\text{Et} + [\text{CH}_3\text{ZrCp}_2]^+ / [\text{CH}_3\text{B}(\text{CF}_2\text{Cl})_3]^-$. The last value, labeled R, gives the correlation coefficient between the fit and the calculated points.

$$V_{Gauss} = \alpha + \beta e^{-\gamma(x-\delta)^2} \quad (3.5)$$

Some constants in the fitted functions bear a special meaning, which I will summarize next. In the case of the Morse fit to the complex basin, the parameter D stands for the distance where the minimum of the function is located (2.906 Å), and thus corresponds to the $\text{Zr}-C_1C_2$ distance for the π -complex. Its energy is given by the value of parameter A (~ 7.3 kcal/mol). In the case of the Gaussian fit to the monomer approach, the most remarkable parameter would be α , which gives us an idea of the basis set superposition error (~ 1.7 kcal/mol), for this parameter should be exactly zero in its absence.

The electron deficiency that the zirconium atom had in the bare cationic species is now offset by the contribution of the counterion, so that the electron excess provided by the ethylene monomer, through its π -bond, is not required

anymore. This fact generates a competition between nucleophiles (ethylene monomer *vs.* $[\text{CH}_3\text{B}(\text{CF}_2\text{Cl})_3]^-$ counterion), and thus the monomer has to overcome an effective “complexation barrier” before it can be inserted into the alkyl-metal bond.

The $d(\text{C}_2\text{-C}_\alpha)$ scan, on the other hand, suggests that once the monomer is complexed, the insertion reaction crosses an energetic *plateau*, with a very low relative barrier for the cleavage of the methyl group and the formation of the new $\text{C}_2\text{-C}_\alpha$ and Zr-C_1 bonds. Two PECs can also be distinguished in this plot: a binding zone at $d(\text{C}_2\text{-C}_\alpha) = 1.30\text{--}1.70$ Å and a $\text{C}_2\text{-C}_\alpha$ bond formation TS zone, from $d(\text{C}_2\text{-C}_\alpha) = 1.75$ Å on. The former has been fitted to a Morse-type function of the kind displayed in Eq. 3.4, and the latter to a third degree polynomial, and the values of the parameters of such fits are also given in Table 3.4.

As in the case of the $d(\text{Zr-C}_1\text{C}_2)$ plot, some of the parameters have a special meaning. In the case of the binding basin, parameter D gives us the $\text{C}_2\text{-C}_\alpha$ equilibrium distance of the reaction product (1.55 Å), and parameter A corresponds to its energy (-21.1 kcal/mol).

The key property here to tell one zone from the other is the Zr-C_α distance. This property bears a constant value of 2.26 Å for distances $d(\text{C}_2\text{-C}_\alpha) > 2.55$ Å, but then it starts to elongate up to 2.72 Å at $d(\text{C}_2\text{-C}_\alpha) = 1.75$ Å. At $d(\text{C}_2\text{-C}_\alpha) = 1.70$ Å the α carbon completely breaks its bond with the zirconium atom, jumping to a distance of 4.05 Å from it, and staying always further than 4.5 Å at smaller $\text{C}_2\text{-C}_\alpha$ distances. This transition is depicted in Figure 3.15, also fitted to a Fermi-Dirac-type function, labeled FD-2 (See the $\text{Zr-C}_1\text{C}_2$ case above).

Once more, the fit parameters tell us a summary of the whole story: the Zr-C_α distance switches from a nearly constant distance of around 2.32 Å (Y_0) at large values of $d(\text{C}_2\text{-C}_\alpha)$, to distances around 4.66 Å ($Y_0 + Y_1$) for small values of $d(\text{C}_2\text{-C}_\alpha)$. This transition happens in a thin region (0.08 Å, 4.6λ) around $d(\text{C}_2\text{-C}_\alpha) = 1.73$ Å (x_0). The “dirty stuff” the Fermi-Dirac function does not tell us is that $d(\text{Zr-C}_\alpha)$ already starts to elongate at $d(\text{C}_2\text{-C}_\alpha) = 2.2$ Å. It is also untrue that it stays constant at small $d(\text{C}_2\text{-C}_\alpha)$; it shortens noticeably.

It is worth noting that, from the insertion TS on, the counterion takes its place back, provided that the coordination of the zirconium cation would otherwise drop formally to 3 again. While the Zr-C_{CI} distance stays at around 4.5 Å for $d(\text{C}_2\text{-C}_\alpha)$ larger than 2.1 Å, it drops to 2.58 Å for $d(\text{C}_2\text{-C}_\alpha)$ smaller than 1.70 Å, with a rapid transition in between. The Zr-C_{CI} *vs.* $d(\text{C}_2\text{-C}_\alpha)$ plot is also given in Figure 3.15, and also fitted to a Fermi-Dirac function (labeled FD-3).

The fitting parameters would say that $d(\text{Zr}-\text{C}_{CI})$ stays at around 4.5 Å for large $d(\text{C}_2-\text{C}_\alpha)$ values (Y_0), and then jumps to a much closer 2.58 Å ($Y_0 + Y_1$) within 0.03 Å (4.6λ) of $d(\text{C}_2-\text{C}_\alpha) = 1.75$ (x_0). It is worth noting that x_0 is very close to the value it has in FD-2. It makes clear that the rupture of the $\text{Zr}-\text{C}_\alpha$ bond and the regeneration of the metal/CI bond happen simultaneously.

As in the FD-2 case, FD-3 also fails to predict the shortening of $d(\text{Zr}-\text{C}_\alpha)$ from $d(\text{C}_2-\text{C}_\alpha) = 2.1$ Å to x_0 . However the values of $d(\text{Zr}-\text{C}_\alpha)$ at both large and small $d(\text{C}_2-\text{C}_\alpha)$ are fairly constant, as described by FD-3.

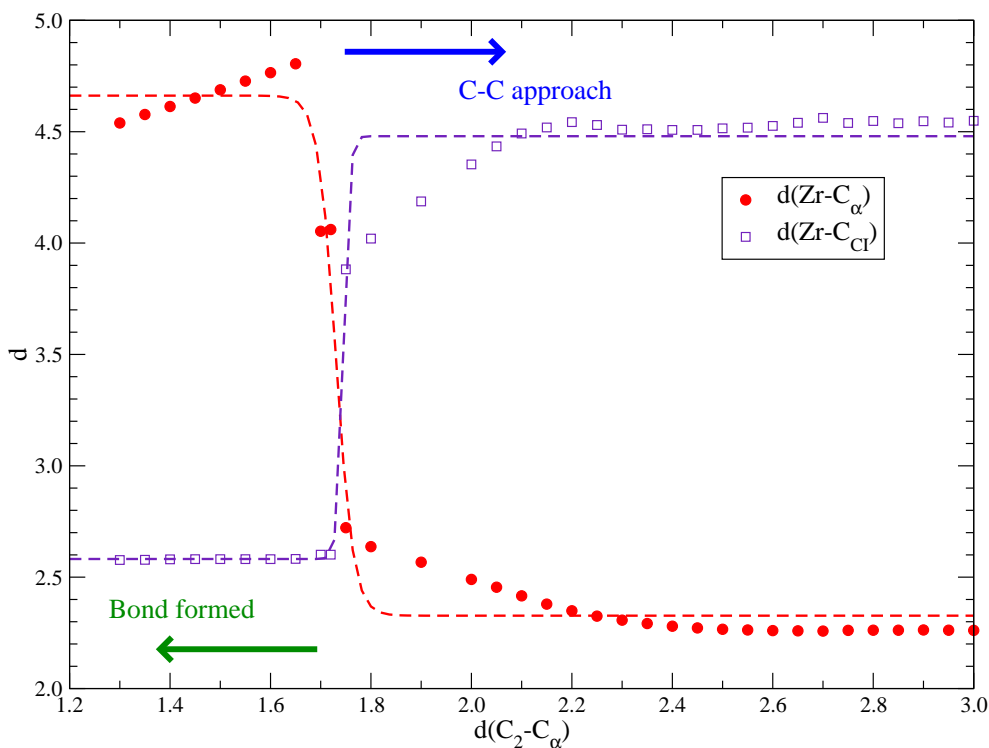


Figure 3.15: Transition between a zone where the C_2 carbon of the ethylene monomer is approaching the α carbon of the $[Cp_2ZrCH_3]^+/[CH_3B(CF_2Cl)_3]^-$ complex, and the region where the C_2-C_α bond is already formed. In the latter the C_α has broken its bond with the metal, namely $d(Zr-C_\alpha)$ abruptly increases to over 4.5 Å. This curve has been fitted to a Fermi-Dirac function (see text), and labeled FD-2 in Table 3.3. In that same region the $Zr-C_{Cl}$ bond is also regenerated, with a fast approach to a $d(Zr-C_{Cl})$ equivalent to that of the MET_{react} reactant. This curve has been also fitted to another Fermi-Dirac function, labeled FD-3 in Table 3.3. The values of both axes are given in Å.

Stationary points

As in the case of the bare cation, I have performed full geometry optimizations at the B3LYP/LanL2DZdp level at the relevant stationary points, namely reactants, π -complex, complexation and insertion TSs and product. *Single point* energies have also been obtained, for the LanL2DZdp geometries, at the B3LYP/TZ level.

A summary of the geometrical features of these stationary points follows. The nomenclature used to designate the atoms should be quite straightforward; however, the atoms mentioned are specified in Figure 3.16 (using MET_{TS2} as an example). The distances and angles mentioned below are summarized in Table 3.5.

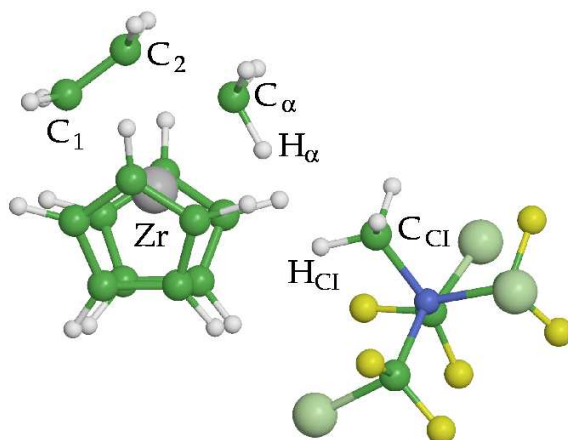


Figure 3.16: Scheme of the nomenclature used to designate relevant atoms in the $\text{Et} + [\text{Cp}_2\text{ZrCH}_3]^+ / [\text{CH}_3\text{B}(\text{CF}_2\text{Cl})_3]^-$ system.

In the $\text{MET}_{\text{react}}$ reactant only the α carbon seems to be directly bound to the metal, with a $\text{Zr}-\text{C}_\alpha$ distance of 2.278 Å, although the carbon in the methyl group of the counterion is actually very close to the zirconium atom, that is $d(\text{Zr}-\text{C}_{\text{Cl}}) = 2.533$ Å. Unlike in the case of the counterionless $\text{CAM}_{\text{react}}$ reactant, here the longest $\text{C}_\alpha-\text{H}_\alpha$ distance is only 1.101 Å, which points to an absence of agostic interaction with the metal center. Nevertheless the hydrogen atoms closest to the zirconium are those of the methyl group in the counterion. Two of them show a regular $d(\text{C}_{\text{Cl}}-\text{H}_{\text{Cl}}) = 1.10$ Å distance, and are 2.540 and

Parameter	MET _{react}	MET _{TS1}	MET _{comp}	MET _{TS2}	MET _{prod}
d(Zr-C _α)	2.278	2.264	2.258	2.305	4.717
d(Zr-C _{CI})	2.533	3.407	4.471	4.327	2.540
d(C ₂ -C _α)	–	3.125	3.161	2.229	1.539
d(Zr-C ₁)	–	3.394	2.896	2.442	2.299
d(Zr-C ₂)	–	3.344	2.921	2.689	3.340
d(C ₁ -C ₂)	1.340	1.344	1.350	1.408	1.542
d(C _{CI} -H _{CI})	1.116	1.115	1.099	1.100	1.116
d(C _α -H _α)	1.100	1.103	1.105	1.136	1.099
a(Zr-C _α -H _α)	115.8	104.6	106.4	69.8	–

Table 3.5: Selected geometric features of the stationary points of the Et + [Cp₂ZrCH₃]⁺/[CH₃B(CF₂Cl)₃]⁻ PEC. d(X-Y) denotes distance between X and Y, in Å. a(X-Y-Z) denotes the corresponding angle, with corner at Y, in degrees.

2.560 Å apart from the metal. The third hydrogen, however, is only 2.285 Å away from it, and shows a noticeable d(C_{CI}-H_{CI}) elongation to 1.116 Å. In Table 3.5, d(C₁-C₂) is also given for MET_{react}, but it refers to the C-C distance of the free ethylene double bond, namely 1.340 Å.

The monomer complexation occurs when an ethylene unit approaches the MET_{react} catalyst ion pair, after crossing a complexation TS labeled MET_{TS1}. In this TS both carbons in the monomer and the one in the methyl group of the counterion are placed at similar distances from the Zr center, namely d(Zr-C₁) = 3.394 Å, d(Zr-C₂) = 3.344 Å and d(Zr-C_{CI}) = 3.407 Å. No α-agostic interaction is noticeable, with a longest C_α-H_α distance of 1.103 Å.

In the MET_{comp} π-complex the Zr-C distances for the monomer carbons are 2.896 and 2.921 Å, and the d(Zr-C_α) distance actually shortens from 2.278 Å in the reactant, to 2.258 Å in the complex. At this stage the C₁-C₂ double bond is only slightly (albeit noticeably) affected, with a C₁-C₂ distance of 1.350 Å, whereas d(C₁-C₂) = 1.340 Å in the isolated monomer. The counterion has left its place completely to the incoming monomer, with a Zr-C_{CI} distance of 4.471 Å.

The π-complex evolves to the insertion product through the TS labeled MET_{TS2}. In this TS the Zr-C_α bond breaks, a C₁-C₂ double bond turns into a single bond and simultaneously two new bonds are formed: the Zr-C₁ one, and the C_α-C₂ one. The corresponding distances are: d(Zr-C_α) = 2.305 Å, d(Zr-C₁) = 2.442 Å, d(C₁-C₂) = 1.408 Å and d(C₂-C_α) = 2.229 Å. In this TS, one of the hydrogens on the α carbon interacts again with the metallic

Species	LanL2DZdp		TZ	
	ΔE	ΔG	ΔE	ΔG
$MET_{react} + Et$	0.00	0.00	0.00	0.00
MET_{TS1}	16.45	27.07	18.06	28.68
MET_{comp}	13.52	22.80	15.04	24.32
MET_{TS2}	16.78	28.87	19.51	31.59
MET_{prod}	-20.38	-6.24	-16.40	-2.26

Table 3.6: Energy differences (in kcal/mol) at selected stationary points for the insertion of ethylene into $[CH_3ZrCp_2]^+/[CH_3B(CF_2Cl)_3]^-$. Values obtained at the theory level shown, on the B3LYP/LanL2DZdp geometries.

center through an agostic interaction, and its $d(C_\alpha-H_\alpha)$ shows an elongation to 1.136 Å, with a Zr– H_α distance of only 2.189 Å, which gives rise to an acute Zr– C_α – H_α angle, even below 70 degrees. The counterion stays far from the metal, namely $d(Zr-C_{CI}) = 4.327$ Å.

The final product of this reaction, MET_{prod} features single Zr– C_1 (2.299 Å), C_1 – C_2 (1.542 Å) and C_2 – C_α (1.539 Å) bonds, with no γ -H agostic interaction in this case, because the propyl chain is oriented away from the metal.

The geometries, energy differences and potential energy profile corresponding to the commented PEC are shown in Figure 3.17, and the energies are given in Table 3.6.

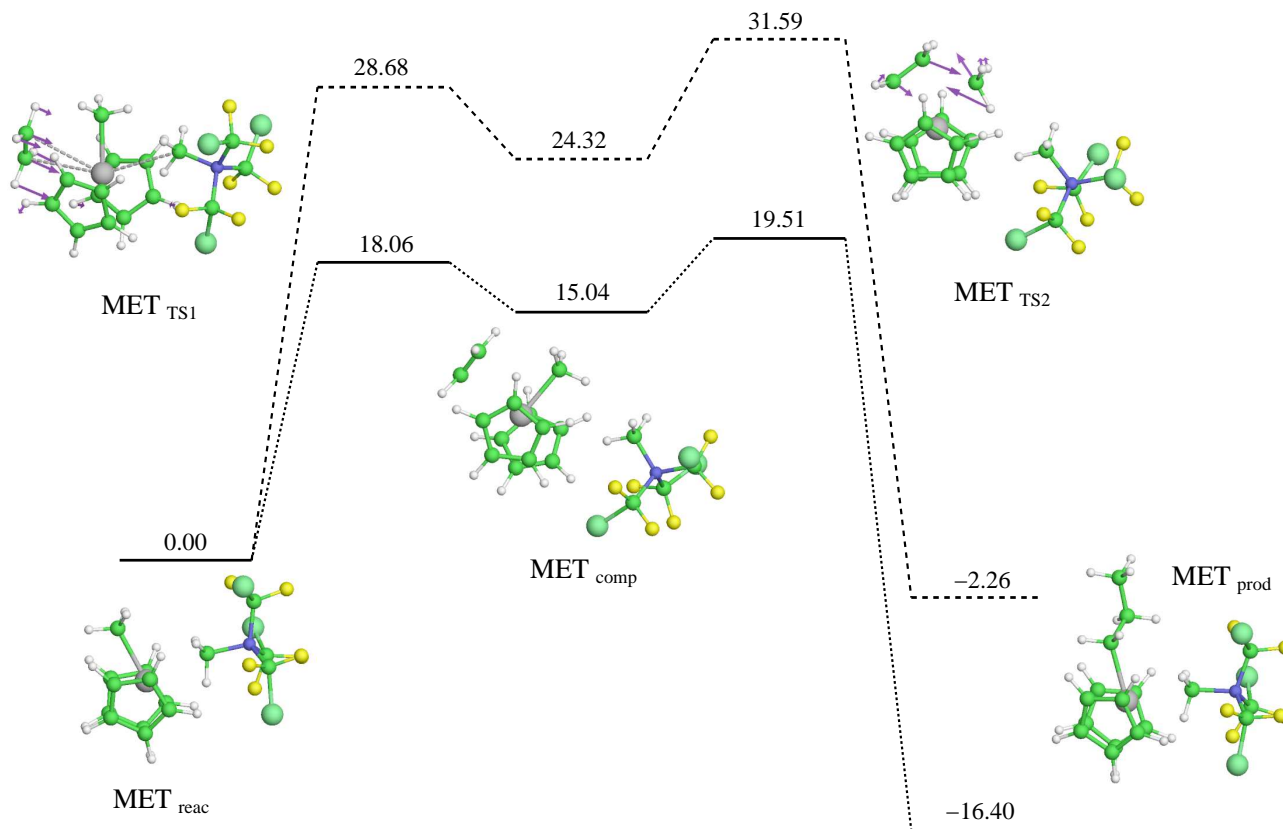


Figure 3.17: Stationary points along the $\text{Et} + [\text{CH}_3\text{ZrCp}_2]^+ / [\text{CH}_3\text{B}(\text{CF}_2\text{Cl})_3]^-$ reaction PEC. Solid lines correspond to electronic energies, and dashed lines to Gibbs free energies, both values in kcal/mol at the B3LYP/TZ//B3LYP/LanL2DZdp level. The arrows in MET_{TS1} and MET_{TS2} correspond to the motion of the atoms according to the normal mode with an imaginary frequency. The scale is arbitrary, but the relative moduli of the vectors match those of the Gaussian output.

Et+[CH₃CH₂ZrCp₂]⁺/[CH₃B(CF₂Cl)₃]⁻ results

In this case I have followed the same procedure as in the case of the methylated catalyst. Firstly a relaxed PEC scan has been performed, and four regions have been differentiated, fitting them to four distinct functions. The results are depicted in figure 3.18

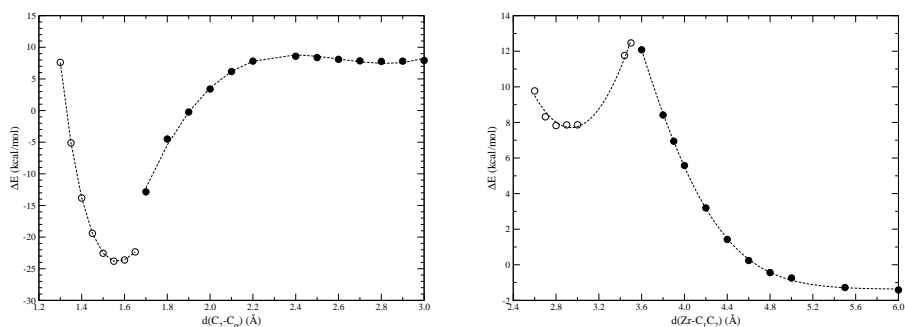


Figure 3.18: PEC corresponding to varying the C₂-C_α (left) and Zr-C₁C₂ (right) distances for the ethylene + [CH₃CH₂ZrCp₂]⁺/[CH₃B(CF₂Cl)₃]⁻ system. In each plot white and solid black circles have been used to distinguish the two surfaces (see text), and the corresponding fitted functions are represented by dashed lines. Distances in Å and energies in kcal/mol.

It is evident from Figure 3.18 that the differences with the methylated case are quantitative, rather than qualitative. The four regions have been fitted to homologous functions, with the optimized parameters shown in Table 3.8.

Stationary points

As in the case of the methylated zirconocene, the geometry optimizations have been performed at the B3LYP/LanL2DZdp level at the reactants, π -complex, complexation and insertion transition states and product. *Single point* energies have also been obtained, for the LanL2DZdp geometries, at the B3LYP/TZ level.

A summary of the geometrical features of these stationary points follows. The nomenclature for labeling the atoms is identical to that of the methylated zirconocene case (see Fig. 3.16), except that the (new) carbon atom bound to C_α has been tagged C_β. The distances and angles mentioned below are summarized in Table 3.7.

In the ET_{reac} reactant only the α carbon seems to be directly bound to the

Parameter	ET _{reac}	ET _{TS1}	ET _{comp}	ET _{TS2}	ET _{prod}
d(Zr-C _α)	2.284	2.273	2.243	2.310	4.725
d(Zr-C _{CI})	2.550	3.433	4.368	4.380	2.534
d(C ₂ -C _α)	–	3.199	2.831	2.319	1.546
d(Zr-C ₁)	–	3.346	2.766	2.475	2.297
d(Zr-C ₂)	–	3.320	2.827	2.677	3.332
d(C ₁ -C ₂)	1.340	1.344	1.359	1.399	1.542
d(C _{CI} -H _{CI})	1.116	1.113	1.099	1.099	1.116
d(C _α -H _α)	1.105	1.106	1.142	1.144	1.101
a(Zr-C _α -H _α)	101.5	98.0	74.3	66.4	–

Table 3.7: Selected geometric features of the stationary points of the Et + [Cp₂ZrCH₃]⁺/[CH₃B(CF₂Cl)₃]⁻ PEC. d(X-Y) denotes distance between X and Y, in Å. a(X-Y-Z) denotes the corresponding angle, with corner at Y, in degrees.

metal, with a Zr-C_α distance of 2.284 Å, although the carbon in the methyl group of the counterion is actually very close to the zirconium atom, that is d(Zr-C_{CI}) = 2.550 Å. As in the case of the methylated MET_{reac} reactant, the hydrogen atoms closest to the zirconium are those of the methyl group in the counterion. One of them is only 2.275 Å away from it, and shows a noticeable d(C_{CI}-H_{CI}) elongation to 1.116 Å.

The monomer complexation occurs when an ethylene unit approaches the ET_{reac} catalyst ion pair, after crossing a complexation TS labeled ET_{TS1}. In this TS both carbons in the monomer and the one in the methyl group of the counterion are placed at similar distances from the Zr center, namely d(Zr-C₁) = 3.346 Å, d(Zr-C₂) = 3.320 Å and d(Zr-C_{CI}) = 3.433 Å. No α-agostic interaction is noticeable, with both α hydrogens at a C_α-H distance of 1.104 and 1.106 Å.

In the π-complex, ET_{comp}, the Zr-C distances for the monomer carbons are 2.766 and 2.827 Å, and the d(Zr-C_α) distance actually shortens from 2.284 Å in the reactant, to 2.243 Å in the complex. At this stage the C₁-C₂ double bond is slightly elongated, with a C₁-C₂ distance of 1.359 Å, whereas d(C₁-C₂) = 1.340 Å in the isolated monomer. The counterion has left its place completely to the incoming monomer, with a Zr-C_{CI} distance of 4.368 Å. The presence of an α-agostic interaction is remarkable, because it contrasts with its absence in the MET_{comp} case. In ET_{comp} the C_α-H_α is elongated to 1.142 Å (3.7 pm longer than in MET_{comp}), and the Zr-C_α-H_α angle is as acute as 74.3° (32.1° more acute than that of MET_{comp}).

The π-complex evolves to the insertion product through the TS labeled

ZrCC Basin		ZrCC Approach		CC Basin		CC Approach	
A	7.68114	α	-1.37113	A	-23.8808	c_0	-563.395
B	25.4299	β	28.14398	B	72.7367	c_1	666.88
C	0.90796	γ	0.669329	C	1.89426	c_2	-257.534
D	2.87488	δ	2.54886	D	1.56691	c_3	32.9195
R	0.99879	R	0.99991	R	1.00000	R	0.99834

Table 3.8: Fitted constants for the Morse (first and third columns), Gaussian (second column), and third order polynomial (fourth column) fits corresponding, respectively, to the π -complex basin, monomer approach to Zr, C_1 - C_α binding and C_1 - C_α approach before binding, for the case of $\text{Et} + [\text{CH}_3\text{CH}_2\text{ZrCp}_2]^+ / [\text{CH}_3\text{B}(\text{CF}_2\text{Cl})_3]^-$. The last value, labeled R, gives the correlation coefficient between the fit and the calculated points.

ET_{TS2} . In this TS the Zr- C_α bond breaks, the C_1 - C_2 double bond turns into a single bond and simultaneously two new bonds are formed: the Zr- C_1 one and the C_α - C_2 one. The corresponding distances are: $d(\text{Zr}-C_\alpha) = 2.310 \text{ \AA}$, $d(\text{Zr}-C_1) = 2.475 \text{ \AA}$, $d(C_1-C_2) = 1.399 \text{ \AA}$ and $d(C_2-C_\alpha) = 2.319 \text{ \AA}$. In this TS, one of the hydrogens on the α carbon interacts again with the metallic center through an agostic interaction, showing an elongation of the C_α - H_α distance to 1.144 \AA , a Zr- C_α - H_α angle of merely 66.4° , and a Zr- H_α distance of only 2.127 \AA . The counterion stays far from the metal, namely $d(\text{Zr}-C_{CI}) = 4.380 \text{ \AA}$.

The final product of this reaction, ET_{prod} , features single Zr- C_1 (2.297 \AA), C_1 - C_2 (1.542 \AA), C_2 - C_α (1.546 \AA) and C_α - C_β (1.534 \AA) bonds, with no γ -H agostic interaction in this case, because the butyl chain is oriented away from the metal.

The geometries, energy differences, and potential energy profile so obtained are depicted in Figure 3.19, and the energy differences are summarized in Table 3.9.

Species	LanL2DZdp		TZ	
	ΔE	ΔG	ΔE	ΔG
$ET_{react} + Et$	0.00	0.00	0.00	0.00
ET_{TS1}	16.72	28.30	18.33	29.91
ET_{comp}	12.93	23.08	14.78	24.93
ET_{TS2}	12.98	25.46	15.36	27.84
ET_{prod}	-23.30	-9.06	-19.98	-5.74

Table 3.9: Energy differences (in kcal/mol) at selected stationary points for the insertion of ethylene into $[\text{CH}_3\text{CH}_2\text{ZrCp}_2]^+ / [\text{CH}_3\text{B}(\text{CF}_2\text{Cl})_3]^-$. Values obtained at the theory level shown, on the B3LYP/LanL2DZdp geometries.

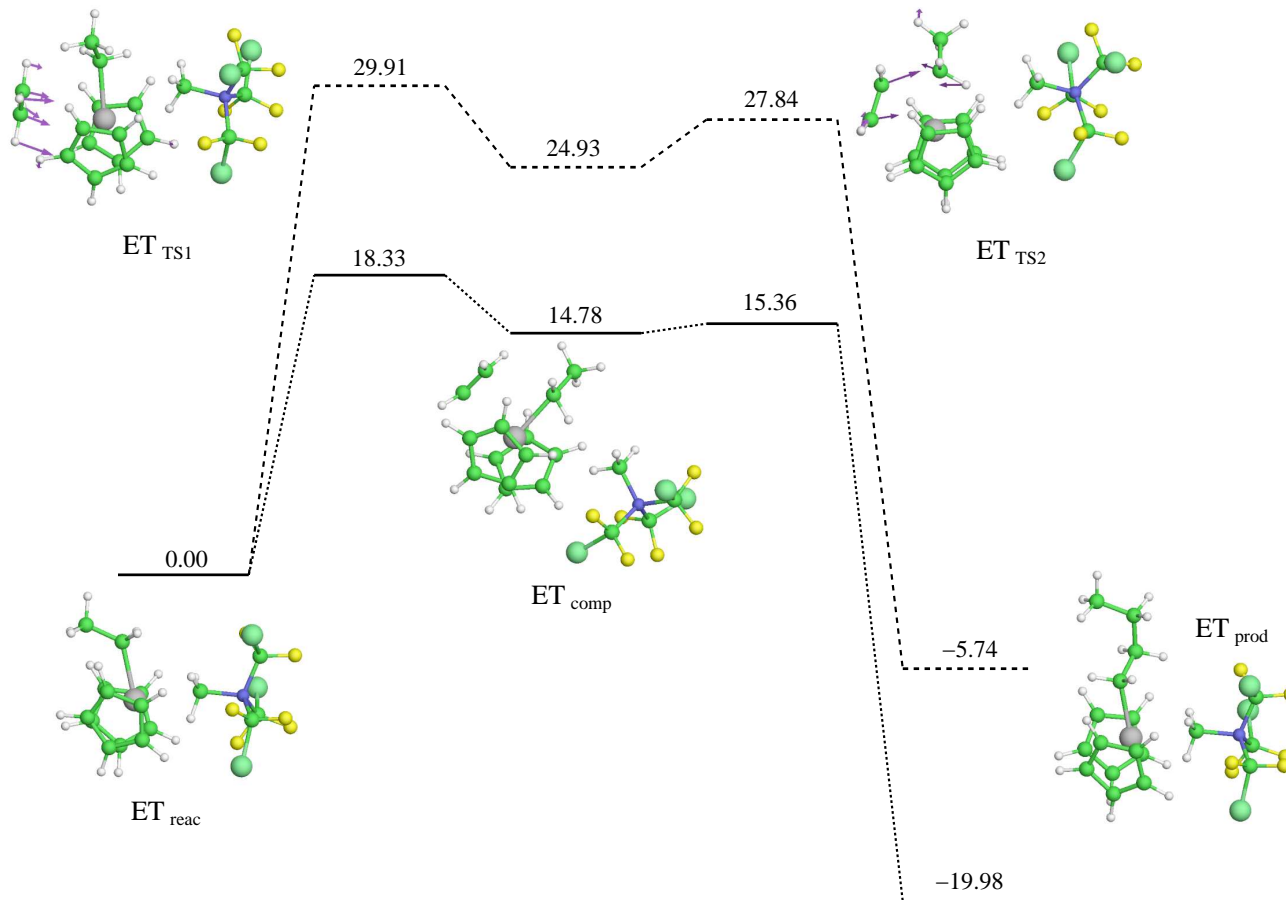


Figure 3.19: Stationary points along the Et + $[\text{CH}_3\text{CH}_2\text{ZrCp}_2]^+ / [\text{CH}_3\text{B}(\text{CF}_2\text{Cl})_3]^-$ reaction PEC. Solid lines correspond to electronic energies, and dashed lines to Gibbs free energies, both values in kcal/mol at the B3LYP/TZ//B3LYP/LanL2DZdp level. The arrows in ET_{TS1} and ET_{TS2} correspond to the motion of the atoms according to the normal mode with an imaginary frequency. The scale is arbitrary, but the relative moduli of the vectors match those of the Gaussian output.

3.5 Conclusions

3.5.1 Bare cation

Our quantum chemical results entitle us to shed some light over the questions posed previously. As we will see, the TM gives straightforward and simple answers to the three of them, but with the CAM, they are not so obvious.

The first question deals with the reaction rate order with respect to the monomer. Of course, all the considerations have to be made taking into account the free energy surface, for that is the surface traveled in any chemical reaction, as mentioned above.

Inspection of the mechanism proposed by Ystenes (see Figure 3.9) leads directly to a kinetic equation in close agreement with what is experimentally known. The reaction has only one step, and it is bimolecular.

In the case of the CAM, the closeness in free energy of the reactants and the complex (species $CAM_{react} + Et$ and CAM_{comp}), and the absence of a classic transition state between them, suggests that a very fast preequilibrium exists. In that case, bimolecularity of the whole reaction (i.e., first order of reaction rate with respect to both catalyst and monomer) could be derived. Recall that our electronic energy barrier for ethylene insertion (8 kcal/mol) and reaction exothermicity (22 kcal/mol), are in good agreement with the values by Morokuma *et al.*[47] for a silylene bridged zirconocene (less than 10 kcal/mol barrier, and around 30 kcal/mol exothermicity), but I go one step further, calculating ΔG , which gives us a different picture of the reaction. Firstly, the free energy barrier is different (higher), and secondly the π -complex is relatively close to the reactants' free energy.

In the case of the chain flipping, the energy barrier I get for the system considered is so low that the position of the growing chain should be expected to be random, equally distributed between both coordination sites. If experimental results make it unacceptable, then either any model that leaves a coordination site empty in some reaction step (e.g. CAM) must be discarded, or our model is too simple to account for some important subtleties that fix the growing chain in place (even when the other coordination site is empty). It is important to note, though, that, as mentioned in Section 2, there are some known metallocenic catalytic systems for which a facile chain inversion is indeed deduced from experiment[79]. Thus, Mohammed *et al.* mention two limit cases. When the chain inversion (flipping) rate is much higher than the monomer insertion one, Curtin-Hammet (CH) conditions are invoked. In this case, both states are fully equilibrated. When the opposite is true (insertion much faster than inversion), they use the term kinetic quenching (KQ). Our calculations predict CH conditions for the case under study, but KQ catalytic

systems must exist in order to obtain syndiotactic polymers. In the latter case, the mechanistical explanation Mohammed *et al.* give is that the effect of the counterion is to bind more or less strongly to the metallocene cation, and consequently to obstruct such inversion. In the case where the binding is stronger, the tacticity will increase (KQ conditions), but the polymerization rate will decrease (it will be harder for the incoming monomer to take the counterion's place).

Regarding the effect of other Lewis bases, I can conclude that their effect must be similar to the one of the counterion I mention above. Small amounts of Lewis bases present will increase tacticity and decrease propagation rate, although their effect will only be significant when the counterion is loosely bound to the metallocene cation (CH conditions), and will be masked by the counterion itself when it binds more strongly (closer to KQ conditions). These ideas do not collide with the ones by Vanka and Ziegler[68].

3.5.2 Inclusion of counterion

As mentioned in Section 3.4.5, the binding energy of the counterion is around 81 kcal/mol (in gas phase), which makes it rather unlikely that immersed in such an apolar solvent as n-heptane or other typical olefin polymerization medium the bare cation could be regarded as the active species. Experimental results[43] confirm that $[\text{CH}_3\text{B}(\text{C}_6\text{F}_5)^-]$ forms a contact ion pair with a similar metallocene (bisindenyl-dimethyl-zirconium), at least at moderate temperatures and in an apolar solvent. The results presented in the second part of the chapter are thus more representative of the reaction medium.

Having found two TSs in either PECs is quite revealing, and further clarification is obtained by the fact that both TSs are really close in energy. In fact, in the ethylated case the insertion barrier has an absolute height three kcal/mol *lower* than the complexation one. This data can help us understand why the reaction kinetics obey a first order law with respect to both catalyst and monomer (overall second order kinetics). It is so because the complexation step has a higher barrier than the one from the complex to the products, or, in other words, the complexation is the limiting step, not the insertion. Our results concur with similar propositions by other authors[72].

The picture we get when including the counterion is thus a hybrid of both CAM and TM. On one hand, the reaction proceeds in a two-step fashion, through a complexation and subsequent insertion, as hypothesized by Cossée and Arlman. On the other hand, the insertion TS is affected by the presence of a second electron donor, as Ystenes proposed in his *trigger* mechanism, albeit this electron donor would be the counterion itself, and not a second monomeric unit.

The effect of the Lewis bases is also evident within this framework: the complexation step can and will be traversed by other (not the monomer) Lewis bases, but it will be reversible, since only the monomer will proceed to insertion. That is why Lewis bases can reduce slightly the polymerization rate (they “occupy” a fraction of the catalyst), but do not inhibit the catalyst action.

With regard to the side-chain flipping, I have to admit that the reaction path presented here would lead, apparently, to a polymer growth where the chain would always remain in the same coordination site of the metal. This would fit into a “chain stationary” insertion type described by some authors[59]. However further study needs to be done on chain inversion mechanisms and barriers.

In summary, I have pointed out the importance of calculating Gibbs free energy profiles, in addition to the usual electronic energy ones, to give insight into the reaction path followed by the system under study, as well as including the counterion into the calculations.

I conclude that detailed energetic calculations are imperative in such systems, provided that there are two TSs apparently very close in energy.

Chapter 4

Extension to Ti and Hf

Contents

4.1	Introduction	68
4.2	Methods	69
4.3	Results and discussion	71
4.3.1	PEC scan	71
4.3.2	Stationary points	82
4.4	Conclusions	91
4.5	Acknowledgements	91

4.1 Introduction

“En las vías, las mismas flores se agitaban por distintos vientos.”¹

Melocotones helados, Espido Freire

The elucidation at a molecular level of the mechanism of olefin polymerization by Group 4 transition metal complexes such as metallocenes[46, 53, 92, 51, 74, 93, 94, 95], “Constrained Geometry Catalyst” (CGC)[51, 93, 59, 96, 97, 98] or other post-metallocenes[99, 72, 100] has attracted great interest. Despite the over 40 years since the proposal of the most widely accepted mechanism by Cossée and Arlman[19, 20, 21, 22, 23] some questions remain, and theoretical calculations on the reactive species should still be helpful to shed light on the reaction mechanism.

In order to model the molecular structures playing an active role in the reaction site, one would like to include in the calculations not only the catalyst cation (which bears the transition metal active site), the incoming monomer and the growing polymer chain, but also the anionic counterpart for the metal, that is, the counterion (CI). The experimentally, and industrially, most used counterion is the methyl aluminoxane (MAO), which, not only activates the metallocenic catalyst making it a cation, but also regulates its affinity towards the monomer complexation, through a higher or lower degree of binding to the metal.

Unfortunately, MAO is not a molecularly well-defined species, and the substance employed in the industry is probably a mixture of different moieties[92]. A common workaround for this situation consists in substituting the MAO with a well-defined molecule that plays the same role. Such a molecule can be found among a family of boron compounds, one of which is $B(C_6F_5)_3$.

In Chapter 3 I stated that the inclusion of the full counterion species $[CH_3B(C_6F_5)_3]^-$, would increase the computational workload considerably, and thus I chose to use a smaller model for it, namely $[CH_3B(CF_2Cl)_3]^-$. However, an increase of computing power has enabled me to extend the calculations to include the actual $[CH_3B(C_6F_5)_3]^-$ counterion, and so I am able to compare the results with both CIs.

The aim of the present chapter is to take advantage of this model to analyze the effect of the substitution of zirconium by its first- and third-row transition metal counterparts, namely titanium and hafnium, in view of the long standing apparent controversy raised by various interpretations of experiments and theoretical calculations. On this regard, some authors[92, 101, 102] consider Zr as the most active metallic center for a number of metallocenic or

¹On the railway, the same flowers were shaken by different winds.

post-metallocenic olefin polymerization catalysts, while others[103, 104] have found a similar activity for Zr and Ti, and yet others[105, 106, 107] reckon Ti as the most active, at least at low temperatures.

Besides the metallic center comparison, the feasibility of three different monomer approach paths will be discussed, namely those depicted in Figure 4.1. Ziegler and Yang[95] have very recently studied a system identical to ours, limited to $M = \text{Zr}$, and $\text{CI} = \text{CI}_R$, and they take into account the *Endo* and *Exo* paths (which they call *cis* and *trans*, respectively).

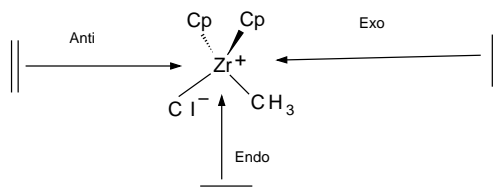


Figure 4.1: Three possible monomer approach paths for the considered metallocenic catalyst.

As a side effect, I gather further evidence of the suitability of my CI model as a convenient theoretical substitute for the real one.

4.2 Methods

My first step is to use relatively low, although reliable enough, level quantum calculations to sketch a potential energy curve (PEC) for the approach of the monomer to the metal, and then to perform more accurate calculations on the stationary points.

My active catalyst consisted in a $[\text{Cp}_2\text{MCH}_3]^+/\text{CI}_X^-$ complex, where $M = \text{Ti}$, Zr and Hf , and CI stands for counterion: $\text{CI}_R^- = [\text{CH}_3\text{B}(\text{C}_6\text{F}_5)_3]^-$ and $\text{CI}_M^- = [\text{CH}_3\text{B}(\text{CF}_2\text{Cl})_3]^-$. The monomer was ethylene in all the calculations. I will refer to the moieties containing $M = \text{Ti}$ as titanocenes (Tc), and similarly zirconocenes (Zc) and hafnocenes (Hc) for $M = \text{Zr}$ and Hf , respectively.

I have performed three types of calculations throughout this work. First, relaxed PEC scans have been performed for the approach and insertion of a monomer unit into the growing chain attached to the zirconocenyl catalyst. For these scans I chose SKBJ effective core potential (ECP) basis set[80, 81, 82], as defined in the Extensible Computational Chemistry Environment Basis Set Database[32]. I chose such basis set for performance considerations, since it has all of the core electrons described by pseudopotential functions, and only the valence shell of each element is described with Gaussian basis functions,

thus reducing the computational expense considerably. In order to better describe the anions, I have extended the SKBJ basis set by adding a set of diffuse functions, consisting of a S-type function with an exponent 1/3 that of the previously most diffuse one for each element. I have called such basis set SKBJ+.

With regard to the theoretical method used, it is worth noting that the lack of a pruned grid for the Zr element for the computation of the spatial integrals in the DFT method leads to a enormous performance loss (through the use of unpruned grids). I have tried to overcome this by optimizing the $[\text{Cp}_2\text{ZrCH}_3]^+/\text{CI}_R^-$ species along the PEC at HF/SKBJ level, then refining the final energy through a B3LYP/SKBJ *single point* calculation. Thus B3LYP/SKBJ//HF/SKBJ energies have been used to build up a PEC for $[\text{Cp}_2\text{ZrCH}_3]^+/\text{CI}_X^-$, where X = real and model, in order to compare the CI_M to CI_R , and then B3LYP/SKBJ energies for $[\text{Cp}_2\text{ZrCH}_3]^+/\text{CI}_M^-$ have also been taken from Chapter 3, to compare B3LYP//HF and full B3LYP PECs.

Second, geometry optimizations and subsequent frequency calculations have been carried out for the stationary points found in this zirconocene PEC, and the titanocene and hafnocene counterparts (for the latter two, PEC calculations have not been performed). For these optimizations I have made use of the LanL2DZdp basis set, which is an extension of the LanL2DZ basis set[83, 84, 85], supplemented with diffuse and polarization functions[86]. Unfortunately there is no such extension for boron, titanium, zirconium or hafnium, so I have used the bare LanL2DZ basis set for these elements. The LanL2DZ basis set is a pseudopotential one, as it is SKBJ, but with a smaller core described with ECPs, so that an increase in accuracy is expected, at the expense of an actual increase in computational cost.

The LanL2DZdp optimizations and frequency calculations have all been performed at the B3LYP level, for reactant, complexation TS, monomer π -complex, insertion TS and inserted product, for CI_M (and all three metals). All the frequency calculations have come up with real frequencies for all the normal modes of the local minima, and one and only one imaginary frequency (negative force constant) for the transition states. I have also confirmed that in every case the negative force constant corresponded to the desired normal mode.

Due to computational limitations, transition states have not been optimized for CI_R , and only two optimized geometries incorporating CI_R have had their frequencies calculated. Although the LanL2DZdp optimizations could have been performed, the subsequent frequency calculations (in order to make sure that one and only one vibrational mode with a negative force constant (imaginary frequency) and appropriate atomic motions was present),

would have been too expensive, and their lack would render the optimized TSs virtually useless. Minima have been accepted without frequency test, but I would not feel confident doing so with the TSs. The frequency calculations indeed performed, namely for Zc_{react}^{real} and Zc_{comp}^{real} (zirconocene with $CI = CI_R$, reactant and π -complex, respectively) in the *Exo* path, were carried out (at a great expense) in order to have at least one model vs. real ΔG .

Third, *single point* energy calculations have been done (on all the geometries previously optimized at the LanL2DZdp level) at the B3LYP/6-311++G(3df,3pd) level. This basis set is widely known, and was used as implemented in Gaussian, for all the elements except for the titanium, zirconium and hafnium, for which the SDD basis set was used, as implemented in Gaussian. I have called this basis set TZ throughout this thesis.

All the calculations have been carried out using the GAUSSIAN 98[34] and GAUSSIAN 03[35] packages, and the Hartree-Fock (HF) and B3LYP density functional (DFT) methods, as implemented therein.

For the ball-and-stick graphical representation of molecules, the Raster3D software[3] has been extensively used throughout this article. Various graphs and schematic figures have been produced with Grace[88], Xfig[89] and ChemTool[87].

4.3 Results and discussion

4.3.1 PEC scan

Relaxed potential energy surface scans were performed for $[Cp_2ZrCH_3]^+/CI_X^-$, $X = R$ (real) or M (model). These scans are equivalent to those performed in the previous chapter, but with a less expensive HF/SKBJ+ optimization, followed by a B3LYP/SKBJ+ *single point* on each optimized geometry. As in that chapter, I have scanned the Zr-C₁C₂ distance, meaning a fixed (and equal) Zr-C distance for both carbon atoms of the incoming ethylene monomer. All other variables were relaxed (optimized) at each Zr-C₁C₂ point. The C₂-C _{α} distance has also been used as pseudo-reaction coordinate in an additional PEC scan. C _{α} designates the carbon atom of the methyl group bound to the metal cation in the reactant. Similarly, C₁ designates the carbon, belonging to the incoming monomer, that will bind to the zirconium cation in the product and C₂ designates the carbon atom of the monomer that will bind to C _{α} . Recall that the reference energy for calculating the ΔE s (the Y-axis values of the PECs) has been taken as the sum of those of infinitely separated ethylene and $[Cp_2ZrCH_3]^+/CI_X^-$ ($X = R$ and M).

The present chapter, however, considers another two possible monomer approach paths, which the previous chapter did not. A careful inspection

of the catalyst geometry shows that there are three possible such paths, as depicted in Figure 4.1, in Section 4.1. The previous chapter featured the “*Exo*” path, and here I consider all three of them.

Two regions have been distinguished in each scan. Figure 4.2 depicts them for the *Exo* approach to $[\text{Cp}_2\text{ZrCH}_3]^+/\text{CI}_M^-$ (circles) and $[\text{Cp}_2\text{ZrCH}_3]^+/\text{CI}_R^-$ (squares). Notice that the qualitative features of the CI_M curves are identical to those of the CI_R ones. A more quantitative comparison of model/real PECs will be done further on in this section.

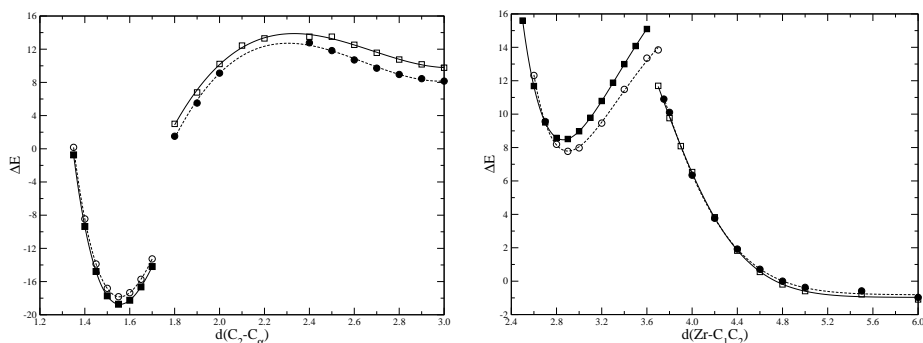


Figure 4.2: PEC corresponding to varying the $\text{C}_2\text{-C}_\alpha$ (left) and $\text{Zr-C}_1\text{C}_2$ (right) distances for the $\text{Et} + [\text{Cp}_2\text{ZrCH}_3]^+/\text{CI}_M^-$ (circles) and $\text{Et} + [\text{Cp}_2\text{ZrCH}_3]^+/\text{CI}_R^-$ (squares) systems at the B3LYP//HF level. In each plot white and solid black symbols have been used to distinguish the two surfaces (see text), and the corresponding fitted functions are represented by solid (CI_R) and dashed (CI_M) lines. Distances in Å and energies in kcal/mol.

A description of these scans follows. In the $\text{Zr-C}_1\text{C}_2$ scan (right hand side of Figure 4.2), as the monomer approaches the metal from $d(\text{Zr-C}_1\text{C}_2) = 6.0$ to 3.7 Å, a monotonically increasing energy profile is found. This region has been fitted to a Gaussian function (Eq. 4.1), and the corresponding parameters are given in Tables 4.1 and 4.2. In the same scan, as the monomer gets still closer, a complexation basin is observed for $d(\text{Zr-C}_1\text{C}_2) = 3.6$ to 2.5 Å. Here the monomer has displaced the counterion in the coordination sphere of the metal. Such region has been fitted to a Morse-type function (Eq. 4.2), and corresponds to the π -complex intermediate (parameters also given in Tables 4.1 and 4.2). These two regions are differentiated because, whereas in the monomer approach curve, the CI is still closely bound to the metal cation, in the complexation basin the CI has been displaced. The $d(\text{Zr-C}_{CI})$ vs. $d(\text{Zr-C}_1\text{C}_2)$ curves are depicted in Figure 4.3 for both CI_M and CI_R .

The rapid transition from a metal-bound counterion and a displaced one

can be given a mathematical treatment, fitting the $d(\text{Zr}-C_{CI})$ vs. $d(\text{Zr}-C_1C_2)$ curves to Fermi-Dirac type functions (Eq. 3.3). The corresponding parameters can be found at Tables 4.3 (model CI) and 4.4 (real CI), under the headers FD-1M and FD-1R, respectively. These parameters can be given a physical meaning, as follows. Y_0 represents the $d(\text{Zr}-C_{CI})$ value (in Å) for infinitely large $d(\text{Zr}-C_1C_2)$. $Y_0 + Y_1$ represents the $\text{Zr}-C_{CI}$ distance when $d(\text{Zr}-C_1C_2)$ is small; in other words, when the monomer is already complexated to the metal. The $\text{Zr}-C_1C_2$ distance for which the transition happens is precisely x_0 , and the width of the transition zone can be considered to be proportional to the value of δ (see Section 3.4.6).

Path	ZrCC Basin		ZrCC Approach		CC Basin		CC Approach	
<i>Exo</i>	A	7.61116	α	-1.84646	A	-18.6701	c_0	-492.446
	B	11.2054	β	26.4354	B	88.5348	c_1	587.591
	C	1.60645	γ	0.727531	C	1.7958	c_2	-225.017
	D	2.89697	δ	2.73705	D	1.55696	c_3	28.248 5
	R	0.999173	R	0.999295	R	0.999998	R	0.997892
<i>Anti</i>	A	5.47548	α	-2.5875	A	-18.6701	c_0	-
	B	21.7581	β	18.8088	B	88.5348	c_1	-
	C	1.27002	γ	0.704715	C	1.7958	c_2	-
	D	2.86108	δ	2.6367	D	1.55696	c_3	-
	R	0.999997	R	0.999827	R	0.999998	R	-
<i>Endo</i>	A	0.194255	α	-2.70287	A	-18.670100	c_0	-541.215
	B	17.1952	β	8.63988	B	88.534800	c_1	675.678
	C	1.45306	γ	0.774687	C	1.795800	c_2	-270.025
	D	2.83936	δ	3.38002	D	1.55696	c_3	35.1313
	R	0.999979	R	0.99997	R	0.999998	R	0.998769

Table 4.1: Fitted constants for the Morse (first and third columns), Gaussian (second column), and third order polynomial (fourth column) fits corresponding (from left to right) to the π -complex basin, monomer approach to Zr, C_2-C_α binding and C_2-C_α approach before binding, for the case of $Et + [CH_3ZrCp_2]^+/Cl_M^-$ at the B3LYP/SKBJ+//HF/SKBJ+ level. The last value, labelled R, gives the correlation coefficient between the fit and the calculated points.

Path	ZrCC Basin		ZrCC Approach		CC Basin		CC Approach	
<i>Exo</i>	A	8.96127	α	-1.10395	A	-18.5028	c_0	-457.767
	B	14.6738	β	38.9636	B	83.0258	c_1	546.276
	C	1.46163	γ	0.561594	C	1.84231	c_2	-208.025
	D	2.82998	δ	2.30872	D	1.55655	c_3	25.981
	R	0.996723	R	0.998912	R	0.999948	R	0.996426
<i>Anti</i>	A	5.76332	α	-2.3905	A	-18.5028	c_0	-764.249
	B	8.60001	β	16.5933	B	83.0258	c_1	921.72
	C	1.85174	γ	1.02316	C	1.84231	c_2	-359.82
	D	2.86627	δ	2.83559	D	1.55655	c_3	46.0947
	R	0.999654	R	0.999328	R	0.999948	R	0.996733
<i>Endo</i>	A	0.371691	α	-2.72463	A	-18.5028	c_0	-505.645
	B	21.9267	β	14.1854	B	83.0258	c_1	634.704
	C	1.31276	γ	0.782209	C	1.84231	c_2	-254.02
	D	2.83141	δ	3.12753	D	1.55655	c_3	32.974
	R	0.999988	R	0.999474	R	0.999948	R	0.998576

Table 4.2: Fitted constants for the Morse (first and third columns), Gaussian (second column), and third order polynomial (fourth column) fits corresponding, respectively, to the π -complex basin, monomer approach to Zr, C₂-C _{α} binding and C₂-C _{α} approach before binding, for the case of Et + [CH₃ZrCp₂]⁺/Cl_R⁻ at the B3LYP//HF level. The last value, labelled R, gives the correlation coefficient between the fit and the calculated points.

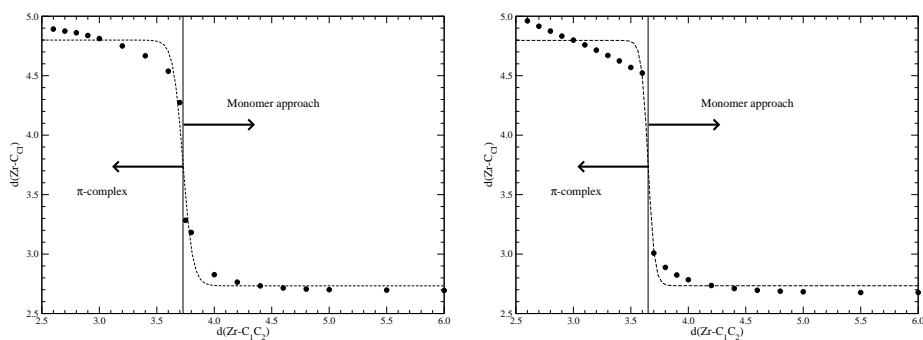


Figure 4.3: From right to left, transition between a zone where the ethylene monomer is merely approaching the metallic center of the $[\text{Cp}_2\text{ZrCH}_3]^+/\text{Cl}_X^-$ complex, and the region where it is already complexated, where $X = \text{M}$ (left) and R (right). The dots correspond to the calculated values, and the dashed line represents a fit to a Fermi-Dirac function. The fitting parameters are given in Tables 4.3 and 4.4 with labels FD-1M and FD-1R, respectively. All values in \AA .

	FD-1M	FD-2M	FD-3M
Y_0	2.73305	Y_0 2.34944	Y_0 4.71964
Y_1	2.06638	Y_1 1.65931	Y_1 -1.99655
x_0	3.72776	x_0 1.79632	x_0 1.77672
λ	0.04213	λ 0.003995	λ 0.01607
R	0.994973	R 0.990925	R 0.999004

Table 4.3: Constants for the Fermi-Dirac fits to the $d(\text{Zr}-\text{C}_{CI})$ vs. $d(\text{Zr}-\text{C}_1\text{C}_2)$ (FD-1M), and $d(\text{Zr}-\text{C}_\alpha)$ and $d(\text{Zr}-\text{C}_{CI})$ vs. $d(\text{C}_2-\text{C}_\alpha)$ (FD-2M and FD-3M, respectively) plots. They all refer to the case of $\text{Cl} = \text{Cl}_M$.

It is apparent that, when the monomer approaches the metallic center, the counterion is displaced (be it Cl_R or Cl_M) from its equilibrium distance of 2.73 \AA from the zirconium, to almost 4.80 \AA away from it, and this happens when the monomer/Zr distance is around $x_0 = 3.73 \text{ \AA}$ (3.65 \AA for Cl_R). This transition happens in around $4.6\lambda = 0.19 \text{ \AA}$ of monomer displacement (0.13 \AA for Cl_R).

The next step of this reaction consists on the formation of the $\text{C}_2-\text{C}_\alpha$ bond. The corresponding scan is depicted in the left hand side of Figure 4.2. In that scan a transition region can be assigned to $d(\text{C}_2-\text{C}_\alpha) = 3.0$ to 1.8 \AA , which has been fitted to a third-order polynomial. This region is characterized by a

	FD-1R	FD-2R	FD-3R
Y_0	2.73376	Y_0 2.35855	Y_0 4.65755
Y_1	2.06299	Y_1 1.67770	Y_1 -1.94717
x_0	3.64982	x_0 1.79670	x_0 1.79535
λ	0.02797	λ 0.00294	λ 0.003159
R	0.994828	R 0.99168	R 0.991175

Table 4.4: Constants for the Fermi-Dirac fits to the $d(\text{Zr}-C_{CI})$ vs. $d(\text{Zr}-C_1C_2)$ (FD-1R), and $d(\text{Zr}-C_\alpha)$ and $d(\text{Zr}-C_{CI})$ vs. $d(C_2-C_\alpha)$ (FD-2R and FD-3R, respectively) plots. They all refer to the case of $CI = CI_R$.

long $\text{Zr}-C_{CI}$ distance (displaced counterion), and a short $\text{Zr}-C_\alpha$ distance (α carbon still bound to the metal).

For closer C_2-C_α distances a C-C bond-formation region is found (which corresponds to the insertion product). This region is characterized by a short $\text{Zr}-C_{CI}$ distance (the counterion takes its place back in the Zr coordination sphere), and a long $\text{Zr}-C_\alpha$ distance (α carbon jumps to a γ position, once the monomer has inserted its two carbons between it and the metal). The $d(\text{Zr}-C_{CI})$ and $d(\text{Zr}-C_\alpha)$ vs. $d(C_2-C_\alpha)$ plots are depicted in Figure 4.4. These plots can also be fitted to Fermi-Dirac equations, and the fitting parameters are given in Table 4.3, under the FD-2M and FD-3M headings (for $CI = CI_M$), and Table 4.4, under the FD-2R and FD3R headings (for $CI = CI_M$).

The PECs of the left hand side of Figure 4.2 have been also fitted to a Morse-type potential. The parameters for these fits are given in Tables 4.1 and 4.2.

$$V_{Gauss} = \alpha + \beta e^{-\gamma(x-\delta)^2} \quad (4.1)$$

$$V_{Morse} = A + B(1 - e^{-C(x-D)})^2 \quad (4.2)$$

For CI_R , the four regions are quite similar to those of the CI_M ones (Figure 4.2). The curves can be fitted to the corresponding model functions, and the fitted parameters are provided in Table 4.2.

In order to be able to assess the reliability of my CI_M compared to CI_R , the fitted functions have been used. With each one of them I have defined a difference ϵ as the square root of the averaged square of the difference between the fitted function for CI_R , and the one for CI_M (see Eq. 4.3). The values of the differences so defined are given in Table 4.5.

$$\epsilon_{\alpha|\beta}^2 = \frac{1}{x_2 - x_1} \int_{x_1}^{x_2} (V_\alpha(x) - V_\beta(x))^2 dx \quad (4.3)$$

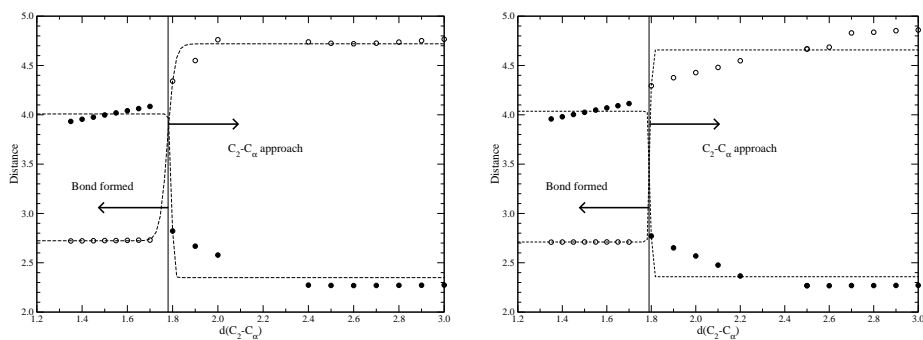


Figure 4.4: From right to left, transition between a zone where a carbon atom of the ethylene monomer is approaching the α carbon of the metallic center of the $[\text{Cp}_2\text{ZrCH}_3]^+/\text{Cl}_X^-$ complex, and the region where they are already bound, where $X = \text{M}$ (left) and R (right). The dots correspond to the calculated values for $d(\text{Zr}-\text{C}_\alpha)$ (black circles) and $d(\text{Zr}-\text{C}_{\text{Cl}})$ (white circles). The dashed lines represent the fits to a Fermi-Dirac function. The fitting parameters are given in Tables 4.3 and 4.4 with labels FD-2M, FD-3M, FD-2R and FC-3R, respectively. All values in \AA .

Region	<i>Exo</i>	<i>Anti</i>	<i>Endo</i>
ZrCC basin	1.84	0.86	0.51
ZrCC approach	1.74	0.48	0.43
CC basin	0.11	0.11	0.11
CC approach	2.14	-	0.73

Table 4.5: Energetic differences defined in Eq. 4.3 for the model/real CI PEC comparisons. Values in kcal/mol.

It is apparent from Table 4.5 that the discrepancy between the results obtained with the model CI and the real one (both at the same level of theory, namely B3LYP/SKBJ+//HF/SKBJ+) is close to, and in some cases even within, chemical accuracy (less than 1 kcal/mol).

Additionally, approximate stationary points have been extracted from the fitted functions, in the following manner: the complexation TS (TS1) has been taken as the calculated crossing point of the V_{Gauss} of the ZrCC approach zone and the V_{Morse} of the ZrCC basin; the π -complex corresponds to the minimum of the V_{Morse} of the ZrCC basin; the insertion TS (TS2) is the maximum in the 3rd grade polynomial of the CC approach zone; and the product is identified with the minimum in the V_{Morse} of the CC basin. The

values obtained for the energies are given in Table 4.6, and the geometrical parameters in Table 4.7. The potential energy values can be briefly compared to those by Yang and Ziegler[95], who also calculate them for the *cis* and *trans* paths (my *Endo* and *Exo*, respectively). Although they perform Car-Parrinello/AMBER95 QM/MM molecular dynamics, some similarities can be found. They find a lower TS1 for the *Endo* approach (6.0 *vs.* 15.9 kcal/mol), as I do (9.2 *vs.* 15.2 kcal/mol), whereas the ordering is reversed for TS2 (16.2 *vs.* 15.3 kcal/mol), which is not true with my results, but still they give much closer TS2 energies for both approaches, than TS1 did (12.5 *vs.* 14.4 kcal/mol). Intriguingly, our CI_M energetic results are much closer to their CI_R ones than our (aforementioned) CI_R results. Regarding the geometries, Yang and Ziegler come up with a $d(\text{Zr-X})$ value (where X denotes the center of masses of C_1 and C_2) of 3.38 Å for the *Endo* approach, and ours would be around 3.54 Å. However, their *Exo* TS1 would feature a significantly shorter Zr-X distance (3.22 Å), while ours has it only slightly shorter (3.49 Å). The π -complexes show a similar trend: their *Endo* $d(\text{Zr-X})$ is longer than their *Exo* one (2.87 *vs.* 2.74 Å), whereas ours are equal (2.75 Å). For the TS2s they obtain almost equal C_2-C_α distances for the *Endo* and *Exo* paths (2.12 and 2.11 Å, respectively). My results agree for the *Endo* path (2.15 Å), but are significantly different for the *Exo* one (2.33 Å).

The energetic and geometric values for the *Anti* and *Endo* products are not given in Tables 4.6 and 4.7 because the C-C bond formation basin has been taken as identical for all three paths (see below). The values for the *Anti* TS2 could not be obtained for $CI = CI_M$, due to technical limitations. This TS has a particularly long $\text{Zr}-C_{CI}$ distance, and my model tended to turn around and bind through a fluorine atom.

It is worth noting the fact that I have considered the CC basins (and thus the reaction products) to be one and the same for all three paths. The rationale behind this is as follows: the counterion is quite separated from the central metal in the insertion TSs (TS2), and it takes back its position in the coordination sphere of the metal quite easily after the C-C bond has been formed[95]. Upon visual inspection of the geometries of the *Endo* and *Anti* TS2 structures, it is apparent that in both cases the CI will go to the same place in the product. In addition to that, the *Exo* product is also equivalent to the *Endo* / *Anti* one, because what separates them is a rotation of the growing chain around the $\text{Zr}-C_\alpha$ bond. The energetic profile for that rotation is given in Figure 4.5. Inspection of that figure shows that, although the three maxima (and minima) do not have the same height and are not exactly equally spaced, they are close to indeed being. It is also evident that transition from any minimum to any other one requires a single jump over a barrier of

around 3.5 kcal/mol. This rotation barrier is not negligible, but, since the propagation reaction barrier is much higher (of the order of 20-30 kcal/mol), and the three rotation minima are close to degeneracy, it can be assumed that the product will distribute equally among the three states much faster than the next polymerization reaction step.

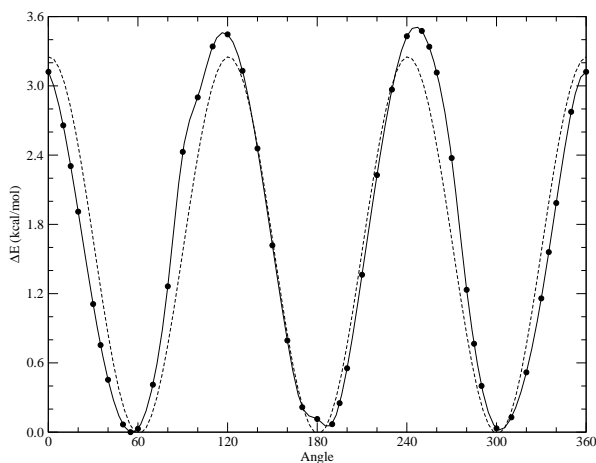


Figure 4.5: Energy profile for the rotation, along the Zr-C_α bond, of the growing chain R in [Cp₂ZrR]⁺/CI_M⁻, where R = propyl. The solid line corresponds to a cubic spline, and the dashed line to a simple period-three cosine fit.

	CI _M			CI _R		
	<i>Exo</i>	<i>Anti</i>	<i>Endo</i>	<i>Exo</i>	<i>Anti</i>	<i>Endo</i>
TS1	13.0	10.9	5.9	15.2	9.2	9.2
π-complex	7.6	5.5	0.2	9.0	5.8	0.4
TS2	12.4	-	12.5	14.4	13.1	12.5
Product	-18.7	-	-	-18.5	-	-

Table 4.6: ΔE values for the reaction stationary points, as obtained from the *Exo* PEC scans for [Cp₂ZrCH₃]⁺/CI_X⁻, X = M and R. All energies in kcal/mol.

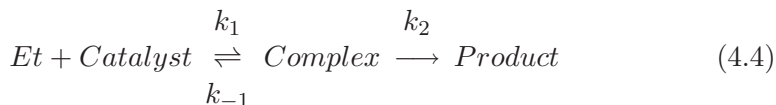
Reaction rate order from the PECs

The previous section makes it evident that I face a two-step reaction, with a high barrier for the (forward) first step, and a low one for both the forward

	Parameter	CI _M			CI _R		
		<i>Exo</i>	<i>Anti</i>	<i>Endo</i>	<i>Exo</i>	<i>Anti</i>	<i>Endo</i>
TS1	d(Zr-C ₁ C ₂)	3.63	3.41	3.43	3.55	3.42	3.60
π-complex	d(Zr-C ₁ C ₂)	2.90	2.86	2.84	2.83	2.87	2.83
TS2	d(C ₂ -C _α)	2.31	-	2.17	2.33	2.28	2.15
Product	d(C ₂ -C _α)	1.56	-	-	1.56	-	-

Table 4.7: Geometric parameters for the reaction stationary points, as obtained from the PEC scans for [Cp₂ZrCH₃]⁺/CI_X⁻, X = M and R. All distances in Å.

second step and the backward first step. The backward second step will be regarded as negligibly slow. This reaction, hence, can be given in short chemical notation as Eq. 4.4.



According to Eq. 4.4, and applying the stationary-state approximation, one obtains Eq. 4.5:

$$0 \sim \frac{d[Complex]}{dt} = k_1[Et][Catalyst] - k_{-1}[Complex] - k_2[Complex] \quad (4.5)$$

Since, by definition, $k_2[Complex] = d[Product]/dt$, minimal algebra gives Eq. 4.6.

$$\frac{d[Product]}{dt} = \frac{k_1 k_2}{k_{-1} + k_2} [Et][Catalyst] \quad (4.6)$$

Equation 4.6 shows that, under the proposed conditions, the propagation reaction rate is a bimolecular one, and that a global $k_T = \frac{k_1 k_2}{k_{-1} + k_2}$ can be calculated from the individual ones. If one assumes that $k_x = A \exp(-\Delta G_x/RT)$, and for pre-exponential factors that cancel out, it turns out that one can calculate a global reaction Gibbs free energy from the individual ΔG s of each step, as given by Eq. 4.7.

$$\Delta G_T = \Delta G_1 + \Delta G_2 + RT \ln \left(e^{-\Delta G_{-1}/RT} + e^{-\Delta G_2/RT} \right) \quad (4.7)$$

I will use Eq. 4.7 in the following section, where I calculate Gibbs free energies. However, up to this point, I have only calculated potential energy

profiles. Substituting Gibbs free energies for electronic energies in that equation, I could find an estimate of the global ΔE s that these scans predict for the three monomer approach paths, in the cases of CI_M and CI_R , for the zirconocene. These “global” ΔE s are given in Table 4.8, using a RT value of 0.596 kcal/mol ($T = 300K$).

Path	CI_M	CI_R
<i>Exo</i>	12.4	14.4
<i>Anti</i>	-	13.1
<i>Endo</i>	12.5	12.5

Table 4.8: Global reaction energy barriers for the propagation step of ethylene polymerization through an *Exo* monomer approach path, as calculated from Eq. 4.7 with values taken from PEC scans. Recall that I am using potential energies, and not free energies. All values in kcal/mol.

4.3.2 Stationary points

I picked the stationary points of the PEC scans, and optimized their geometries with the LanL2DZdp basis set: the maximum (complexation TS) and minimum (π -complex) of the $d(Zr-C_1C_2)$ scans, and the maximum (insertion TS) and minimum (product) of the $d(C_2-C_\alpha)$ scans, as well as the ethylene and metallocene moieties infinitely separated (reactants), and their energies were refined by means of *single point* energy calculations with the TZ basis set. This procedure was followed for the three monomer approach paths, and similar starting point geometries were used for $M = Ti$ and Hf (for which PEC scans were not performed). All the stationary points were calculated for $CI = CI_M$, but only local minima for $CI = CI_R$.

Figure 4.6 depicts the potential energy (PEC) and free energy (FEC) curves for each path of the zirconocenic catalyst. Titanocenic and hafnocenic catalyst curves are given in Appendix I. The optimized geometries for the reactant, complexation TS (TS1), π -complex, insertion TS (TS2) and product, are given in Figures 4.7–4.12, for the *Exo*, *Anti* and *Endo* monomer approach paths to zirconocene. Geometries for the titanocenic and hafnocenic counterparts is also available in Appendix I.

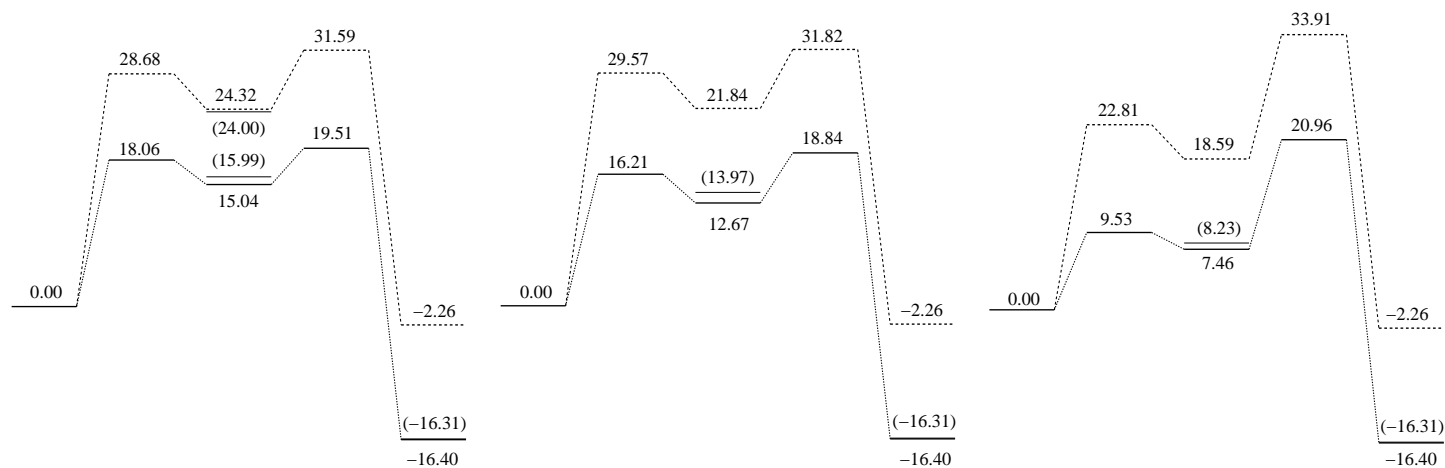


Figure 4.6: Stationary points along the $\text{Et} + [\text{Cp}_2\text{ZrCH}_3]^+/\text{CI}_M^-$ reaction PECs (solid line) and FECs (dashed line), for the *Exo* (left), *Anti* (middle) and *Endo* (right) monomer approach paths. The values for $\text{CI} = \text{CI}_R$ are given in parentheses, where calculated. All values in kcal/mol at the B3LYP/TZ//B3LYP/LanL2DZdp level.

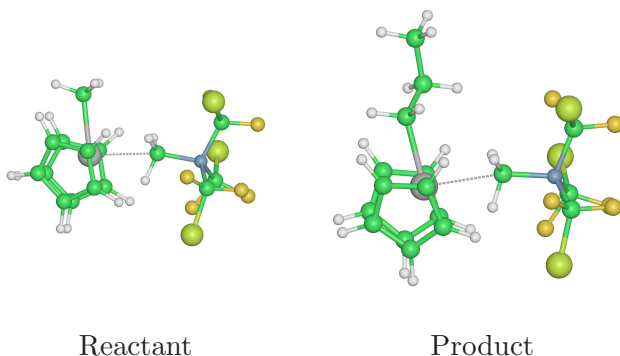


Figure 4.7: Geometries for the reactant and product of the insertion reaction of the first ethylene monomer into the $[\text{Cp}_2\text{ZrCH}_3]^+/\text{Cl}_M^-$ catalyst. These two geometries are common for the three different approach paths to the zirconocene catalyst.

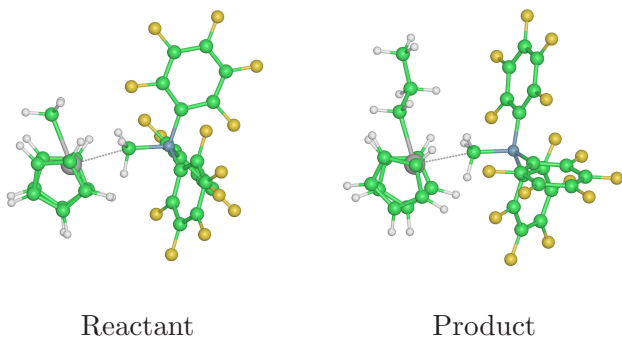


Figure 4.8: Geometries for the reactant and product of the insertion reaction of the first ethylene monomer into the $[\text{Cp}_2\text{ZrCH}_3]^+/\text{Cl}_R^-$ catalyst. These two geometries are common for the three different approach paths to the zirconocene catalyst.

The model/real counterion energetic discrepancies are depicted in Figure 4.13. As can be seen, the differences are small in general, only seldom rising slightly over chemical accuracy values (1 kcal/mol). Additionally the one $\Delta\Delta G$ calculated, namely $\Delta\Delta G = \Delta G(\text{Zc}_{comp}^M) - \Delta G(\text{Zc}_{comp}^R)$, gives a discrepancy of only 0.32 kcal/mol.

All the electronic energies are summarized in Table 4.9, and the Gibbs free energies in Table 4.10. The potential energy values can be briefly compared

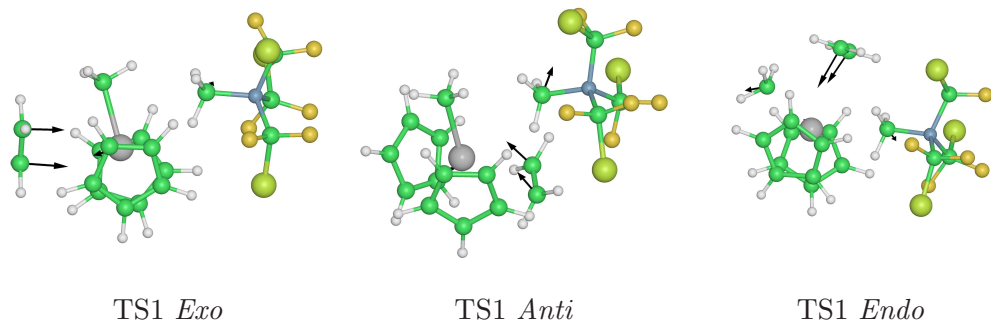


Figure 4.9: Geometries for the TS1 transition states for the three different monomer approach paths to the $[\text{Cp}_2\text{ZrCH}_3]^+/\text{Cl}_M^-$ catalyst. The black arrows depict the movement of the relevant atoms ($\text{C}_1, \text{C}_2, \text{Zr}, \text{C}_\alpha, \text{C}_{\text{Cl}}$) in the vibrational mode corresponding to the imaginary frequency that characterizes the transition state.

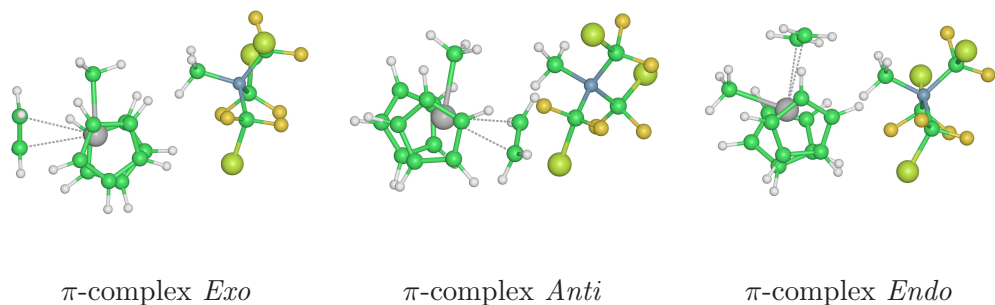


Figure 4.10: Geometries for the monomer/metal π -complex geometries for the three different approach paths to the $[\text{Cp}_2\text{ZrCH}_3]^+/\text{Cl}_M^-$ catalyst.

to those by Yang and Ziegler[95], who also calculate them for the *cis* and *trans* paths (my *Endo* and *Exo*, respectively). Although they perform Car-Parrinello/AMBER95 QM/MM molecular dynamics, some similarities can be found. They find a lower TS1 for the *Endo* approach (6.0 *vs.* 15.9 kcal/mol), as I do (9.53 *vs.* 18.06 kcal/mol), whereas the ordering is reversed for TS2 (16.2 *vs.* 15.3 kcal/mol), in agreement with my results (20.96 *vs.* 19.51 kcal/mol). Bear in mind that I am comparing their Cl_R results with my Cl_M ones, because I did not calculate TSs for Cl_R .

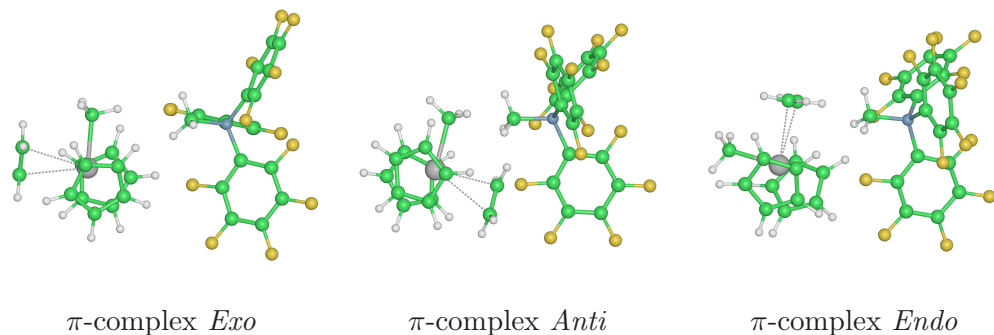


Figure 4.11: Geometries for the monomer/metal π -complex geometries for the three different approach paths to the $[\text{Cp}_2\text{ZrCH}_3]^+/\text{Cl}_R^-$ catalyst.

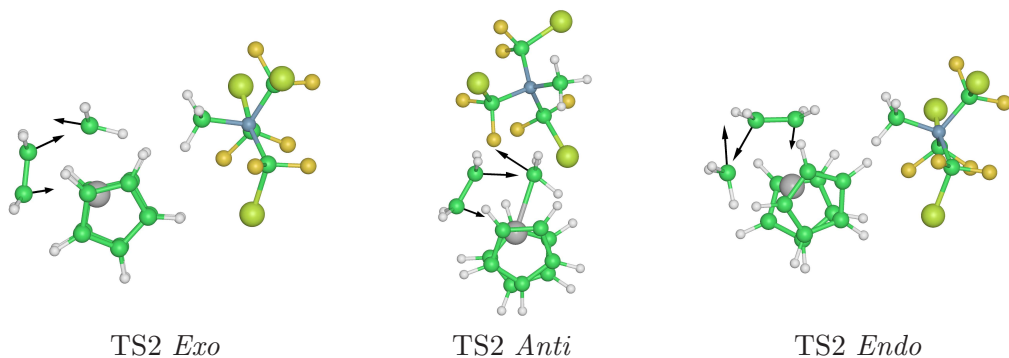


Figure 4.12: Geometries for the TS2 transition states for the three different monomer approach paths to the $[\text{Cp}_2\text{ZrCH}_3]^+/\text{Cl}_M^-$ catalyst. The black arrows depict the movement of the relevant atoms ($\text{C}_1, \text{C}_2, \text{Zr}, \text{C}_\alpha, \text{C}_{\text{Cl}}$) in the vibrational mode corresponding to the imaginary frequency that characterizes the transition state.

It is worth mentioning that the TS1 is slightly lower than π -complex in the *Exo* FEC for $[\text{Cp}_2\text{TiCH}_3]^+/\text{Cl}_M^-$. This is no paradox, of course, because it is indeed higher in the electronic energy surface, and that is the space where the geometry optimization calculations take place. However, the energy corrections obtained from the frequency calculations raise the π -complex more than they do the TS, and hence it looks like the structure that is a TS in the PEC is not so in the Gibbs free energy curve (FEC). Unfortunately, it is not presently feasible to optimize directly in the FEC.

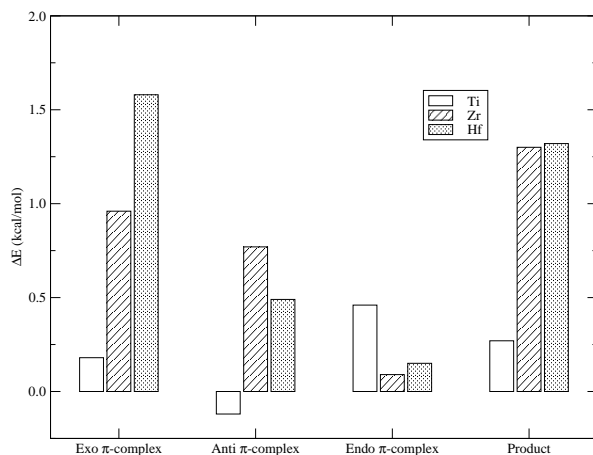


Figure 4.13: Energy differences between species calculated with real and model counterions. Values in kcal/mol.

In order to have more compact numbers to quantify differences, one can resort to Eq. 4.7. Assuming an example RT of 0.576 kcal/mol ($T = 300\text{K}$), I come up with the global ΔG values tabulated in Table 4.11.

One can compare the energies in the right hand side of Table 4.11 with those in Table 4.8, as well as geometrical parameters in Table 4.12 with those in Table 4.7, in order to assess the accuracy of the B3LYP/SKBJ+//HF/SKBJ+ scans, with respect to the B3LYP/TZ//B3LYP/LanL2DZdp optimizations. All one can conclude is that the SKBJ+ energies seem to be underestimated by around 7 kcal/mol. However, when it comes to geometry, the concordance is not that bad, at least for local minima. SKBJ+ scans correctly predict a longer *Exo* TS1 $d(\text{Zr}-\text{C}_1\text{C}_2)$ and TS2 $d(\text{C}_2-\text{C}_\alpha)$, but greatly overestimating the $d(\text{Zr}-\text{C}_1\text{C}_2)$ of all TS1s. For the π -complex, the SKBJ+ $\text{Zr}-\text{C}_1\text{C}_2$ distances seem to be quite accurate, if only a bit underestimated for $\text{CI} = \text{CI}_R$. The product $\text{C}_2-\text{C}_\alpha$ distances do not change much from the scans to the optimizations.

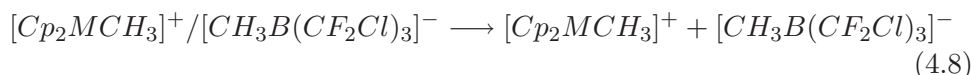
Regarding a prediction of a preferred path for each metal, looking at Table 4.11 it seems that both *Exo* and *Anti* approach paths have almost the same free energy barrier for each metal, whereas the *Endo* approach path is always unfavorable. Take into account that for my achiral catalyst, and ethylene as monomer, all the paths lead to equivalent products. This might not be the case for other polymerizing systems, where one path might be greatly favored over the others. Particularly, when an alternating monomer complexation site (growing chain swinging) is required to explain the experimentally obtained

Metal	Path	CI _M				CI _R	
		TS1	π -comp	TS2	Product	π -comp	Product
Ti	<i>Exo</i>	13.39	11.59	14.42	-16.24	11.77	-15.78
	<i>Anti</i>	18.10	11.42	14.89	-16.24	11.68	-15.78
	<i>Endo</i>	13.80	7.63	17.12	-16.24	7.52	-15.78
Zr	<i>Exo</i>	18.06	15.04	19.51	-16.40	15.99	-16.31
	<i>Anti</i>	16.21	12.67	18.84	-16.40	13.97	-16.31
	<i>Endo</i>	9.53	7.46	20.96	-16.40	8.23	-16.31
Hf	<i>Exo</i>	18.51	15.40	21.15	-16.23	16.99	-16.07
	<i>Anti</i>	18.20	13.10	21.33	-16.23	14.42	-16.07
	<i>Endo</i>	11.33	8.03	22.60	-16.23	8.52	-16.07

Table 4.9: Summary of electronic energies of stationary points in the $[\text{Cp}_2\text{MCH}_3]^+/\text{CI}_X^-$ + ethylene reaction potential energy curves (PECs), M = Ti, Zr and Hf, and X = M and R.

tacticity, it seems intuitive that the *Exo* path should be the preferential one, as it seems the only one including such a swing.

On the other hand, if one compares the metals among them, it is observed that the heavier metals have higher overall reaction barriers. This can be tracked back to the binding energies (BE) of the counterions (Eq. 4.8).



The values of these BEs (see Table 4.13) indicate a clearly less tightly bound CI for M = Ti (by around 10 kcal/mol), and similar tightness for M = Zr and Hf (within 1 kcal/mol). This seems to imply that, as expect, the stronger the metal/CI bond, the harder for the monomer to displace the latter and form the π -complex; moreover, my data also shows a similar correlation for the insertion barrier, for reasons still unclear. This results agree with experimental results[108] that observe a greater catalytic activity when a greater cationic character is induced into the metal (presumably this means greater charge separation, which is expected for weaker binding).

It may come as a surprise that for this system the activity of the M = Ti case would be higher than that of Zr and Hf (because the complexation and insertion barriers are lower). There is, indeed, literature regarding zirconium as the most active metal of the three, followed by hafnium, and titanium at a far

Metal	Path	TS1	π -complex	TS2	Product
Ti	<i>Exo</i>	20.55	21.52	26.46	0.16
	<i>Anti</i>	27.65	21.29	26.07	0.16
	<i>Endo</i>	23.89	19.57	29.91	0.16
Zr	<i>Exo</i>	28.68	24.32	31.59	-2.26
	<i>Anti</i>	29.57	21.84	31.82	-2.26
	<i>Endo</i>	22.81	18.59	33.91	-2.26
Hf	<i>Exo</i>	29.08	25.27	32.96	-2.49
	<i>Anti</i>	31.67	22.40	32.45	-2.49
	<i>Endo</i>	24.61	18.97	35.49	-2.49

Table 4.10: Summary of Gibbs free energies of stationary points in the $[\text{Cp}_2\text{MCH}_3]^+/\text{Cl}_M^-$ + ethylene reaction potential energy curves (PECs), M = Ti, Zr and Hf, and X = m. The π -complex ΔG value the *Exo* approach to $[\text{Cp}_2\text{ZrCH}_3]^+/\text{Cl}_R^-$ is 24.00 kcal/mol. All values in kcal/mol.

	ΔG			ΔE		
	<i>Exo</i>	<i>Anti</i>	<i>Endo</i>	<i>Exo</i>	<i>Anti</i>	<i>Endo</i>
Ti	26.46	27.69	29.91	14.52	18.10	17.12
Zr	31.60	31.84	33.91	19.56	18.85	20.96
Hf	32.96	32.60	35.49	21.85	21.33	22.60

Table 4.11: Global propagation reaction Gibbs free energy barriers (left), as obtained from data in Table 4.10 and Eq. 4.7. Global electronic energy barriers also tabulated (right), for comparison purposes with data in Table 4.8. All values in kcal/mol.

third position[92]. Other comparisons between Ti and Zr germanium-bridged *ansa*-metallocenes[101] regard Zr as around double as active as Ti towards ethylene and propylene polymerization. Beckerle *et al.*[102] studied some post-metallocenic bisphenolic compounds of the type $[\{\text{S}(\text{CH}_2)_2\text{S}\}(\text{OC}_6\text{H}_2\text{-}^t\text{Bu}_2\text{-}4,6)_2\text{MX}_2]$, and found that for M = Ti and Hf the activity towards styrene polymerization was similar (with Hf slightly more active) and M = Zr was clearly more active than any of the former two. Theoretical studies by Vanka *et al.* on a nitrogenated post-metallocene[72], also come up with a lower barrier for the polymerization by zirconium, than by titanium.

However, the data on the subject is far from uncontroversial, since recent

	Parameter	CI _M			CI _R		
		<i>Exo</i>	<i>Anti</i>	<i>Endo</i>	<i>Exo</i>	<i>Anti</i>	<i>Endo</i>
TS1	d(Zr–C ₁ C ₂)	3.394	3.080	3.296	-	-	-
π -complex	d(Zr–C ₁ C ₂)	2.896	2.841	2.857	2.924	2.981	2.845
TS2	d(C ₂ –C _{α})	2.229	2.215	2.117	-	-	-
Product	d(C ₂ –C _{α})	1.539	-	-	1.539	-	-

Table 4.12: Geometric parameters for the reaction stationary points, as optimized for [Cp₂ZrCH₃]⁺/CI_X⁻, X = M and R. All distances in Å.

M	BE (CI _M)	BE (CI _R)
Ti	-74.33	-71.47
Zr	-83.55	-81.21
Hf	-84.48	-82.08

Table 4.13: Counterion Binding Energies for M = Ti, Zr and Hf. Electronic energies calculated at the B3LYP/TZ//B3LYP/LanL2DZdp theory level.

works by Bott *et al.*[103] report similar activities for Ti- and Zr-bearing monocyclopentadienyl phenoxy-imines and -amines, as well as for Cp₂MCl₂/MAO, M = Ti and Zr. Even more recent studies by Gil and Casagrande[104] on exotic hydrotris(pyrazolyl)borateMCl₃ derivatives conclude that, depending on some substituents, Ti can have slightly more or slightly less activity than Zr towards ethylene polymerization.

However, some metallocenic catalysts show outright higher activity for the titanated system than for the zirconated one, e.g. some β -diketiminato complexes[105]. Early work by Kaminsky [106] regards Ti as more active than Zr, but reckon a decrease in titanium activity caused by its reduction from Ti(IV) to Ti(III)[109], which is believed to be more active for polystyrene (PS) polymerization, whereas Ti(IV) is more active towards ethylene[110]. This deactivation through reduction is observed to increase as the reaction temperature increases[74]. Kaminsky also discusses a propylene polymerization case where hafnium is approximately three times less active than zirconium. The decrease in polymerization activity as temperature increases, for Ti(IV) compounds, is also observed by Lee *et al.*[111]. Kim *et al.* are also “surprised”[107] that for their silacycloalkane-bridged *ansa*-metallocenes the activity of the titanated complexes is indeed higher than that of the zirconated ones, by almost an order of magnitude in some cases.

It is of great interest the fact that titanium complexes have been reported

to have their activity reduced when increasing the reaction temperature. This means that there are competitive deactivating processes, e.g. the reduction to Ti(III) mentioned above, but also that these processes are more sensitive to temperature changes than the propagation step itself is, because *both* polymer chain growth and deactivation must *a priori* be accelerated when increasing the temperature, but the latter accelerates more, resulting in an overall activity decrease.

My results so far predict a lower barrier for the titanated metallocene, which rationalizes fairly well the experimentally observed [106, 107, 74, 111] high activity at low temperatures, and small temperature sensitivity of the base reaction rate constant. The latter is inferred from the observed decrease of the overall reaction rate at higher temperatures, where the thermal deactivation of Ti(IV) to Ti(III) takes over.

4.4 Conclusions

The substitution of Zr by group 4 Ti and Hf transition metals has been analyzed. The monomer complexation and insertion barriers are found to be lower for titanium than for its heavier counterparts. This, although not an ubiquitous trend in metallocenic and post-metallocenic catalysts, is in good agreement with the superior activity for Ti at lower temperatures, found at least in some titanocenes.

It is also apparent from the results obtained that $[\text{CH}_3\text{B}(\text{CF}_2\text{Cl})_3]^-$ is indeed a convenient and accurate replacement for $[\text{CH}_3\text{B}(\text{C}_6\text{F}_5)_3]^-$ in quantum mechanical calculations of metallocene-catalyzed olefin polymerizations.

The energetic differences when sketching a PES at the B3LYP/SKBJ//HF/SKBJ theory level are close to chemical accuracy. Although the error introduced by not considering correlation in the optimization (see Table 4.5), is small in general, in the C–C bond formation zone it seems to go above 2.5 kcal/mol. On the other hand, the error introduced by substituting CI_R by CI_M is consistently small, and below 1.5 kcal/mol for the four regions depicted in Figure 4.2.

The model/real CI energetic discrepancies are even smaller in the case of the B3LYP/LanL2DZdp stationary points, where they are all around the chemical accuracy threshold.

4.5 Acknowledgements

This research was funded by Euskal Herriko Unibertsitatea (the University of the Basque Country), Gipuzkoako Foru Aldundia (the Provincial Govern-

ment of Gipuzkoa), and Eusko Jaurlaritza (the Basque Government). The SGI/IZO-SGIker UPV/EHU (supported by Fondo Social Europeo and MCyT) is gratefully acknowledged for generous allocation of computational resources.

*“Scully: Did you find what you were looking for?
Mulder: No, but I found something I thought I’d lost:
the faith to keep looking.”*

The X-Files, Season 2, Episode *End Game*

Appendix I

PECs

I.a Titanocene PECs and FECs

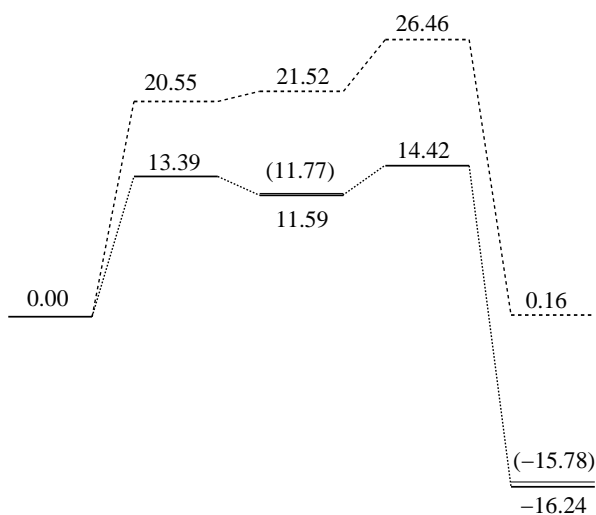


Figure I.1: PEC (dotted line) and FEC (dashed line) for the *Exo* monomer approach path to $[\text{Cp}_2\text{TiCH}_3]^+/\text{Cl}_M^-$.

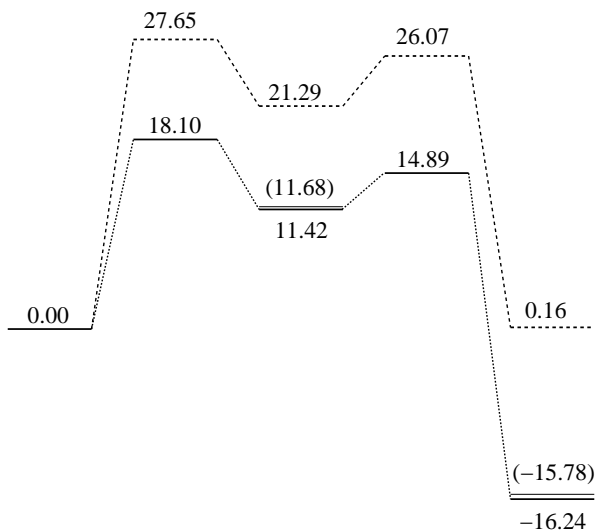


Figure I.2: PEC (dotted line) and FEC (dashed line) for the *Anti* monomer approach path to $[\text{Cp}_2\text{TiCH}_3]^+/\text{Cl}_M^-$.

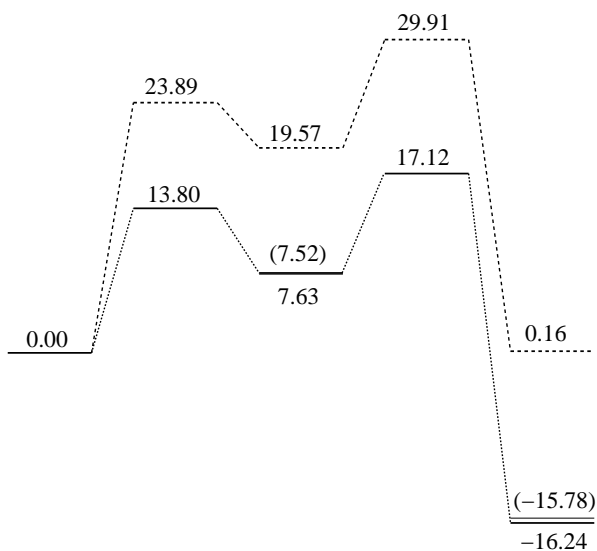


Figure I.3: PEC (dotted line) and FEC (dashed line) for the *Endo* monomer approach path to $[\text{Cp}_2\text{TiCH}_3]^+/\text{Cl}_M^-$.

I.b Zirconocene PECs and FECs

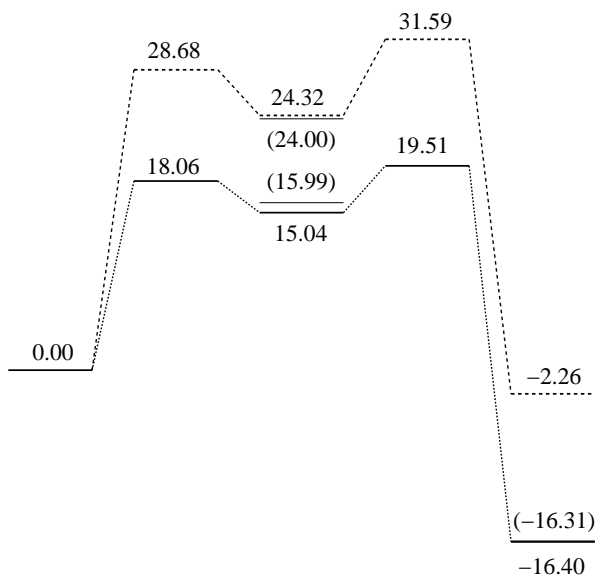


Figure I.4: PEC (dotted line) and FEC (dashed line) for the *Exo* monomer approach path to $[\text{Cp}_2\text{ZrCH}_3]^+/\text{Cl}_M^-$.

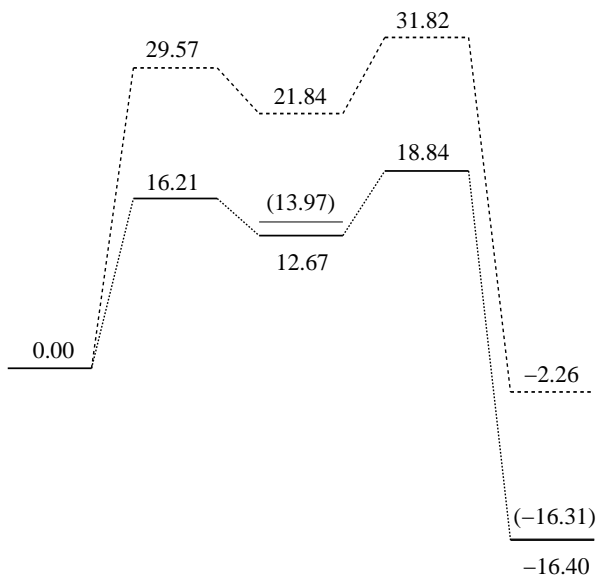


Figure I.5: PEC (dotted line) and FEC (dashed line) for the *Anti* monomer approach path to $[\text{Cp}_2\text{ZrCH}_3]^+/\text{Cl}_M^-$.

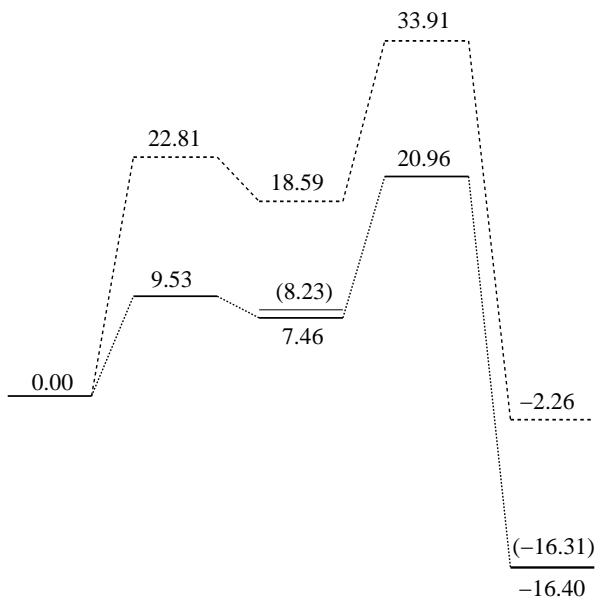


Figure I.6: PEC (dotted line) and FEC (dashed line) for the *Endo* monomer approach path to $[\text{Cp}_2\text{ZrCH}_3]^+/\text{Cl}_M^-$.

I.c Hafnocene PECs and FECs

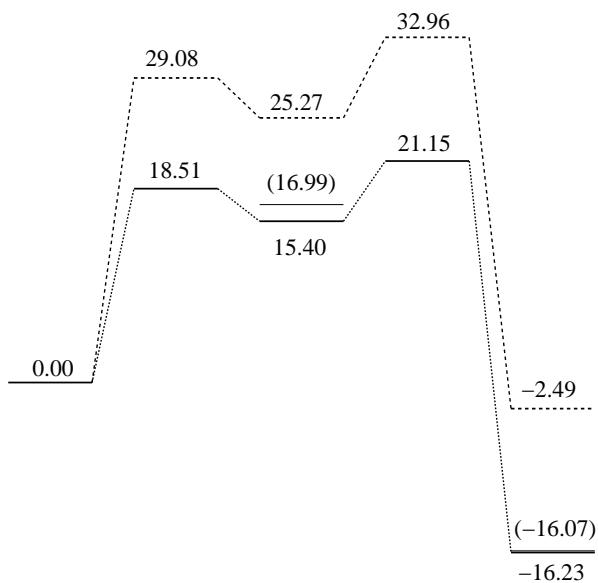


Figure I.7: PEC (dotted line) and FEC (dashed line) for the *Exo* monomer approach path to $[\text{Cp}_2\text{HfCH}_3]^+/\text{Cl}_M^-$.

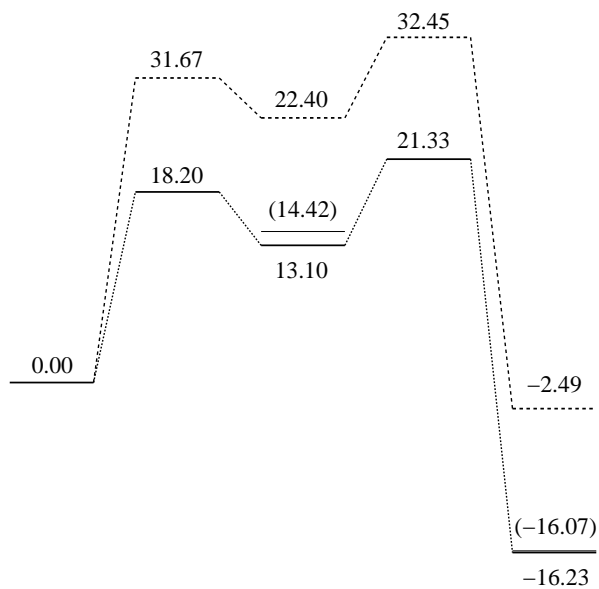


Figure I.8: PEC (dotted line) and FEC (dashed line) for the *Anti* monomer approach path to $[\text{Cp}_2\text{HfCH}_3]^+/\text{Cl}_M^-$.

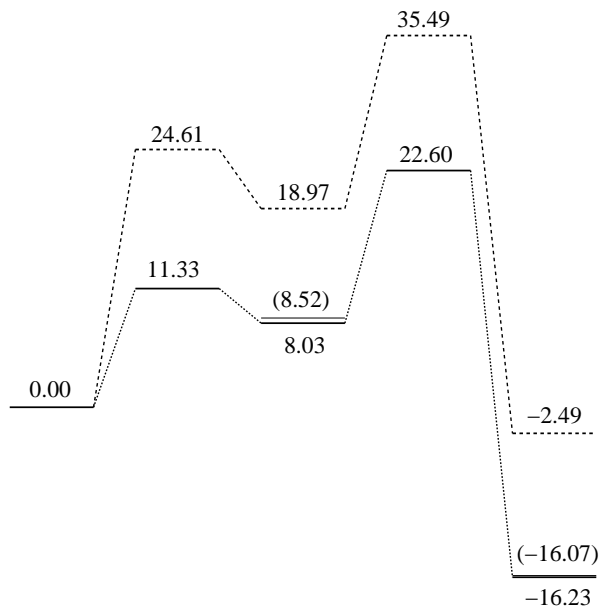


Figure I.9: PEC (dotted line) and FEC (dashed line) for the *Endo* monomer approach path to $[\text{Cp}_2\text{HfCH}_3]^+/\text{Cl}_M^-$.

Appendix II

Geometries

II.a Titanocene geometries

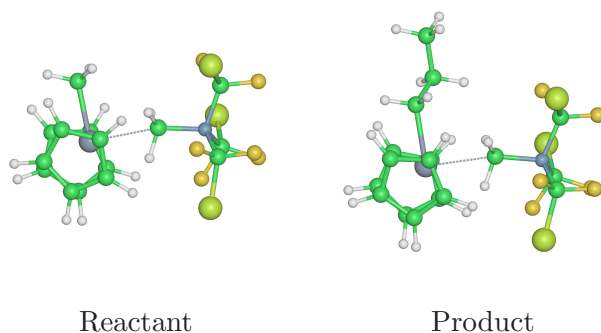


Figure II.1: Geometries for the reactant and product of the insertion reaction of the first ethylene monomer into the $[\text{Cp}_2\text{TiCH}_3]^+/\text{Cl}_M^-$ catalyst. These two geometries are common for the three different approach paths to the zirconocene catalyst.

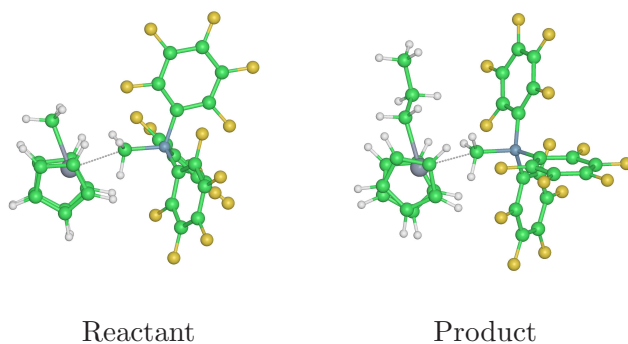


Figure II.2: Geometries for the reactant and product of the insertion reaction of the first ethylene monomer into the $[\text{Cp}_2\text{TiCH}_3]^+/\text{Cl}_R^-$ catalyst. These two geometries are common for the three different approach paths to the zirconocene catalyst.

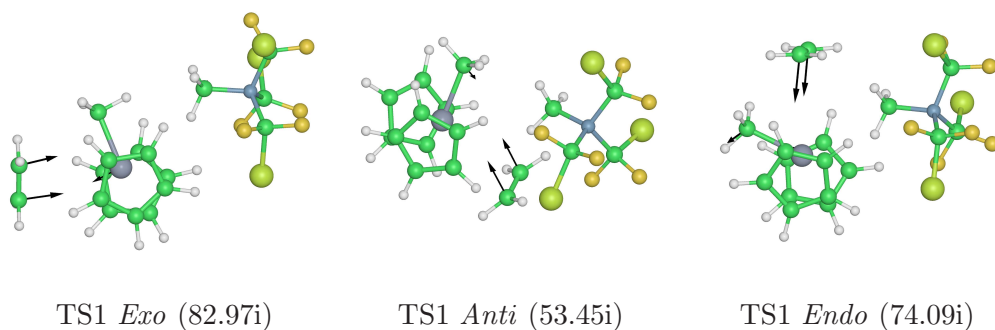


Figure II.3: Geometries for the TS1 transition states for the three different monomer approach paths to the $[\text{Cp}_2\text{TiCH}_3]^+/\text{Cl}_M^-$ catalyst. The black arrows depict the movement of the relevant atoms ($\text{C}_1, \text{C}_2, \text{Zr}, \text{C}_\alpha, \text{Cl}$) in the vibrational mode corresponding to the imaginary frequency that characterizes the transition state.

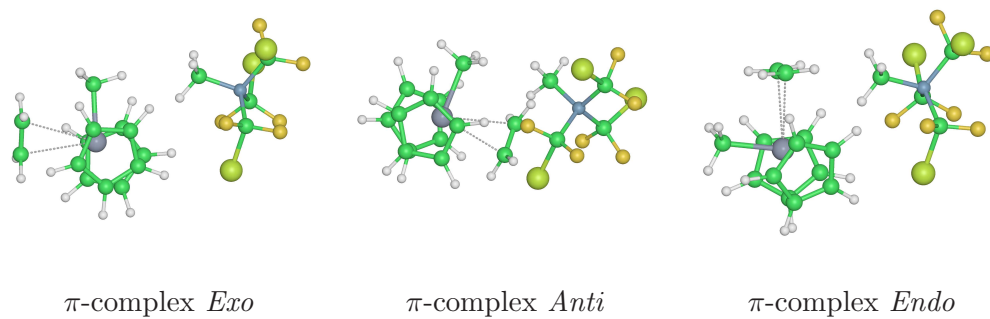


Figure II.4: Geometries for the monomer/metal π -complex geometries for the three different approach paths to the $[\text{Cp}_2\text{TiCH}_3]^+/\text{Cl}_M^-$ catalyst.

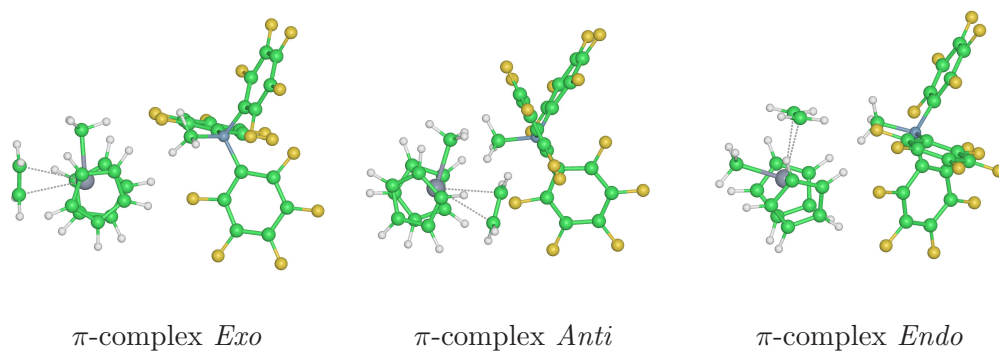


Figure II.5: Geometries for the monomer/metal π -complex geometries for the three different approach paths to the $[\text{Cp}_2\text{TiCH}_3]^+/\text{Cl}_R^-$ catalyst.

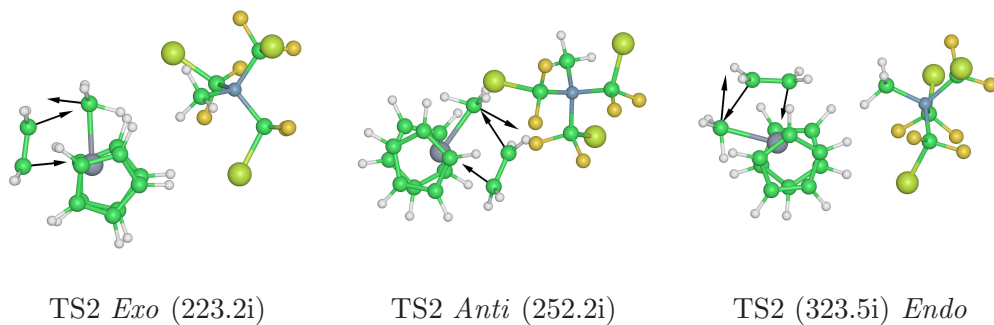


Figure II.6: Geometries for the TS2 transition states for the three different monomer approach paths to the $[\text{Cp}_2\text{TiCH}_3]^+/\text{Cl}_M^-$ catalyst. The black arrows depict the movement of the relevant atoms ($\text{C}_1, \text{C}_2, \text{Zr}, \text{C}_\alpha, \text{C}_{\text{Cl}}$) in the vibrational mode corresponding to the imaginary frequency that characterizes the transition state.

		Ti-C ₁	Ti-C ₂	Ti-C _α	Ti-C _{CI}	C ₁ -C ₂	C ₂ -C _α	
CI _M	Reactant	-	-	2.160	2.459	-	-	
	<i>Exo</i>	TS1	3.798	3.786	2.102	4.033	1.342	3.367
		π-complex	2.864	2.858	2.139	4.546	1.349	2.997
		TS2	2.429	2.604	2.144	4.647	1.388	2.302
	<i>Anti</i>	TS1	3.713	3.845	2.140	4.040	1.344	4.921
		π-complex	2.731	2.827	2.145	5.006	1.352	3.082
		TS2	2.371	2.570	2.141	6.342	1.395	2.257
	<i>Endo</i>	TS1	3.724	3.737	2.168	3.553	1.343	3.506
		π-complex	2.796	2.814	2.163	4.303	1.351	3.326
		TS2	2.335	2.557	2.191	4.602	1.403	2.182
		Product	2.194	3.270	4.627	2.467	1.537	1.540
	CI _R	Reactant	-	-	2.159	2.453	-	-
		<i>Exo</i>	π-complex	2.874	2.846	2.138	4.973	1.349
<i>Anti</i>		π-complex	2.846	2.749	2.140	5.134	1.351	3.101
<i>Endo</i>		π-complex	2.818	2.813	2.159	4.655	1.351	3.320
		Product	2.197	3.295	4.641	2.507	1.535	1.540

Table II.1: Selected interatomic distances for the stationary points in the titanocenic catalyst reaction paths. All values in Å.

II.b Zirconocene geometries

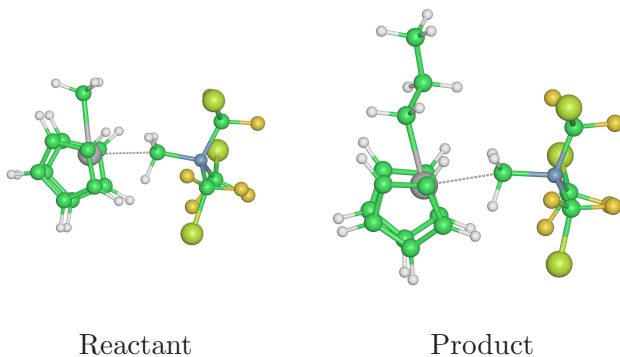


Figure II.7: Geometries for the reactant and product of the insertion reaction of the first ethylene monomer into the $[\text{Cp}_2\text{ZrCH}_3]^+/\text{Cl}_M^-$ catalyst. These two geometries are common for the three different approach paths to the zirconocene catalyst.

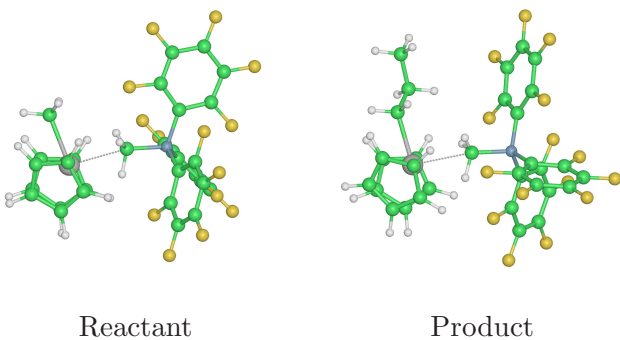


Figure II.8: Geometries for the reactant and product of the insertion reaction of the first ethylene monomer into the $[\text{Cp}_2\text{ZrCH}_3]^+/\text{Cl}_R^-$ catalyst. These two geometries are common for the three different approach paths to the zirconocene catalyst.

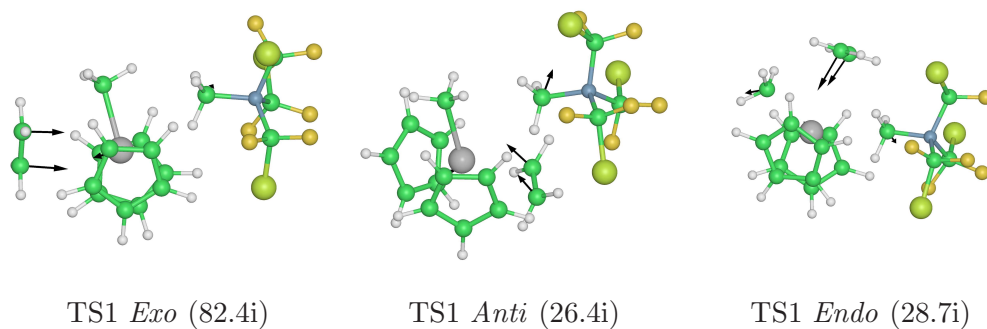


Figure II.9: Geometries for the TS1 transition states for the three different monomer approach paths to the $[\text{Cp}_2\text{ZrCH}_3]^+/\text{Cl}_M^-$ catalyst. The black arrows depict the movement of the relevant atoms ($\text{C}_1, \text{C}_2, \text{Zr}, \text{C}_\alpha, \text{C}_{\text{Cl}}$) in the vibrational mode corresponding to the imaginary frequency that characterizes the transition state.

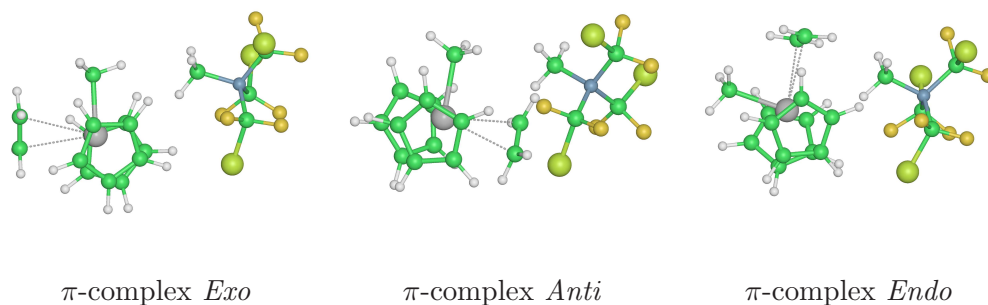


Figure II.10: Geometries for the monomer/metal π -complex geometries for the three different approach paths to the $[\text{Cp}_2\text{ZrCH}_3]^+/\text{Cl}_M^-$ catalyst.

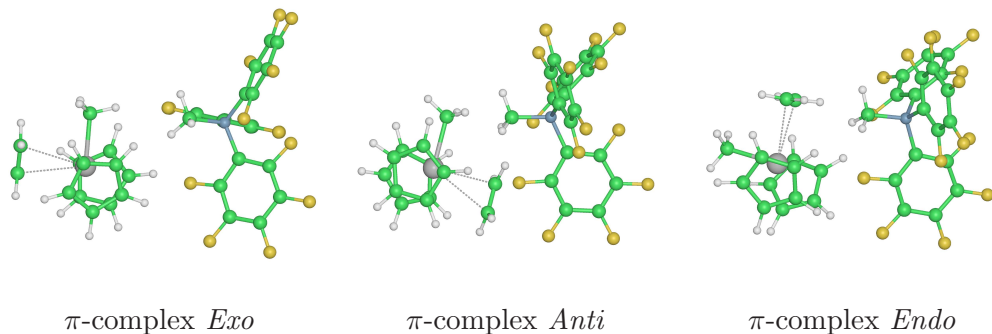


Figure II.11: Geometries for the monomer/metal π -complex geometries for the three different approach paths to the $[\text{Cp}_2\text{ZrCH}_3]^+/\text{Cl}_R^-$ catalyst.

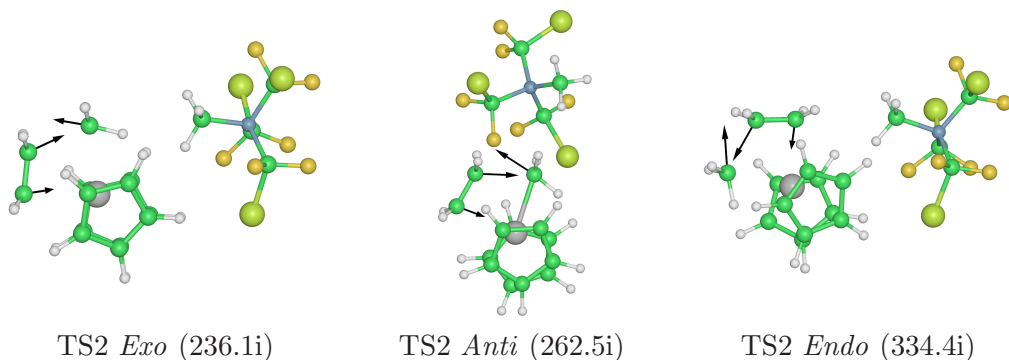


Figure II.12: Geometries for the TS2 transition states for the three different monomer approach paths to the $[\text{Cp}_2\text{ZrCH}_3]^+/\text{Cl}_M^-$ catalyst. The black arrows depict the movement of the relevant atoms ($\text{C}_1, \text{C}_2, \text{Zr}, \text{C}_\alpha, \text{C}_{\text{Cl}}$) in the vibrational mode corresponding to the imaginary frequency that characterizes the transition state.

		Zr-C ₁	Zr-C ₂	Zr-C _α	Zr-C _{CI}	C ₁ -C ₂	C ₂ -C _α	
CI _M	Reactant	-	-	2.278	2.533	-	-	
	<i>Exo</i>	TS1	3.394	3.344	2.264	3.407	1.344	3.125
		π-complex	2.896	2.921	2.258	4.471	1.350	3.161
		TS2	2.442	2.689	2.305	4.327	1.408	2.229
	<i>Anti</i>	TS1	3.080	3.252	2.289	3.419	1.348	4.880
		π-complex	2.841	2.906	2.256	4.757	1.352	3.538
		TS2	2.413	2.673	2.285	6.350	1.412	2.215
	<i>Endo</i>	TS1	3.296	3.296	2.318	2.871	1.347	3.332
		π-complex	2.857	2.861	2.291	3.939	1.352	3.424
		TS2	2.374	2.665	2.345	4.452	1.423	2.117
		Product	2.299	3.340	4.717	2.540	1.542	1.539
	CI _R	Reactant	-	-	2.274	2.528	-	-
		<i>Exo</i>	π-complex	2.925	2.889	2.254	5.008	1.350
<i>Anti</i>		π-complex	2.981	2.717	2.254	5.036	1.351	3.513
<i>Endo</i>		π-complex	2.849	2.845	2.281	4.769	1.353	3.531
		Product	2.303	3.366	4.737	2.557	1.540	1.539

Table II.2: Selected interatomic distances for the stationary points in the zirconocenic catalyst reaction paths. All values in Å.

II.c Hafnocene geometries

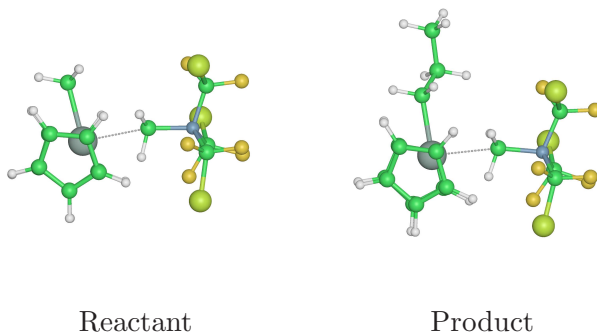


Figure II.13: Geometries for the reactant and product of the insertion reaction of the first ethylene monomer into the $[\text{Cp}_2\text{HfCH}_3]^+/\text{Cl}_M^-$ catalyst. These two geometries are common for the three different approach paths to the hafnocene catalyst.

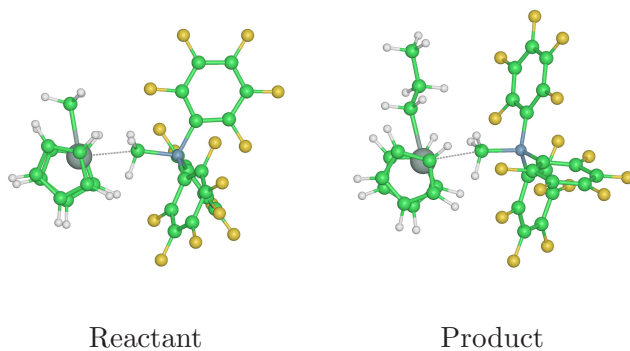


Figure II.14: Geometries for the reactant and product of the insertion reaction of the first ethylene monomer into the $[\text{Cp}_2\text{HfCH}_3]^+/\text{Cl}_R^-$ catalyst. These two geometries are common for the three different approach paths to the hafnocene catalyst.

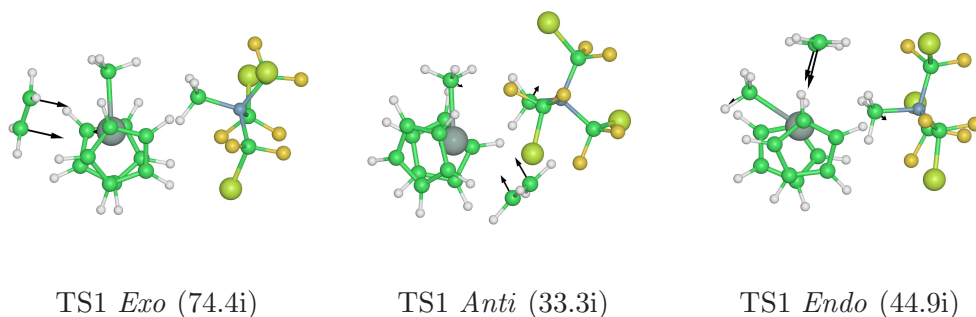


Figure II.15: Geometries for the TS1 transition states for the three different monomer approach paths to the $[\text{Cp}_2\text{HfCH}_3]^+/\text{Cl}_R^-$ catalyst. The black arrows depict the movement of the relevant atoms ($\text{C}_1, \text{C}_2, \text{Zr}, \text{C}_\alpha, \text{C}_{CI}$) in the vibrational mode corresponding to the imaginary frequency that characterizes the transition state.

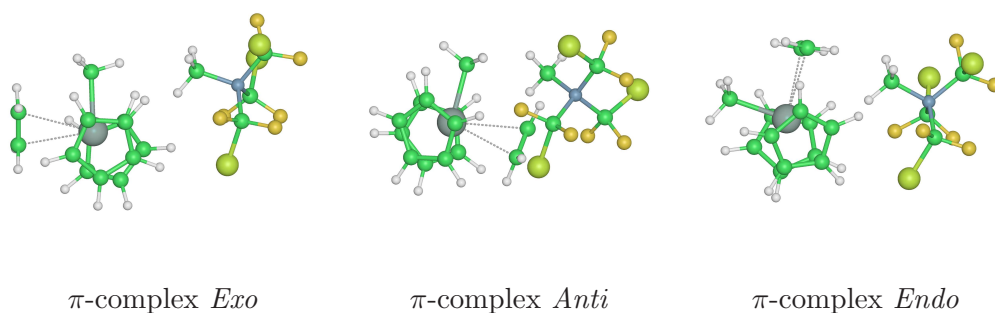


Figure II.16: Geometries for the monomer/metal π -complex geometries for the three different approach paths to the $[\text{Cp}_2\text{HfCH}_3]^+/\text{Cl}_M^-$ catalyst.

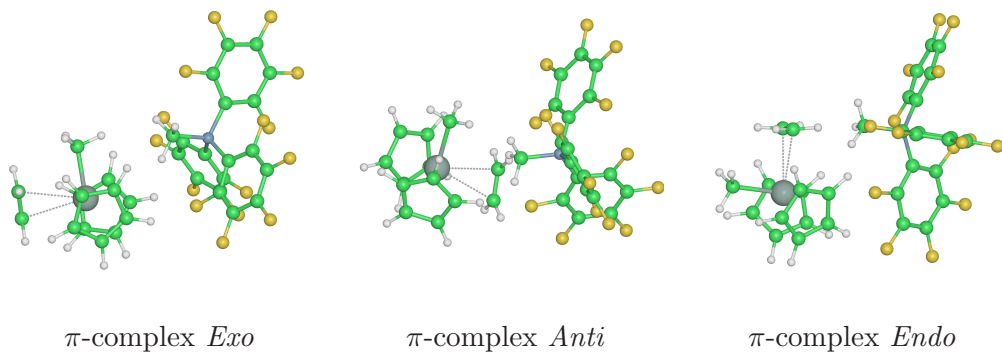


Figure II.17: Geometries for the monomer/metal π -complex geometries for the three different approach paths to the $[\text{Cp}_2\text{HfCH}_3]^+/\text{Cl}_R^-$ catalyst.

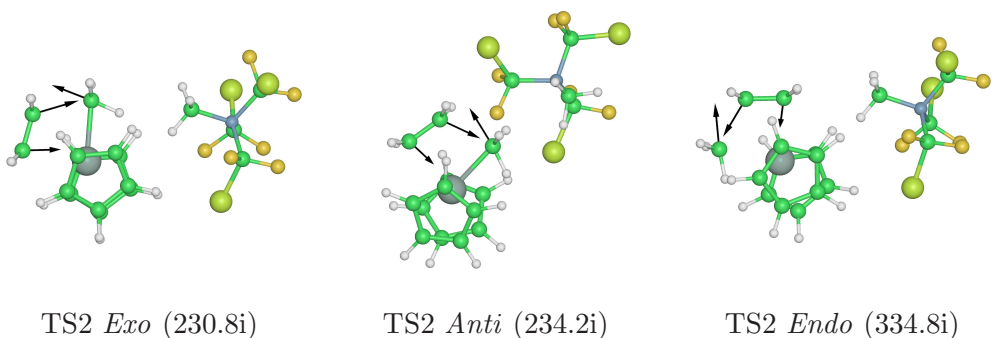


Figure II.18: Geometries for the TS2 transition states for the three different monomer approach paths to the zirconocene catalyst. The black arrows depict the movement of the relevant atoms ($\text{C}_1, \text{C}_2, \text{Zr}, \text{C}_\alpha, \text{C}_{\text{Cl}}$) in the vibrational mode corresponding to the imaginary frequency that characterizes the transition state.

		Hf-C ₁	Zr-C ₂	Hf-C _α	Hf-C _{CI}	C ₁ -C ₂	C ₂ -C _α	
CI _M	Reactant	-	-	2.252	2.487	-	-	
	<i>Exo</i>	TS1	3.390	3.324	2.235	3.488	1.344	3.135
		π-complex	2.874	2.879	2.231	4.472	1.351	3.101
		TS2	2.422	2.668	2.270	4.368	1.408	2.245
	<i>Anti</i>	TS1	3.122	3.320	2.260	3.404	1.348	4.900
		π-complex	2.777	2.865	2.233	4.901	1.352	3.318
		TS2	2.403	2.660	2.252	5.801	1.411	2.236
	<i>Endo</i>	TS1	3.250	3.254	2.288	2.904	1.348	3.305
		π-complex	2.798	2.810	2.256	4.184	1.354	3.450
		TS2	2.349	2.643	2.313	4.459	1.424	2.124
		Product	2.270	3.340	4.713	2.492	1.545	1.538
	CI _R	Reactant	-	-	2.249	2.481	-	-
		<i>Exo</i>	π-complex	2.870	2.865	2.228	4.556	1.351
<i>Anti</i>		π-complex	2.937	2.709	2.227	3.975	1.352	3.342
<i>Endo</i>		π-complex	2.805	2.802	2.252	4.726	1.354	3.472
		Product	2.275	3.367	4.732	2.510	1.543	1.538

Table II.3: Selected interatomic distances for the stationary points in the hafnocenic catalyst reaction paths. All values in Å.

Bibliography

- [1] Harrington, B.; Byak, B.; Cruz, J. A.; MenTaLguY. Inkscape 0.44. Downloadable under the GPL license at: <http://www.inkscape.org/download.php>, 2006.
- [2] Wolfram Inc. Mathematica 5.2. <http://www.wolfram.com/>, 2005.
- [3] Merrit, E. A.; Bacon, D. J. *Meth. Enzymol.*, **1997**, *277*, 505. Downloadable free of charge at: <http://www.bmsc.washington.edu/raster3d/>.
- [4] Silanes, I.; Ugalde, J. M. *Organometallics*, **2005**, *24(13)*, 3233.
- [5] Silanes, I.; Mercero, J. M.; Ugalde, J. M. *Organometallics*, **2006**, *25(19)*, 4483.
- [6] Ziegler, K.; Hozkamp, E.; Breil, H.; Martin, H. *Angew. Chem.*, **1955**, *67*, 541.
- [7] Natta, G. *J. Polym. Sci.*, **1955**, *16*, 143.
- [8] Natta, G. *Angew. Chem.*, **1956**, *68*, 393.
- [9] Natta, G.; Pino, P.; Mazzanti, G. *Gazz. Chem. Ital.*, **1957**, *87*, 528.
- [10] Natta, G. *Angew. Chem.*, **1964**, *76*, 553.
- [11] Kealy, T. J.; Pauson, P. J. *Nature(London)*, **1951**, *168*, 1039.
- [12] Miller, S. A.; Tebboth, J. A.; Tremaine, J. F. *J. Chem. Soc.*, **1952**, p 632.
- [13] Breslow, D. S.; Newburg, N. R. *J. Am. Chem. Soc.*, **1957**, *79*, 5072.
- [14] Natta, G.; Pino, P.; Mazzanti, G.; Lauzo, R. *Chim. Ind. (Milan)*, **1957**, *39*, 1032.

- [15] Natta, G.; Pino, P.; Mazzanti, G.; Giannini, U. *J. Am. Chem. Soc.*, **1957**, *79*, 2975.
- [16] Breslow, D. S.; Newburg, N. R. *J. Am. Chem. Soc.*, **1959**, *81*, 81.
- [17] Causey, P. W.; Baird, M. C.; Cole, S. P. C. . *Organometallics*, **2004**, *23*, 4486.
- [18] Allen, O. R.; Croll, L.; Gott, A. L.; Knox, R. J.; McGowan, P. C. *Organometallics*, **2004**, *23*, 288.
- [19] Cossée, P. *Tetrahedron Lett.*, **1960**, *38*, 12.
- [20] Cossée, P. *J. Catal.*, **1964**, *3*, 80.
- [21] Arlman, E. J. *J. Catal.*, **1964**, *3*, 89.
- [22] Arlman, E. J.; Cossée, P. *J. Catal.*, **1964**, *3*, 99.
- [23] Arlman, E. J. *J. Catal.*, **1966**, *5*, 178.
- [24] Kaminsky, W.; Steiger, R. *Polyhedron*, **1988**, *7(22/23)*, 2375.
- [25] Corradini, P.; Guerra, G. *Prog. Polym. Sci.*, **1991**, *16*, 239.
- [26] Vosko, S. H.; Wilk, L.; Nussair, M. M. *Can. J. Phys.*, **1980**, *58*, 1200.
- [27] Becke, A. D. *Phys. Rev. A*, **1988**, *38*, 3098.
- [28] Lee, C.; Yang, W.; Parr, R. G. *Phys. Rev. B*, **1980**, *37*, 785.
- [29] Adcock, S. A.; McCammon, J. A. *Chem. Rev.*, **2006**, *106*, 1589.
- [30] Svensson, M.; Humbel, S.; Froese, R. D. J.; Matsubara, T.; Sieber, S.; Morokuma, K. *J. Phys. Chem.*, **1996**, *100*, 19357.
- [31] Dapprich, S.; Komáromi, I.; Byun, K. S.; Morokuma, K.; Frisch, M. J. *J. Mol. Struct. (Theochem)*, **1999**, *462*, 1.
- [32] Basis sets were obtained from the Extensible Computational Chemistry Environment Basis Set Database, Version 02/25/04, as developed and distributed by the Molecular Science Computing Facility, Environmental and Molecular Sciences Laboratory which is part of the Pacific Northwest Laboratory, P.O. Box 999, Richland, Washington 99352, USA, and funded by the U.S. Department of Energy. The Pacific Northwest Laboratory is a multi-program laboratory operated by Battelle Memorial

Institute for the U.S. Department of Energy under contract DE-AC06-76RLO 1830. Contact David Feller or Karen Schuchardt for further information.

- [33] Schaftenaar, G.; Noordik, J. H. *J. Comput.-Aided Mol. Design*, **2000**, *14*, 123.
- [34] Frisch, M. J.; Trucks, G. W.; Schlegel, H. B.; Scuseria, G. E.; Robb, M. A.; Cheeseman, J. R.; Zakrzewski, V. G.; Montgomery, J. A.; Stratmann, R. E.; Burant, J. C.; Dapprich, S.; Millam, J. M.; Daniels, A. D.; Kudin, K. N.; Strain, M. C.; Farkas, O.; Tomasi, J.; Barone, V.; Cossi, M.; Cammi, R.; Mennucci, B.; Pomelli, C.; Adamo, C.; Clifford, S.; Ochterski, J.; Petersson, G. A.; Ayala, P. Y.; Cui, Q.; Morokuma, K.; Malick, D. K.; Rabuck, A. D.; Raghavachari, K.; Foresman, J. B.; Cioslowski, J.; Ortiz, J. V.; Stefanov, B. B.; Liu, G.; Liashenko, A.; Piskorz, P.; Komaromi, I.; Gomperts, R.; Martin, R. L.; Fox, D. J.; Keith, T.; Al-Laham, M. A.; Peng, C. Y.; Nanayakkara, A.; Gonzalez, C.; Challacombe, M.; Gill, P. M. W.; Johnson, B. G.; Chen, W.; Wong, M. W.; Andres, J. L.; Head-Gordon, M.; Replogle, E. S.; Pople, J. A. Gaussian 98, revision a.11.3. Gaussian, Inc., Pittsburgh PA, 2002.
- [35] Frisch, M. J.; Trucks, G. W.; Schlegel, H. B.; Scuseria, G. E.; Robb, M. A.; Cheeseman, J. R.; Montgomery, J. A. Jr; Vreven, T.; Kudin, K. N.; Burant, J. C.; Millam, J. M.; Iyengar, S. S.; Tomasi, J.; Barone, V.; Mennucci, B.; Cossi, M.; Scalmani, G.; Rega, N.; Petersson, G. A.; Nakatsuji, H.; Hada, M.; Ehara, M.; Toyota, K.; Fukuda, R.; Hasegawa, J.; Ishida, M.; Nakajima, T.; Honda, Y.; Kitao, O.; Nakai, H.; Klene, M.; Li, X.; Knox, J. E.; Hratchian, H. P.; Cross, J. B.; Adamo, C.; Jaramillo, J.; Gomperts, R.; Stratmann, R. E.; Yazyev, O.; Austin, A. J.; Cammi, R.; Pomelli, C.; Ochterski, J. W.; Ayala, P. Y.; Morokuma, K.; Voth, G. A.; Salvador, P.; Dannenberg, J. J.; Zakrzewski, V. G.; Dapprich, S.; Daniels, A. D.; Strain, M. C.; Farkas, O.; Malick, D. K.; Rabuck, A. D.; Raghavachari, K.; Foresman, J. B.; Ortiz, J. V.; Cui, Q.; Baboul, A. G.; Clifford, S.; Cioslowski, J.; Stefanov, B. B.; Liu, G.; Liashenko, A.; Piskorz, P.; Komaromi, I.; Martin, R. L.; Fox, D. J.; Keith, T.; Al-Laham, M. A.; Peng, C. Y.; Nanayakkara, A.; Challacombe, M.; Gill, P. M. W.; Johnson, B.; Chen, W.; Wong, M. W.; Gonzalez, C.; Pople, J. A. Gaussian 03, revision c.02. Gaussian, Inc., Wallingford CT, 2004.
- [36] Ochoteco, E. *Polimerización de propileno con catalizadores de metaloceno*. Ph.d. diss., University of the Basque Country, 2001.

- [37] John, L.; Utiko, J.; Jerzykiewicz, L. B.; Sobota, P. *Inorg. Chem.*, **2005**, *44*(25), 9131.
- [38] Yang, S. H.; Huh, J.; Jo, W. H. *Macromolecules*, **2005**, *38*, 1402.
- [39] Fusco, R.; Longo, L.; Proto, A.; Masi, F.; Garbassi, F. *Macromol. Rapid Commun.*, **1998**, *19*, 257.
- [40] Zurek, E.; Woo, T. K.; Firman, T. K.; Ziegler, T. *Inorg. Chem.*, **2001**, *40*, 361.
- [41] Zurek, E.; Ziegler, T. *Organometallics*, **2002**, *21*(1), 83.
- [42] Beck, S.; Prosenč, M.-H.; Brintzinger, H.-H.; Goretzki, R.; Herfert, N.; Fink, G. *J. Mol. Catal. A: Chem.*, **1996**, *111*, 67.
- [43] Beringhelli, T.; D'Alfonso, G.; Maggioni, D.; Mercandelli, P.; Sironi, A. *Chem. Eur. J.*, **2005**, *11*, 650.
- [44] Fiske, S. T.; Harris, L. T.; Cuddy, A. J. C. *Science*, **2004**, *306*, 1482.
- [45] Kawamura-Kuribayashi, H.; Koga, N.; Morokuma, K. *J. Am. Chem. Soc.*, **1992**, *114*, 2359.
- [46] Kawamura-Kuribayashi, H.; Koga, N.; Morokuma, K. *J. Am. Chem. Soc.*, **1992**, *114*, 8687.
- [47] Yoshida, T.; Koga, N.; Morokuma, K. *Organometallics*, **1995**, *14*, 746.
- [48] Musaev, D. G.; Froese, R. D. J.; Svensson, M.; Morokuma, K. *J. Am. Chem. Soc.*, **1997**, *119*, 367.
- [49] Froese, R. D. J.; Musaev, D. G.; Morokuma, K. *J. Mol. Struct. (Theochem)*, **1999**, *121*, 461.
- [50] Das, P. K.; et. al. in *Transition State Modeling for Catalysis*, Truhlar, D. G.; Morokuma, K., Eds. volume ACS SympSer 721. 1998.
- [51] Woo, T. K.; Fan, L.; Ziegler, T. *Organometallics*, **1994**, *13*, 2252.
- [52] Weiss, H.; Ehrig, M.; Ahlrichs, R. *J. Am. Chem. Soc.*, **1994**, *116*, 4919.
- [53] Meier, R. J.; van Doremaele, G. H. J.; Iarlori, S.; Buda, F. *J. Am. Chem. Soc.*, **1994**, *116*, 7274.
- [54] van Doremaele, G. H. J.; Meier, R. J.; Iarlori, S.; Buda, F. *J. Mol. Struct. (Theochem)*, **1996**, *363*, 269.

- [55] Ystenes, M. *J. Catal.*, **1991**, *129*, 383.
- [56] Ystenes, M. *Makromol. Chem. Macromol. Symp.*, **1993**, *66*, 71.
- [57] Thorshaug, K.; Støvneng, J. A.; Rytter, E.; Ystenes, M. *Macromol.*, **1998**, *31*, 7149.
- [58] Deng, L.; Margl, P.; Ziegler, T. *J. Am. Chem. Soc.*, **1997**, *119*, 1094.
- [59] Lanza, G.; Fragala, I. L.; Marks, T. J. *Organometallics*, **2002**, *21*, 5594.
- [60] Yang, X.; Stern, C. L.; Marks, T. J. *J. Am. Chem. Soc.*, **1991**, *113(9)*, 3623.
- [61] Eisch, J. J.; Caldwell, K. R.; Werner, S.; Krueger, C. *Organometallics*, **1991**, *10*, 3417.
- [62] Chan, M. S. W.; Ziegler, T. *Organometallics*, **2000**, *19*, 5182.
- [63] Nifant'ev, I. E.; Ustynyuk, L. Y.; Laikov, D. N. *Organometallics*, **2001**, *20*, 5375.
- [64] Philipp, D. M.; Muller, R. P.; III, W. A. G.; Storer, J.; McAdon, M.; Mullins, M. *J. Am. Chem. Soc.*, **2002**, *124*, 10198.
- [65] Chen, M.-C.; Roberts, J. A. S.; Marks, T. J. *J. Am. Chem. Soc.*, **2004**, *126(14)*, 4605.
- [66] Landis, C. R.; Sillars, D. R.; Batterton, J. M. *J. Am. Chem. Soc.*, **2004**, *126*, 8890.
- [67] Strauch, J. W.; Faure, J.-L.; Bredeau, S.; Wang, C.; Kehr, G.; Frohlich, R.; Luftmann, H.; Erker, G. *J. Am. Chem. Soc.*, **2004**, *126(7)*, 2089.
- [68] Vanka, K.; Ziegler, T. *Organometallics*, **2001**, *20*, 905.
- [69] Xu, Z.; Vanka, K.; Firman, T. K.; Michalak, A.; Zurek, E.; Zhu, C.; Ziegler, T. *Organometallics*, **2002**, *21*, 2444.
- [70] Song, F.; Lancaster, S. J.; Cannon, R. D.; Schormann, M.; Humphrey, S. M.; Zuccaccia, C.; Macchioni, A.; Bochmann, M. *Organometallics*, **2005**, *24(6)*, 1315.
- [71] Song, F.; Cannon, R. D.; Bochmann, M. *J. Am. Chem. Soc.*, **2003**, *125(25)*, 7641.
- [72] Vanka, K.; Xu, Z.; Ziegler, T. *Organometallics*, **2004**, *23(12)*, 2900.

- [73] Talarico, G.; Budzelaar, P. H. M. *J. Am. Chem. Soc.*, **2006**, *128*(14), 4524.
- [74] Brintzinger, H. H.; Fischer, D.; Mülhaupt, R.; Rieger, B.; Waymouth, R. M. *Angew. Chem. Int. Ed. Engl.*, **1995**, *34*, 1143.
- [75] Liu, Z.; Somsook, E.; Landis, C. R. *J. Am. Chem. Soc.*, **2001**, *123*, 2915.
- [76] Busico, V.; Cipullo, R.; Esposito, V. *Macromol. Rapid Commun.*, **1999**, *20*, 116.
- [77] Bierwagen, E. P.; Bercaw, J. E.; III, W. A. G. *J. Am. Chem. Soc.*, **1994**, *116*(4), 1481.
- [78] Razavi, A.; Bellia, V.; De Brauwer, Y.; Hortmann, K.; Peters, L.; Sirole, S.; Belle, S. V.; Marin, V.; Lopez, M. *J. Organ. Chem.*, **2003**, *684*, 206.
- [79] Mohammed, M.; Nele, M.; Al-Humydi, A.; Xin, S.; Stapleton, R. A.; Collins, S. *J. Am. Chem. Soc.*, **2003**, *125*(26), 7930.
- [80] Stevens, W. J.; Basch, H.; Krauss, M. *J. Chem. Phys.*, **1984**, *81*, 6026.
- [81] Stevens, W. J.; Krauss, M.; Bausch, H.; Jasien, P. G. *Can. J. Chem.*, **1992**, *70*, 612.
- [82] Cundari, T. R.; Stevens, W. J. *J. Chem. Phys.*, **1993**, *98*, 5555.
- [83] Dunning Jr., D. H.; Hay, P. J. in *Methods of Electronic Structure Theory*, Vol. 2, III, H. F. S., Ed. 1977.
- [84] Hay, P. J.; Wadt, W. R. *J. Chem. Phys.*, **1985**, *82*, 270.
- [85] Ortiz, J. V.; Hay, P. J.; Martin, R. L. *J. Am. Chem. Soc.*, **1992**, *114*, 2736.
- [86] Check, C. E.; Faust, T. O.; Bailey, J. M.; Wright, B. J.; Gilbert, T. M.; Sunderlin, L. S. *J. Phys. Chem. A*, **2001**, *105*, 8111.
- [87] Kroeker, M.; Liboska, R.; Banck, M.; Volk, T. Chemtool 1.6.9. Downloadable under the GPL license at: <http://ruby.chemie.uni-freiburg.de/martin/chemtool/chemtool.html>, 2006.
- [88] Grace 5.1.20. Downloadable under the GPL license at: <http://plasmagate.weizmann.ac.il/Grace/>, 2006.

- [89] Sutanthavibul, S.; Yap, K.; Smith, B. V.; King, P.; Boyter, B.; Sato, T. Xfig 3.2.5. Downloadable free of charge at: <http://www.xfig.org/>, 2004.
- [90] Busico, V.; Cipullo, R.; Cutillo, F.; Vacatello, M.; Castelli, V. V. A. *Macromolecules (Communication)*, **2003**, *36(12)*, 4258.
- [91] Busico, V.; Castelli, V. V. A.; Aprea, P.; Cipullo, R.; Segre, A.; Talarico, G.; Vacatello, M. *J. Am. Chem. Soc.*, **2003**, *125(18)*, 5451.
- [92] Möhring, P. C.; Coville, N. J. *J. Organomet. Chem.*, **1994**, *479*, 1.
- [93] Lanza, G.; Fragala, I. L.; Marks, T. J. *Organometallics*, **2001**, *20*, 4006.
- [94] Borrelli, M.; Busico, V.; Cipullo, R.; Ronca, S.; Budzelaar, P. H. M. *Macromolecules*, **2003**, *36*, 8171.
- [95] Yang, S.-Y.; Ziegler, T. *Organometallics*, **2006**, *25(4)*, 887.
- [96] de Rosa, C.; Auriemma, F.; Ruiz de Ballesteros, O.; Resconti, L.; Fait, A.; Ciaccia, E.; Camurati, I. *J. Am. Chem. Soc.*, **2003**, *125*, 10913.
- [97] Xu, Z.; Vanka, K.; Ziegler, T. *Organometallics*, **2004**, *23(1)*, 104.
- [98] Irwin, L. J.; Reibenspies, J. H.; Miller, S. A. *J. Am. Chem. Soc.*, **2004**, *126(51)*, 16716.
- [99] Hagadorn, J. R.; McNevin, M. J.; Wiedenfeld, G.; Shoemaker, R. *Organometallics*, **2003**, *22*, 4818.
- [100] Capacchione, C.; Manivannan, R.; Barone, M.; Beckerle, K.; Centore, R.; Oliva, L.; Proto, A.; Tuzi, A.; Spaniol, T. P.; Okuda, J. *Organometallics*, **2005**, *24(12)*, 2971.
- [101] Alonso-Moreno, C.; Antiñolo, A.; López-Solera, I.; Otero, A.; Prashar, S.; Rodríguez, A. M.; Villaseñor, E. *J. Organomet. Chem.*, **2002**, *656*, 129.
- [102] Beckerle, K.; Capacchione, C.; Ebeling, H.; Manivannan, R.; Mülhaupt, R.; Proto, A.; Spaniol, T. P.; Okuda, J. *J. Organomet. Chem.*, **2004**, *689*, 4636.
- [103] Bott, R. K. J.; Hughes, D. L.; Schormann, M.; Bochmann, M.; Lancaster, S. J. *J. Organomet. Chem.*, **2003**, *665*, 135.
- [104] Gil, M. P.; Casagrande Jr., O. L. *J. Organomet. Chem.*, **2004**, *689*, 286.

-
- [105] Andrés, R.; de Jesús, E.; de la Mata, F. J.; Flores, J. C.; Gómez, R. *J. Organomet. Chem.*, **2005**, *690*, 939.
- [106] Kaminsky, W. *Catal. Today*, **1994**, *20*, 257.
- [107] Kim, S.-J.; Lee, Y.-J.; Kang, E.; Kim, S. H.; Ko, J.; Cheong, B. L. M.; Suh, I.-H.; Kang, S. O. *Organometallics*, **2003**, *22*, 3958.
- [108] Stahl, N. G.; Salata, M. R.; Marks, T. J. *J. Am. Chem. Soc.*, **2005**, *127*(31), 10898.
- [109] Michiue, K.; Jordan, R. F. *Macromolecules*, **2003**, *36*, 9707.
- [110] Mahanthappa, M. K.; Waymouth, R. M. *J. Am. Chem. Soc.*, **2001**, *123*, 12093.
- [111] Lee, M. H.; Han, Y.; Kim, D.-H.; Hwang, J.-W.; Do, Y. *Organometallics*, **2003**, *22*, 2790.

Publications

- **Self-assembly of heterogeneous supramolecular structures with uniaxial anisotropy**
M. Ruiz-Osés, N. González-Lakunza, I. Silanes, A. Gourdon, A. Arnau and J.E. Ortega
J. Phys. Chem. B **2006**, *110(51)*, 25573-25577
- **Comparison of Ti, Zr and Hf as cations for metallocene-catalyzed olefin polymerization**
I. Silanes, J.M. Mercero and J.M. Ugalde
Organometallics **2006**, *25(19)*, 4483-4490.
- **A joint experimental and theoretical study of cation- π interactions: Multiple-decker sandwich complexes of ferrocene with alkali metal ions (Li^+ , Na^+ , Rb^+ , Cs^+)**
A.H. Ilkhechi, J.M. Mercero, I. Silanes, M. Bolte, M. Scheibitz, H-W. Lerner, J.M. Ugalde and M. Wagner
J. Am. Chem. Soc. **2005**, *127*, 10656-10666
- **Comparative study of various mechanisms for metallocene-catalyzed α -olefin polymerization**
I. Silanes and J.M. Ugalde
Organometallics **2005**, *24(13)*, 3233-3246.
- **Minimal dipole charge for a dipole-bound dianion**
I. Silanes, H.J.J. van Dam and J.M. Ugalde
Mol. Phys. **2003**, *101*, 2529-2532
- **Electron correlation studies by means of electron-pair density functions**
E. Valderrama, X. Fradera, I. Silanes, J.M. Ugalde and R.J. Boyd
Reviews in Modern Quantum Chemistry: A celebration of the contributions of Robert G. Parr. Ed. K.D. Sen, World Scientific, Singapore, **2002**

- **Atomic charge states in a weakly coupled plasma environment**
I. Silanes and J. M. Mercero and J.M. Ugalde
Phys. Rev. E **2002**, *66*, 026408
- **The ferrocene-lithium cation complex in the gas phase**
A. Irigoras, J.M. Mercero, I. Silanes and J. M. Ugalde
J. Am. Chem. Soc. **2002**, *123*, 5040-5043
- **Cusp conditions for non-Coulombic interactions**
I. Silanes, J.M. Ugalde and R.J. Boyd
J. Mol. Struc. (Theochem) **2000**, *527*, 27-33
- **Reactivity of $\text{Co}^+(^3\text{F}, ^5\text{F})$, $\text{Ni}^+(^2\text{D}, ^4\text{F})$, and $\text{Cu}^+(^1\text{S}, ^3\text{D})$: reaction of Co^+ , Ni^+ and Cu^+ with water**
A. Irigoras, O. Elizalde, I. Silanes, J.E. Fowler and J.M. Ugalde
J. Am. Chem. Soc. **2000**, *122(1)*, 114-122